Mars Sample Return ascent trajectory optimisation using Taylor Series integration
Master Thesis

S.D. Petrovic

Faculty Aerospace, Section Spaceflight

T̃U Delft
Delft
University of
Technology

Challenge the future

PREFACE

Back in December 2013 Warren Gebbett gave a presentation on his work at the Jet Propulsion Laboratory (JPL) in Pasadena, California, USA and the opportunity for a new student to go and perform research at JPL. At this point I sent in my application together with eight other students. Then at the end of December I heard that I was invited for an interview in the first week of January 2014. In this interview it was concluded that I met all the requirements and that I was the perfect candidate to follow Warren up as the next student at JPL with financial backing of Dutch Space (now Airbus Defence and Space, the Netherlands). Financial backing was also going to be provided by the Stichting Prof.dr.ir. H.J. van der Maas Fonds (Aerospace Engineering Faculty, TU Delft) and the Stichting Universiteitsfonds Delft (TU Delft). Communication with JPL was thus started and in March 2015 it was clear that I would be working for the Mars Program Formulation Office under the supervision of Roby Wilson (Inner Solar System group, NASA JPL). He told me to focus on subjects that dealt with Mars missions. At that point I was doing my internship at DLR Bremen on Lunar rocket ascent and descent, which lasted till June 2015. When I came back to Delft me and my supervisors Erwin Mooij (rockets, trajectories, entry and descent, TU Delft) and Ron Noomen (mission design and orbit analysis, TU Delft) agreed that it would be best to perform a study on these Mars subjects to prepare for my visit to JPL and to formulate proposal thesis topics. The first week at JPL I presented these initial thesis topics to both people from the Inner Solar System group and the Mars program formulation office. The next few weeks were spent choosing and refining one of these topics. This document is the result of the two-month literature study on that topic to prepare for the thesis project.

S.D. Petrovic
Pasadena, California, February 2016

CONTENTS

NOMENCLATURE

Greek

η	Numerical approximation	-
η	Step multiplication factor	-
τ	Local error tolerance	-
Φ	Increment function	-

Roman

h	(Current) step-size	s
t_0	Initial time	s
$T_{n,k}$	Truncation error	-
$\mathbf{x}_i$	Current data point	-
$\mathbf{x}_{i+1}$	Next data point	-
x_n	n^{th} variable	-
$\mathbf{X}$	State vector	-

ABBREVIATIONS

AB4	Adams-Bashforth 4th order	**MEE**	Modified Equinoctial Elements
AB6	Adams-Bashforth 6th order	**MOLA**	Mars Orbiter Laser Altimeter
ABM4	Adams-Bashforth-Moulton 4th order	**MSR**	Mars Sample Return
ABM12	Adams-Bashforth-Moulton 12th order	**RF**	Frame of Reference
BF	Body-fixed	**RHR**	Right-hand-rule
DLR	German Aerospace Center (Deutsches Zentrum für Luft- und Raumfahrt)	**RKF45**	Runge-Kutta-Fehlberg 4th $\left(5^{th}\right)$ order
DOPRIN87	Dormand-Prince 8th $\left(7^{th}\right)$ order	**RKF56**	Runge-Kutta-Fehlberg 5th $\left(6^{th}\right)$ order
ESA	European Space Agency	**RKF78**	Runge-Kutta-Fehlberg 7th $\left(8^{th}\right)$ order
FPA	Flight-path angle	**RKF**	Runge-Kutta-Fehlberg
GLOM	Gross Lift-Off Mass	**RK4**	Runge-Kutta 4th order
GMT	Greenwich Mean Time	**RKN12**	Runge-Kutta-Nyström 12th order
GRAM	Global Reference Atmospheric Model	**s/c**	Spacecraft
JPL	Jet Propulsion Laboratory	**SC14**	Störmer-Cowell 14th order
MAV	Mars Ascent Vehicle	**SG**	Shampine-Gordon
MCI	Mars-centred inertial	**SSTO**	Single Stage to Orbit
MCMF	Mars-centred Mars-fixed	**TSI**	Taylor Series integration
		Tudat	TU Delft Astrodynamics Toolbox

1

INTRODUCTION

Mars Sample Return (MSR) has been a mission concept that has been proposed many times in the past two decades. Even today, research into this mission is still being done. And although it is not yet an official project proposal, NASAs Jet Propulsion Laboratory (JPL) is currently working on pre-cursor missions to eventually launch an MSR mission. To prepare for this, research is being conducted on different aspects of MSR, such as the Mars Ascent Vehicle (MAV) responsible for transporting the dirt and soil samples into a Martian orbit and the orbiter which will then transport the samples back to Earth. The current orbiter proposed by JPL is a low-thrust orbiter called Mars 2022. Such an MSR mission requires precise and optimum (optimised for lowest Gross Lift-Off Mass (GLOM)) trajectories to be able to bring back as many samples as possible. But how does one determine the optimum MAV trajectory? Especially when it is combined with the optimum trajectory of the low-thrust orbiter.

The proposed research would focus on the combined optimisation of an MAV trajectory and the trajectory of the low-thrust Mars 2022 orbiter. Also, one hypothesis is that great mass saving can be made if the orbiter and MAV would rendezvous within one single orbital revolution after MAV lift-off. Therefore, the question that should be answered is: what is the optimal trajectory solution for the combined trajectory problem of a high-thrust MAV and a low-thrust Mars orbiter performing a single-revolution rendezvous in Mars orbit? More information on the proposed topic is provided in **??**.

A mission such as MSR and the corresponding trajectories can be described in many different reference frames, or RF, and the motion of the MAV and the orbiter can be modelled in different ways. Therefore it is important to use the proper equations and environmental models. Also, the trajectory has to be determined or rather a prediction will have to be made. This can be done using integration methods. And finally, the optimum will have to be found using an optimisation method. All these different aspects are addressed in this literature study.

First however, it is important to determine the knowledge that already exists and the research that has already been performed. Therefore, **??** will describe previous sample return missions, low-thrust Spacecraft (s/c) missions, single-revolution rendezvous missions and the research performed in those fields. It will also describe the current MAV designs. Then before mathematically representing the problem it is important to understand in what kind of RF it has to be described. This will be done in **??**, followed by the MAV ascent and low-thrust Mars 2022 orbiter model descriptions in **????** respectively. Here, both chapters explain the assumptions and corresponding equations for each phase. One important aspect of the MAV ascent, which sets it apart from other sample return missions, is that Mars has an atmosphere which cannot be neglected. Accordingly **??** describes the different atmospheric models and the trade-off that was performed to decide which model to use in this thesis problem. Then the integration and optimisation are discussed in **????** respectively. In the integrators chapter, different integration methods are described and a selection is made of the integration methods that will be used. The same is done for the different optimisers. All of this information will be used to define the final thesis topic, which is presented in **??**. For some of the aspects that will be treated in the final thesis problem, certain software is already available. A summary of this software is provided in **??**. Finally, a proposed schedule is presented in **??**, which shows the work which will have to be performed during the thesis work and the time that will have to be spend on each aspect of it. This literature study will serve as a guideline during the thesis project and provide background information for the final thesis report.

2

PROBLEM BACKGROUND

The majority of this research was performed at NASA's JPL in Pasadena, California. For that reason it was decided that the research of this thesis should focus on something related to either current research being done at JPL or missions being flown by JPL[1]. One of the focuses of JPL these days is Mars and the exploration of the Martian system. There are currently two planned missions to Mars: InSight and Mars 2020. InSight is a mission similar to the Viking and the Phoenix missions and primarily based on the last one. It is a lander that will perform experiments on the surface of Mars at a fixed location. Mars 2020 is the next Mars rover and is based on the current Curiosity rover. It has a similar design but will carry different scientific instruments and will focus more on finding life on Mars. Mars 2020 is part of a larger JPL effort to eventually return samples from the Martian surface back to Earth. This mission concepts has been on the drawing board for several years now, but seems to be getting closer to approval. This sample return mission, or MSR, will consist of three different systems and is spread out over three different missions as shown by the proposed mission architecture in Figure 2.1. Mars 2020 is the first step of this plan where the rover will collect samples from the surface of Mars. These samples will then be put into containment tubes and dropped on the surface of Mars. A second mission will then carry a system that will collect these samples from the surface and deliver them into a Martian orbit (Shotwell *et al.*, 2016). Then a third mission, currently proposed as the Mars 2022 orbiter, will collect the sample containment sphere in orbit and eventually deliver them back to Earth (Woolley *et al.*, 2011). Because of the potential of the MSR mission concept and the amount of research that can be done, the focus was put on this JPL effort when looking at research subjects.

2.1. CHOSEN MISSION

The Mars 2020 rover is an approved mission that is currently in the design phase, and the Mars 2022 is a proposed mission that will have to be build in order to enhance the current communication capabilities between Mars and Earth. Therefore it is almost certain that these two missions will fly. However, this does not guarantee that the entire MSR endeavour will also be realised. This is because there is no official approval yet for the second system that will actually bring the samples from the surface back to earth. However, this does not mean that no research is being done on the return system. Many designs have been envisioned over the past few years and even now engineers cannot decide on the best design. Shotwell *et al.* (2016) shows two of the proposed designs that are currently being considered. One design involves a mobile launch system based on the Curiosity rover, which will fetch the samples and then directly put them into the spherical container. Once this container is completely filled, the sphere will be placed on top of the MAV, which the rover will be carrying on its back, and launch it into Mars orbit. The second design uses two systems, one fetch rover that will grab the samples and return them to the lander, and the lander containing the MAV. Once the lander returns with all the samples, the sample sphere will be put on top of the MAV and launched into orbit. There are advantages and disadvantages to both of these systems and more research is being done to determine the best option. What both of these systems have in common though is that they have to launch the sample sphere into orbit using a MAV. An ascent on another celestial body with an atmosphere has never been attempted before, which makes it a crucial part of the MSR campaign. This is also why in the last several years, many researchers have looked at the MAV launch trajectory problem.

---

[1]All past, current and proposed JPL missions: http://www.jpl.nasa.gov/missions/ [Accessed 17 November 2016]
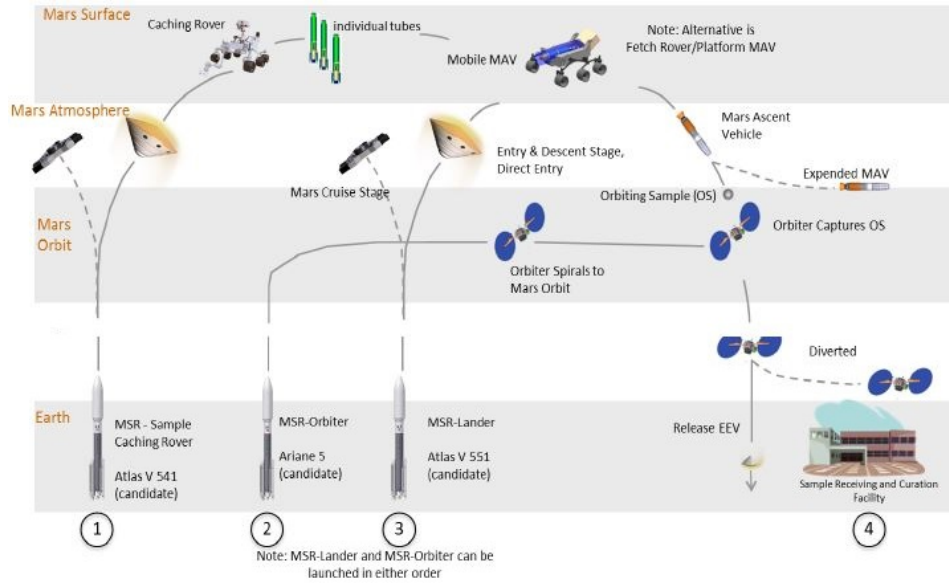
Figure 2.1: Proposed MSR mission architecture (Vaughan *et al.*, 2016).

2.2. PREVIOUS MARS ASCENT RESEARCH

Not only JPL but also many other institutions around the world are working on the Mars ascent problem, for instance the German Aerospace Center (Deutsches Zentrum für Luft- und Raumfahrt) (DLR). A selection of reference research is provided in Table 2.1.

Table 2.1: Previous and current Mars ascent trajectory research.

Author	Organisation	Country
Fanning and Pierson (1996)	Iowa State University	United States
Desai *et al.* (1998)	NASA Langley and JPL	United States
Whitehead (2004, 2005)	Lawrence Livermore National Laboratory	United States
Di Sotto *et al.* (2007)	DEIMOS Engenharia and ESA	Portugal/Europe
Woolley *et al.* (2011)	JPL	United States
Trinidad *et al.* (2012)	Northrop Grumman and JPL	United States
Dumont (2015) (Ongoing)	DLR	Germany
Woolley (2015) (Ongoing)	JPL	United States
Benito and Johnson (2016) (Ongoing)	JPL	United States

Most of the papers before 2015 focus on an older MAV concept, however the newer JPL research focuses more on a Single Stage to Orbit (SSTO) design. This is why this thesis research will also be focusing on the ascent of a SSTO MAV.

Many of the research that was done used either publicly available simulation software or trajectory simulation software that was developed in-house. There are several ways in which an ascent trajectory can be simulated, and these different methods of how to simulate such a launch can results in different outcomes. Therefore, a closer look was taken at the method of ascent trajectory propagation and simulation.

2.3. RESEARCH FOCUS

In order to compute an ascent trajectory, the initial state is taken and provided perturbations the state is propagated until a final condition is met. In most of the research mentioned in Table 2.1 this was done using numerical integration methods. However, often it is not mentioned which specific methods were used. When looking at integration methods, there are a number of methods that are widely used for space related problems, such as the standard integration methods (more information on these standard integration methods can be found in Chapter 4). In recent years however, another method, that has not generally been applied

in space problems, has seen potential to increase performance resulting in faster and more accurate results. This method is called Taylor Series integration (TSI) and was first used in a space trajectory problem by Montenbruck (1992a). A few years later, a comparison between a higher order Runge-Kutta method and TSI was performed on orbital trajectory problems by Scott and Martini (2008) showing that the application of TSI to such problems can be very beneficial. Bergsma and Mooij (2016) showed that TSI shows similar improvements compared to Runge-Kutta-Fehlberg for re-entry cases, where TSI was both faster and more accurate. However, TSI has not yet been applied to ascent cases, leaving a very important knowledge gap that has to be filled.. This is why the Mars ascent trajectory propagation is a good additional test case to add to the knowledge of TSI performance in space related problems. The TSI will have to be compared to a standard integration method to determine its performance.

From the two previous cases (orbital trajectories and re-entry) it is expected that TSI will be faster and more accurate than the standard integration methods. In this thesis, it will be tested whether or not this also holds for ascent cases. However, before this can be tested, an accurate representation of an ascent scenario has to be modelled.

2.4. MAV DESIGN

An important aspect of running an accurate simulation is making sure that the assumed vehicle is representative of the actual vehicle that will be used. Therefore, the most up to date representation of the MAV is required. Over the past 20 years there have been many different iterations of the MAV. Some of the earliest concepts were described by Desai *et al.* (1998); Whitehead (1997); Guernsey (1998); Stone (1999) and were prominently focussed on two-stage liquid rockets (also see Table 2.2. After a change in mission requirements in the early 2000's the leading baseline design changed to a two-stage solid (Whitehead, 2005; Stephenson, 2002; Stephenson and Willenberg, 2006). However, the requirements kept changing and the design kept getting better defined by (among others) Trinidad *et al.* (2012); Sengupta *et al.* (2012); Mungas *et al.* (2012); Mars Program Planning Group (2012) resulting in a two-stage liquid as the updated baseline. The past 4 years however have seen a slight change in the design. Most of the MAV work is now being carried out in-house at JPL. Research is still being performed on the two-stage solids, but SSTO designs are showing that they have an overall better performance. Recently presented designs include a SSTO liquid (Vaughan *et al.*, 2016) and a SSTO hybrid as presented by (Karp *et al.*, 2016). These two papers however focused more on the propulsion systems. Because the mission requirements kept changing leading to many different MAV designs, it can become difficult to keep track of all the differences. Shotwell (2016) provides a good overview of the different designs leading up to the current baseline designs.

Currently there is no clear baseline design, however, the preference leads towards the SSTO designs. Two of those designs are shown in Figure 2.2.
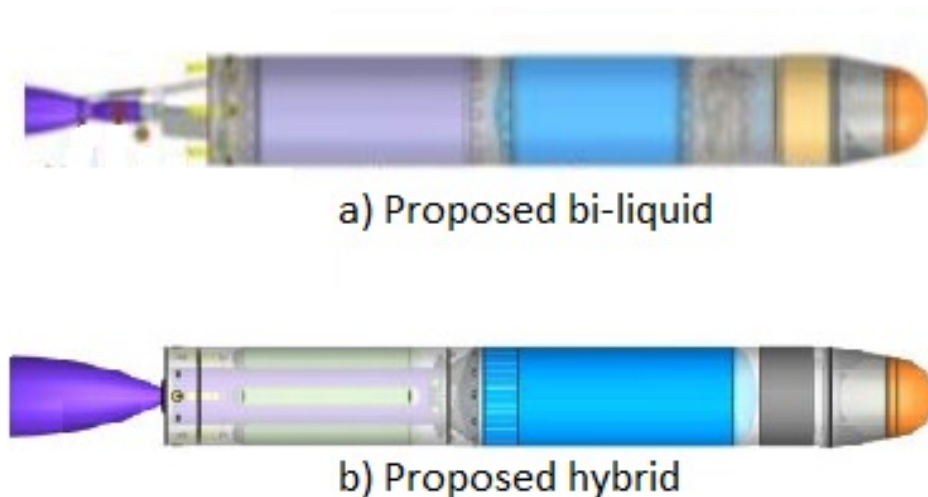

Figure 2.2: Current proposed designs. a) is one of the bi-liquid designs proposed by Vaughan *et al.* (2016). b) is the hybrid design proposed by Karp *et al.* (2016). Not to scale.

Table 2.2: Previous MAV studies.

Author	Rocket	Propellant(s)
Whitehead (1997)	two-stage rockets (comparison study)	solid and liquid (and gel recommended as well)
Guernsey (1998)	two-stage rocket	2x liquid
Desai *et al.* (1998)	two-stage rocket	2x liquid
Stone (1999)	two-stage rocket	hybrid
Stephenson (2002)	two-stage rocket (three different designs)	2x solid (best), solid and liquid or hybrid and 2x gel (best)
Whitehead (2005)	one-, two- and three-stage rockets (variational study)	solid and liquid
Stephenson and Willenberg (2006)	two-stage rocket	2x solid
Sengupta *et al.* (2012)	two-stage rocket	2x liquid
Trinidad *et al.* (2012)	1 to 4 stages (comparison study) two-stage rocket (best)	solid, liquid, hybrid and gel (comparison) 2x liquid (best)
Mungas *et al.* (2012)	single-stage rocket	liquid mono-propellant
Mars Program Planning Group (2012)	undefined rocket	solid and liquid
Vaughan *et al.* (2016)	single-stage rocket	liquid
Karp *et al.* (2016)	single-stage rocket	hybrid

Unfortunately, not much has been published on the specific flight characteristics such as drag coefficient and reference area of these new designs. Fortunately, the size requirements of the MAV have not changed (much) between the 2012 studies and the current designs. Therefore these parameters can be approximated by looking at some of the previous baseline designs such as the two-stage liquid rocket shown in Figure 2.3.
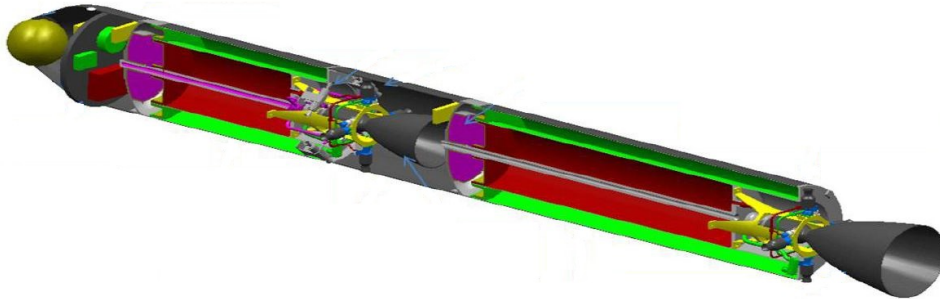
Figure 2.3: Old baseline design (**?**).

This concept had a diameter of approximately 340 mm. This results in a cross sectional area of approximately 0.09079 m^2. Unfortunately, the paper did not mention anything about the drag coefficient. However, **?** provided a general drag coefficient graph as a function of the Mach number for a generalized shape very similar to most MAV concepts. Therefore, this simplified relation, shown in Figure 2.4 is used in this thesis research as well.

These two parameters are used to determine the drag acting on the MAV during the ascent. This drag acts on the MAV in what is called the body frame. One of the problems with trajectories is that different perturbations act differently on the vehicle and are easier to express in different reference frames and systems. In the end however, the state will have to be expressed in one reference frame and system, which means that the drag might have to be transformed to another frame. More information on these different frames is provided in the Section 2.5.
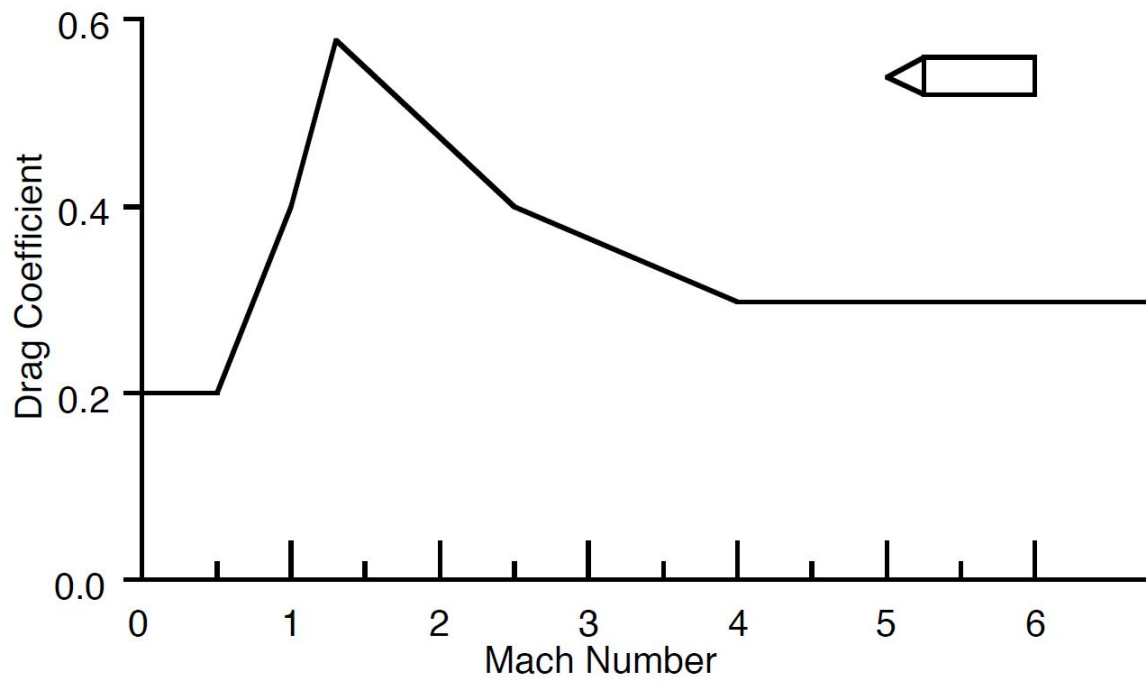
Figure 2.4: Drag coefficient as a function of Mach number Whitehead (2004)

2.5. REFERENCE SYSTEMS

Add a section on reference systems (maybe including appendix on the transformations etc.)
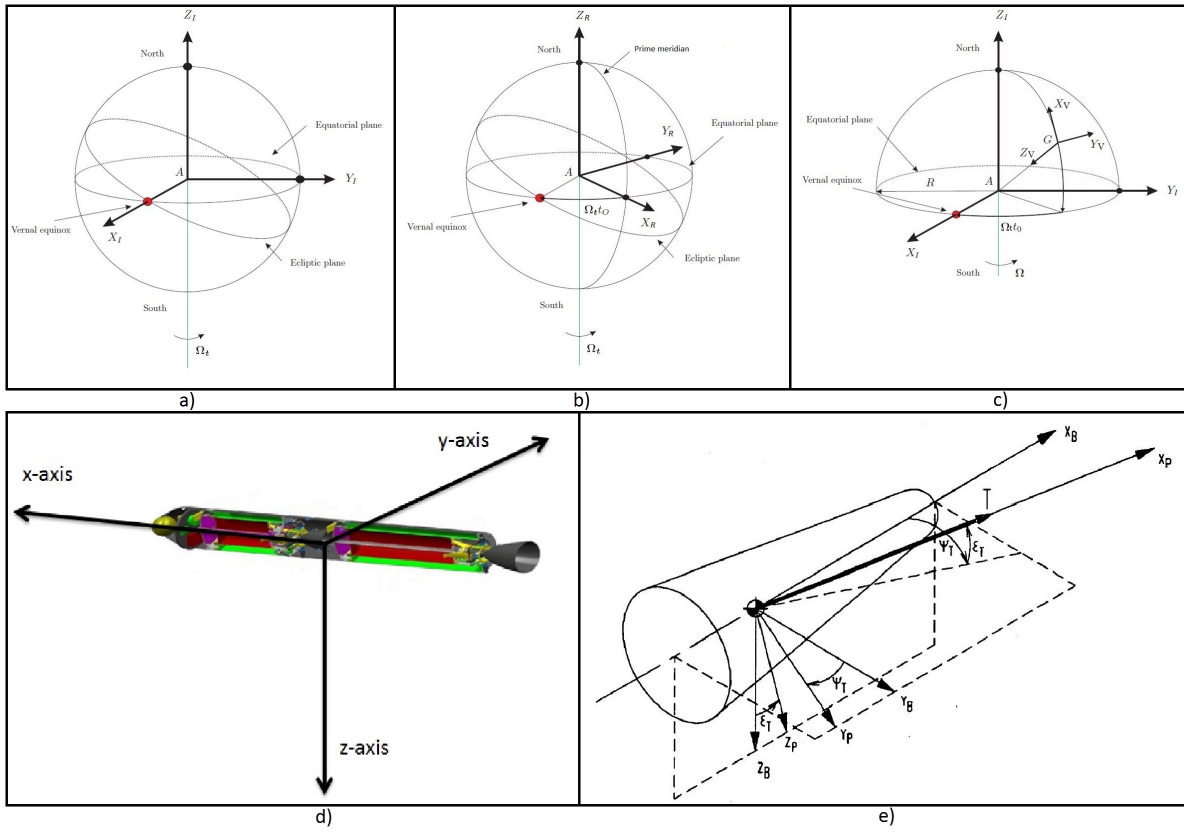
Figure 2.5: a) (Mars centred) Inertial frame, b) (Mars centred) Rotational frame, c) (Vehicle centred) Vertical frame (**?**). d) (Vehicle centred) Body frame (Trinidad *et al.*, 2012). e) (Vehicle centred) Propulsion frame (Mooij, 1994).

3

MODELS

The MAV and the corresponding ascent can be modelled in many different ways. Depending on the desired accuracy of the final solution compared to the real-life expected trajectory, different perturbations and freedom in motion can be defined and included, ranging from a low fidelity to a high fidelity program. The main goal of this thesis is to determine if TSI is an integrator that can be used for ascent cases and determine its performance compared to previously established methods. Therefore, it should be close to a real-life ascent, but not include too many aspects as to make the problem too complex to test. Therefore, it was decided to design a low fidelity program to propagate the trajectory using accelerations in the x-, y- and z-direction (3DOF). The MAV system can then be modelled as a point-mass system with different accelerations acting on it. The change in position can be described by the kinematic equations and the change in velocity by the corresponding dynamic equations. The change in mass is then described by the mass-flow. All these equations are provided in Section 3.1. For this model, three perturbing accelerations will be taken into account: the gravity, the thrust and the drag. The effect of third bodies can be neglected because of the short mission time. All the accelerations are described in Sections 3.2 to 3.4 respectively.

3.1. STATE AND STATE DERIVATIVES

Maybe include more assumptions and corresponding explanations!! The general model is described in terms of the Cartesian state; position and velocity in the x-, y-, and z-direction and the mass. The notation is shown in Equation (3.1), where m_{MAV} is the mass of the MAV and the subscript I refers to the inertial frame.

$$\mathbf{r} = \begin{pmatrix} x_I \\ y_I \\ z_I \end{pmatrix} \qquad \mathbf{V} = \begin{pmatrix} V_{x_I} \\ V_{y_I} \\ V_{z_I} \end{pmatrix} \qquad m_{MAV} \tag{3.1}$$

In order to determine the next state, the change in the state parameters over time have to be computed. This is done by taking the time derivatives of the state as described by Equation (3.2).

$$\begin{aligned} \dot{x}_I &= V_{x_I} \\ \dot{y}_I &= V_{y_I} \\ \dot{z}_I &= V_{z_I} \end{aligned} \qquad \begin{aligned} \ddot{x}_I &= \dot{V}_{x_I} = a_{x_I} \\ \ddot{y}_I &= \dot{V}_{y_I} = a_{y_I} \\ \ddot{z}_I &= \dot{V}_{z_I} = a_{z_I} \end{aligned} \qquad \dot{m}_{MAV} = -\frac{T}{g_0 I_{sp}} \tag{3.2}$$

From this point on, the subscript I is omitted, because the state and the state derivatives are always presented in the inertial frame. If variables have to be presented in any other reference frame the corresponding subscripts will be provided and explained. The accelerations in the x-, y- and z-direction have three contributing components: gravitational acceleration, drag acceleration and thrust acceleration. In this model it is assumed that there is a homogeneous gravitational field acting on the point mass with a direction towards the centre of the inertial frame. The gravitational acceleration can therefore be directly expressed in the inertial frame.

The drag is assumed to work in the opposite direction of the MAV velocity vector, which in turn is assumed

to be in the positive x-direction of the body frame associated with the MAV. This way the MAV velocity, or ground velocity, is acting through the nose of the ascent vehicle. The drag acceleration is therefore expressed in the body frame. This effect in the body frame has to be translated into an acceleration in the inertial frame. This can be done using transformation matrices. A traditional transformation matrix uses an Euler angle to rotate a coordinate frame in a certain reference frame to another. Using the proper Euler, or rotation, angles, the acceleration in the x-, y- and z-direction in the body frame can be transformed into acceleration components acting in the x-, y- and z-direction of the inertial frame. Once it is expressed in the inertial frame it can be added to the effect caused by the gravitational acceleration.

It is also assumed that the nozzle of the MAV engine can be pivoted in two different directions: the y-, and z-direction of the body frame. This means that the thrust acceleration is not acting directly in the body frame, but in what is called the propulsion frame. Because the nozzle can move in two directions, or rather pivot over two different angles, the thrust acceleration can be translated to the body frame using these two thrust angles. Once the thrust acceleration is expressed in the body frame, the same transformations that are used for the drag can be used to determine the thrust acceleration components in the inertial frame.

Combining this in one equation then results in the expression for the acceleration vector as shown by Equation (3.3). The subscript G shows that the parameter is a function of the ground velocity. $\mathbb{T}$ stands for a transformation and the subscript determines the rotation axis. The parameter in the brackets for each transformation is the rotation angle.

$$
\begin{pmatrix} a_x \\ a_y \\ a_z \end{pmatrix} = \begin{pmatrix} a_{x,Grav} \\ a_{y,Grav} \\ a_{z,Grav} \end{pmatrix} + \Bigg|_{\mathbf{I}} \mathbb{T}_{\mathbf{z}}\left(-\Omega_M t_O + \omega_P\right) \Bigg|_{\mathbf{R}} \mathbb{T}_{\mathbf{z}}\left(-\tau\right) \mathbb{T}_{\mathbf{y}}\left(\frac{\pi}{2}+\delta\right) \Bigg|_{\mathbf{V}} \mathbb{T}_{\mathbf{z}}\left(-\chi_G\right) \mathbb{T}_{\mathbf{y}}\left(-\gamma_G\right) \Bigg|_{\mathbf{B}} \Bigg[\begin{pmatrix} a_{Drag} \\ 0 \\ 0 \end{pmatrix} + \dots
$$

$$
\dots \Bigg|_{\mathbf{B}} \mathbb{T}_{\mathbf{z}}\left(-\psi_T\right) \mathbb{T}_{\mathbf{y}}\left(-\epsilon_T\right) \Bigg|_{\mathbf{P}} \begin{pmatrix} a_{Thrust} \\ 0 \\ 0 \end{pmatrix} \Bigg] \tag{3.3}
$$

The rotations required to go from the body frame to the inertial frame are all a function of the current state. Both thrust angles are an input value that is set by the user or the program. $-\Omega_M t_O + \omega_P$ represents the angle between the rotating frame and the inertial frame and consists of three parts. Ω_M is the rotational velocity of Mars around it's own axis, t_O is the difference between the current time and the time at which the inertial frame was set on Mars, and ω_P is the angle between the x-axis of the inertial frame and the zero meridian at the time that the inertial frame was set on Mars. In this thesis the inertial frame is set at the beginning of the simulation (so at $t = 0$, $t_O = 0$) and is aligned with the rotating frame (so $\omega_P = 0$). The transformation from the vertical to the rotating frame requires the latitude and longitude of the MAV, which is a function of the current state. Mooij (1994) provides equations to determine the different rotation angles. These expressions can be used to compute the latitude and longitude as well as shown by Equation (3.4).

$$
r = \sqrt{x^2 + y^2 + z^2}
$$
$$
\delta = \arcsin\left(\frac{z}{r}\right)
$$

$$
x_R = \cos\left(\Omega_M t_O\right) x + \sin\left(\Omega_M t_O\right) y
$$
$$
y_R = -\sin\left(\Omega_M t_O\right) x + \cos\left(\Omega_M t_O\right) y
$$
$$
\tau = \text{atan2}\left(\frac{y_R}{x_R}\right)
$$

$$\tag{3.4}$$

It can be seen that in order to compute the longitude in the rotating frame (τ) the position of the MAV in the rotating frame was required. This position was found by transforming the inertial position to the rotational position using $\Omega_M t_O$ as described before. Working out that transformation matrix results in the sines and cosines presented in Equation (3.4).

Similarly, the flight-path angle and the azimuth angle can be described as a function of the current state. For this, some intermediate parameters have to be computed first and are given by Equation (3.5).

$$V_I = \sqrt{V_x^2 + V_y^2 + V_z^2}$$

$$V_G = \sqrt{V_I^2 + \Omega_M^2\left(x^2 + y^2\right) + 2\Omega_M\left(xy - yx\right)}$$

$$V_{x,V} = \left(V_x + \Omega_M y\right) \cdot \left(\sin\left(\delta\right)\sin\left(\Omega_M t_O\right)\sin\left(\tau\right) - \cos\left(\Omega_M t_O\right)\cos\left(\tau\right)\sin\left(\delta\right)\right) +$$
$$\left(V_y - \Omega_M x\right) \cdot \left(-\cos\left(\tau\right)\sin\left(\delta\right)\sin\left(\Omega_M t_O\right) - \cos\left(\Omega_M t_O\right)\sin\left(\delta\right)\sin\left(\tau\right)\right) + V_z\cos\left(\delta\right)$$

$$V_{y,V} = \left(V_x + \Omega_M y\right) \cdot \left(-\cos\left(\tau\right)\sin\left(\Omega_M t_O\right) - \cos\left(\Omega_M t_O\right)\sin\left(\tau\right)\right) +$$
$$\left(V_y - \Omega_M x\right) \cdot \left(\cos\left(\Omega_M t_O\right)\cos\left(\tau\right) - \sin\left(\Omega_M t_O\right)\sin\left(\tau\right)\right)$$

$$V_{z,V} = \left(V_x + \Omega_M y\right) \cdot \left(\cos\left(\delta\right)\sin\left(\Omega_M t_O\right)\sin\left(\tau\right) - \cos\left(\Omega_M t_O\right)\cos\left(\tau\right)\cos\left(\delta\right)\right) +$$
$$\left(V_y - \Omega_M x\right) \cdot \left(-\cos\left(\tau\right)\cos\left(\delta\right)\sin\left(\Omega_M t_O\right) - \cos\left(\Omega_M t_O\right)\cos\left(\delta\right)\sin\left(\tau\right)\right) - V_z\sin\left(\delta\right)$$

(3.5)

Then the angles can be computed using those parameters as shown by Equation (3.6).

$$\chi_G = \text{atan2}\left(\frac{V_{y,V}}{V_{x,V}}\right)$$

$$\gamma_G = -\arcsin\left(\frac{V_{z,V}}{V_G}\right)$$

(3.6)

In this case, a transformation from the inertial frame to the vertical frame was required to get information on the velocity in the vertical frame. This transformation is written out at sines and cosines in Equation (3.5) resulting in lengthy expressions.

Now that the rotation angles from the body frame to the inertial frame are known, only the thrust angles and the different accelerations have yet to be defined. This is done in the next sections.

3.2. GRAVITY

The gravity acceleration is a function of the position of the MAV and the standard gravitational parameter of the planet, in this case Mars. Often, irregularities in the mass distribution of a planet also have to be taken into account ($J_{2,0}$ etc.), however, because the mission time is very short and the MAV does not even complete one revolution around Mars, these effects can be neglected. Therefore, the gravitational acceleration in the inertial frame can be represented by Equation (3.7).

$$\begin{pmatrix} a_{x,Grav} \\ a_{y,Grav} \\ a_{z,Grav} \end{pmatrix} = \begin{pmatrix} -\mu_M \dfrac{x}{r^3} \\ -\mu_M \dfrac{y}{r^3} \\ -\mu_M \dfrac{z}{r^3} \end{pmatrix}$$

(3.7)

3.3. THRUST

The thrust acceleration in the propulsion frame is simply the thrust divided by the current mass of the MAV, which can be written as shown by Equation (3.8).

$$a_{Thrust} = \frac{T}{m_{MAV}}$$

(3.8)

However, this acceleration has to be transformed to the body frame using the thrust angles. These thrust angles are the thrust elevation (ϵ_T) and thrust azimuth (ψ_T) angle, and are defined in Figure A.5.

These angles will not be computed, but are set as an input for the program.

3.4. DRAG

The drag acceleration can be represented similarly to the thrust acceleration taking into account that the drag is acting in the negative x-direction in the body frame. The acceleration can then be written as Equation (3.9).

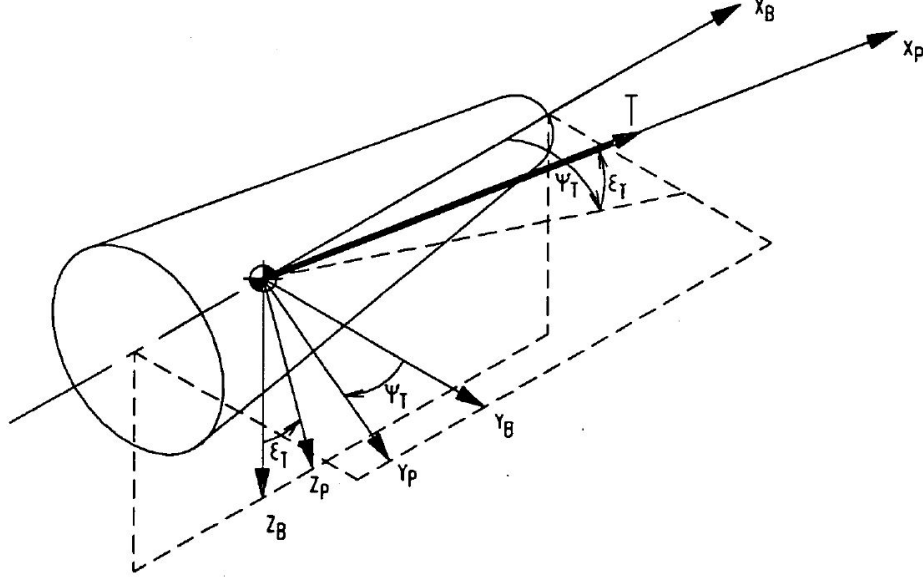$$a_{drag} = -\frac{D}{m_{MAV}}$$

(3.9)

Figure 3.1: Definition of the thrust elevation and thrust azimuth angle with respect to the body frame (Mooij, 1994).

Here the drag is given by Equation (3.10).

$$D = \frac{1}{2}\rho V_G^2 S C_D \qquad (3.10)$$

Where S is the reference area of the MAV set by the user, ρ is the air density which is a function of the altitude $h\,(= r - R_{MOLA})$ and C_D is the drag coefficient of the MAV which is a function of the Mach number. The Mach number in turn is a function of the speed of sound, which depends on the air temperature as can be seen in Equation (3.11).

$$M = \frac{V_G}{a}$$
$$a = \sqrt{\gamma_a R_a^* T_a} \quad \text{where} \quad R_a^* = \frac{R_a}{M_a} \qquad (3.11)$$

Here, R_a is the molar gas constant, γ_a is the adiabatic index for Mars, which according to Ho *et al.* (2002) can be set as ~1.35. M_a is the molecular mass of the Martian atmosphere and depends on it's composition. Williams (2015) mentions a volumetric composition of Mars which results in a mean molecular mass of 0.04334 kg/mol. This value has been used in this research to compute the speed of sound.

The air pressure and temperature (T_a) change as a function of the altitude of the MAV. This means that a pressure and temperature model of the atmosphere of Mars will have to be used to approximate these values as the ascent vehicle moves through the atmosphere. This is done through a function fit of an atmospheric model, as is described in Section 3.4.1.

The drag coefficient changes with the Mach number, however, this change is not constant over the entire Mach range. Therefore, this also requires a function fit in order to be used in the simulation program. This fit is presented in Section 3.4.2.

3.4.1. ATMOSPHERIC GRAPH FUNCTION FIT

Using Mars-GRAM 2005, a table containing altitude, latitude and longitude dependent temperature and density data was produced. The altitude range was -0.6 to 320 km Mars Orbiter Laser Altimeter (MOLA) with a step-size of 0.01 km, the latitude and longitude ranges were centred around the launch site (21.0 °N and 74.5 °E) with a 10 degree range in each direction and a step-size of 1 degree. The rest of the input parameters were

constant and can be seen in Appendix B. The temperature and density data produced is shown in Figures 3.2 and 3.3 respectively for 9 latitude and longitude combinations including the launch site itself.
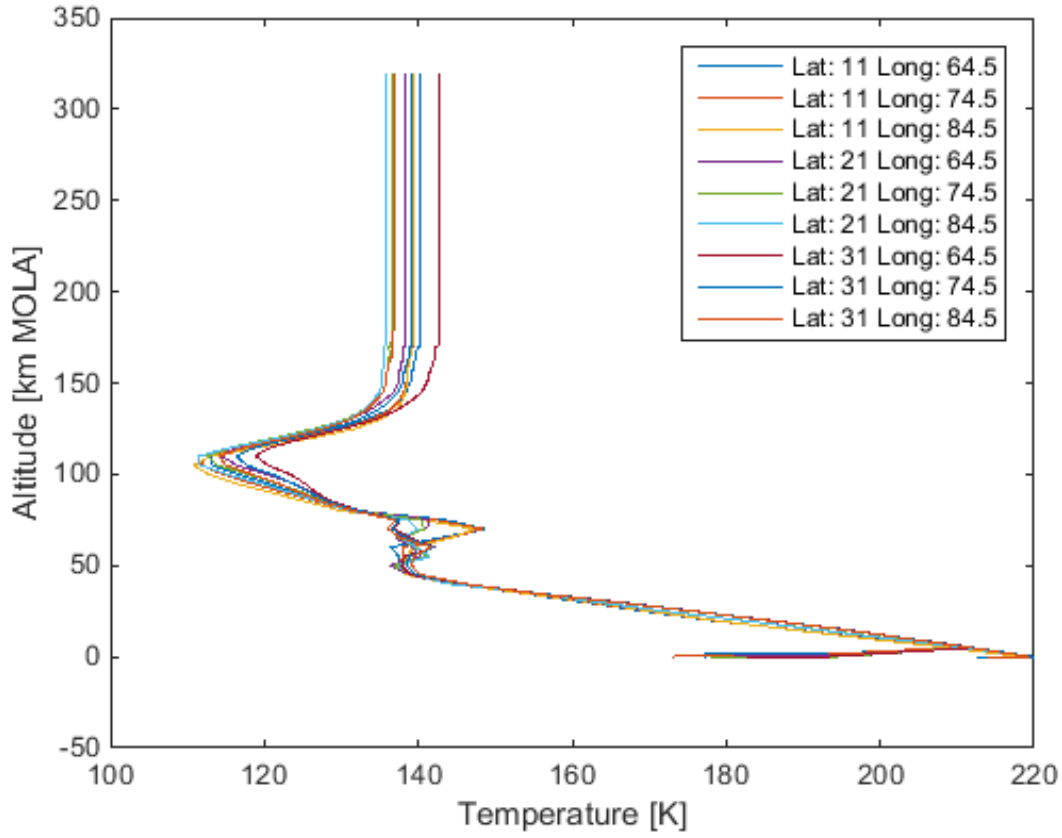

Figure 3.2: Temperature data generated with Mars-GRAM 2005 showing 9 different latitude and longitude combinations

Unfortunately discontinuous data tables cannot be used when integrating using TSI, which is why both these data tables had to be fitted with continuous functions. The temperature data could not be smoothly fit with one continuous function. Therefore, depending on the altitude range, a different approximation function is required. The condition to be met for a proper fit came from the differences in the temperature-altitude and density-altitude curves, where the maximum difference with respect to the launch site curve was taken. The requirement for the standard deviation of the polynomial curve fit was then to be (at least) one order lower than this maximum difference and that the maximum difference between the fit and the launch site curve was lower than the maximum difference. The temperature-altitude curve was split into 5 sections as roughly visualised in Figure 3.4. The number of sections come from both the shape of the curves and the requirement for accuracy and maximum order of the polynomial, which is set at 8 because otherwise the polynomial would get too long. Also, the number of sections were to be kept at a minimum. More information on the fitting process and early results is provided in Appendix C.

Each section was fit with a polynomial function of the nth order where the function is represented by Equation (3.12). The last section shows a constant temperature, thus the temperature of the launch site curve was chosen to represent this final section, which is equal to 136.5 K.

$$y = p_n x^n + p_{n-1} x^{n-1} + \cdots + p_1 x + p_0 \tag{3.12}$$

A lower order is preferred, because then the fitted function will be simpler to evaluate and contain fewer terms. However the order has to be high enough to meet the accuracy requirements. Table 3.1 shows the orders that were required and the deviations to the launch site temperature-altitude curve. The actual corresponding parameters are provided in Table 3.2. It should be noted that the first few temperature data values were so different from the rest of the curve that it was assumed that this is a lack of the Mars-GRAM program
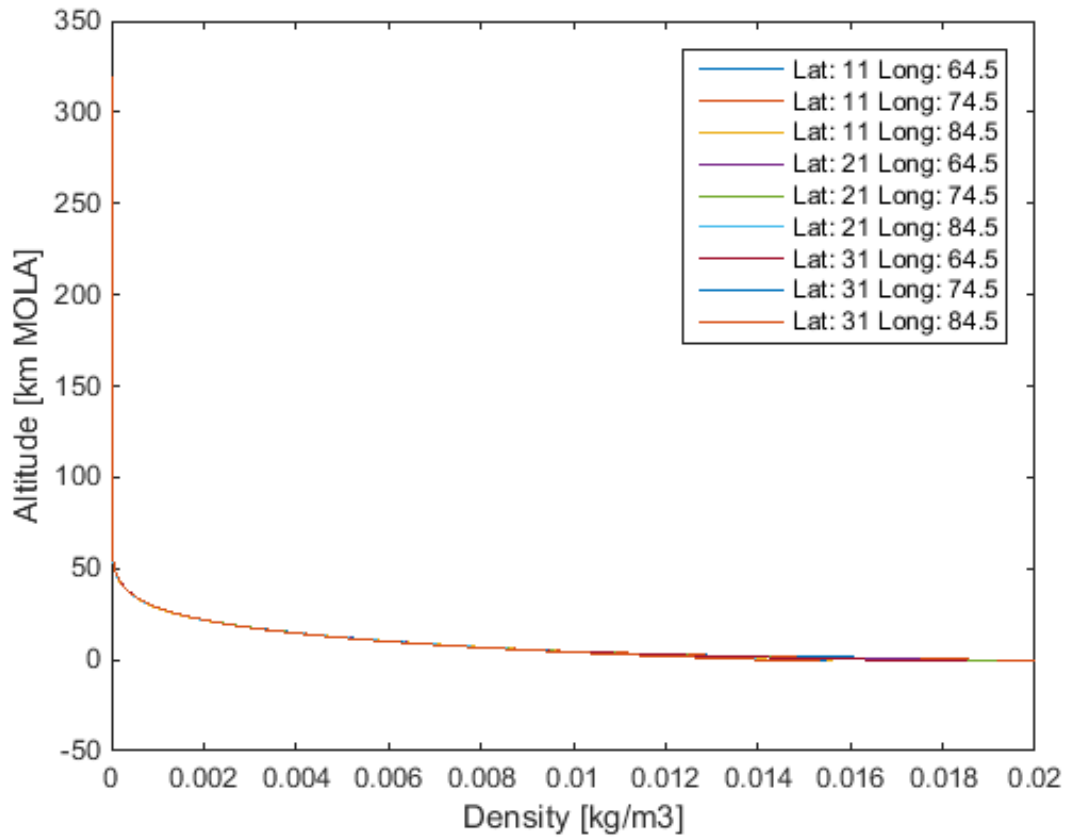
Figure 3.3: Density data generated with Mars-GRAM 2005 showing 9 different latitude and longitude combinations

and were thus treated as outliers.

Table 3.1: Temperature curve fit data all with respect to the launch site curve (Latitude and longitude of the launch site)

Section	Altitude range [km MOLA]	Order	Maximum polynomial standard deviation [K]	Maximum polynomial difference [K]	Maximum data curves difference [K]
1	-0.6 to 5.04	1	0.0312	25.8	0.177
2	5.04 to 35.53	2	0.287	3.90	0.7056
3	35.53 to 75.07	6	0.624	8.00	1.69
4	75.07 to 170.05	8	0.523	6.60	2.45

Table 3.2: Temperature curve fit parameters (rounded to 3 decimal points)

Section	p_8	p_7	p_6	p_5	p_4	p_3	p_2	p_1	p_0
1								3.415	194.165
2							0.006	-2.130	222.052
3			$-5.388 \cdot 10^{-7}$	$1.785 \cdot 10^{-4}$	-0.0243	1.733	-68.294	$1.407 \cdot 10^3$	$-1.167 \cdot 10^4$
4	$4.1942 \cdot 10^{-12}$	$-4.328 \cdot 10^{-9}$	$1.931 \cdot 10^{-6}$	$-4.862 \cdot 10^{-4}$	0.076	-7.405	447.378	$-1.523 \cdot 10^4$	$2.236 \cdot 10^5$

The complete polynomial fit for the launch site curve for the temperature is shown in Figure 3.5.
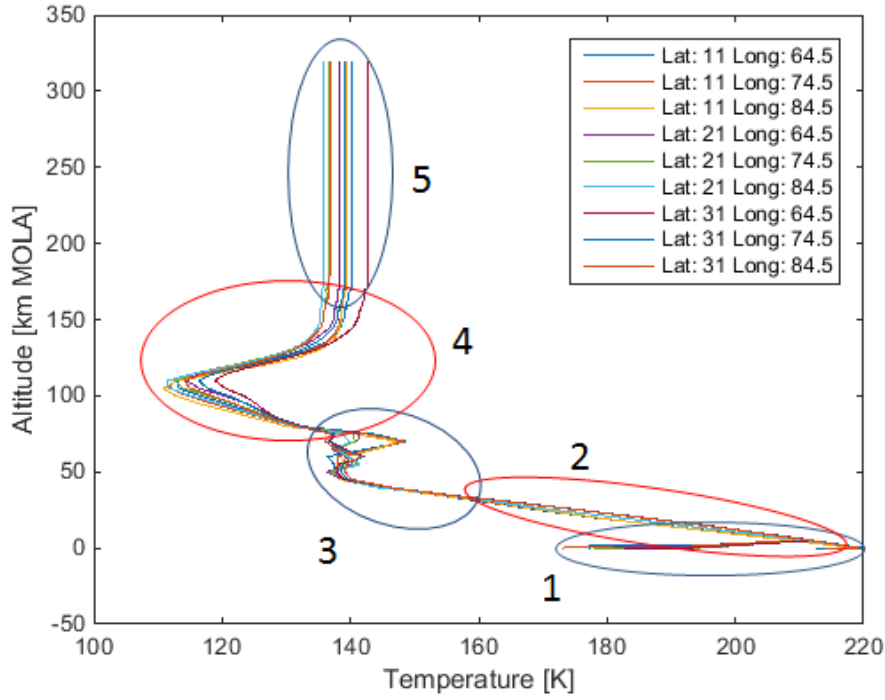
Figure 3.4: Different temperature curve sections

The density fit was slightly more difficult because the curves are all very similar and thus result in a higher accuracy requirement for the fit. At first glance it looks like a natural logarithmic function, unfortunately an ordinary exponential did not fit the curve. This is why a more extensive exponential fit was required. The natural logarithm of the data has been plotted in Figure 3.6.

With the data represented in the logarithmic domain, again a polynomial function can be fit. The total fit would then satisfy Equation (3.13).

$$y = exp\left(p_n x^n + p_{n-1} x^{n-1} + \cdots + p_1 x + p_0\right) \tag{3.13}$$

The same polynomial requirements as for the temperature curve were enforced for the density curve as well. However, because the polynomial is used in an exponential, some extra requirements are needed to assure the accuracy of the fit. One requirement is that the maximum difference between the final exponential fit and the normal launch site density curve is smaller than the maximum difference between all the data curves. Also, in this case the standard deviation of the difference between the exponential fit and the normal launch site curve had to be within the range of standard deviations of the difference between the different data curves. This meant that even though an 8th order polynomial fit could be achieved for the natural logarithmic data with the required accuracy, when converted to the exponential fit, the last two requirements were not met. Before it was mentioned that an order higher than 8 was not desirable. However, in this case, a single exponential fit could be achieved using a 10th order polynomial. This fit meant that the density curve did not have to be split up at all, which makes the integration slightly easier. Therefore, it was decided that a 10th order polynomial was acceptable in this case. The results of the fit is presented in Tables 3.3 and 3.4 and the polynomial and exponential fit curves are shown in Figures 3.7 and 3.8 respectively.

3.4.2. DRAG COEFFICIENT GRAPH FUNCTION FIT
Similar to the temperature and density curves, the relation between Mach number and drag coefficient, as depicted in Figure 2.4, had to be modelled as a continuous function as well. Again, it could not be fitted using one continuous function, but instead had to be modelled by different functions.
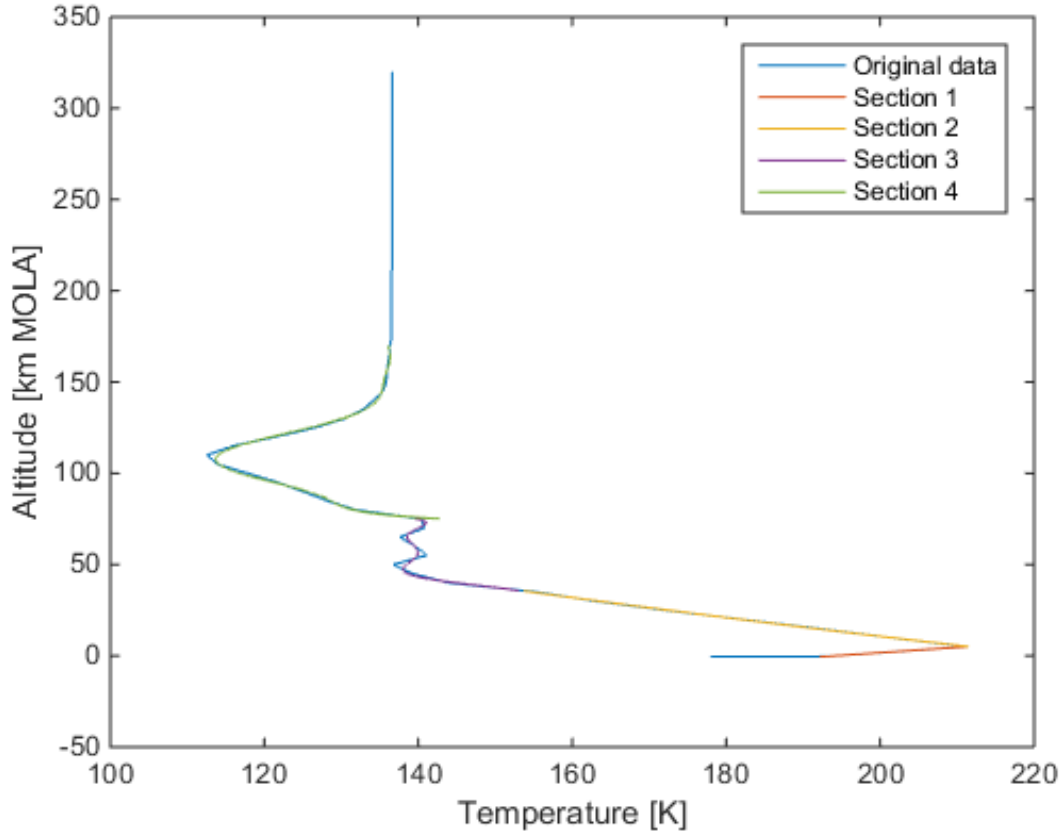
Figure 3.5: All section fits for the launch site temperature data curve

Table 3.3: Density curve fit data (10th order polynomial) with respect to the launch site curve (Latitude and longitude of the launch site)

Maximum polynomial standard deviation [kg/m^3]	0.0501
Maximum polynomial difference [kg/m^3]	0.160
Maximum natural logarithmic data curves difference [kg/m^3]	0.460
Maximum exponential difference with launch site curve [kg/m^3]	$2.826 \cdot 10^{-3}$
Maximum data curves difference [kg/m^3]	$3.910 \cdot 10^{-3}$
Standard deviation exponential fit difference [kg/m^3]	$1.167 \cdot 10^{-4}$
Maximum standard deviation data curves difference [kg/m^3]	$2.106 \cdot 10^{-4}$

Table 3.4: Density curve fit parameters (rounded to 3 decimal points)

p_{10}	p_9	p_8	p_7	p_6	p_5	p_4	p_3	p_2	p_1	p_0
2.287 $\cdot 10^{-21}$	-3.724 $\cdot 10^{-18}$	2.559 $\cdot 10^{-15}$	-9.620 $\cdot 10^{-13}$	2.146 $\cdot 10^{-10}$	-2.884 $\cdot 10^{-8}$	2.273 $\cdot 10^{-6}$	-9.604 $\cdot 10^{-5}$	1.414 $\cdot 10^{-3}$	-0.0962	-4.172

Fortunately, this curve is already an approximation and thus consists of linear elements only. It can be split up into 6 different sections where the first and last section are constant (C_D is 0.2 and 0.3 respectively). Using a similar polynomial fit as before, but now for 1 order only, a linear fit could be made for each of the remaining 4 sections. The corresponding parameters are shown in Table 3.5 and the curve fit is shown in Figure 3.9.
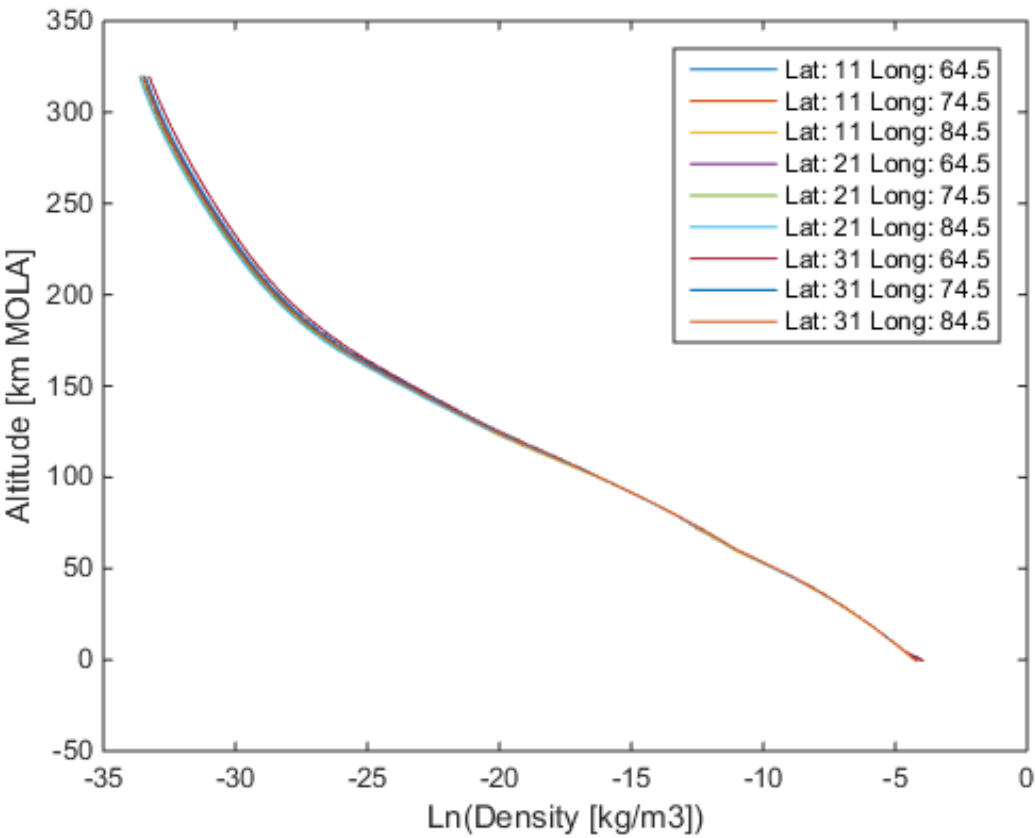
Figure 3.6: Natural logarithmic plot of the density data

Table 3.5: Drag coefficient curve fit parameters (rounded to 3 decimal points)

Section	Mach range	p_1	p_0
2	0.5 to 1	0.400	$-2.483 \cdot 10^{-16}$
3	1 to 1.3	0.567	-0.167
4	1.3 to 2.5	-0.142	0.754
5	2.5 to 4	-0.0667	0.567

3.5. CIRCULARISATION
This section still has to be added!!
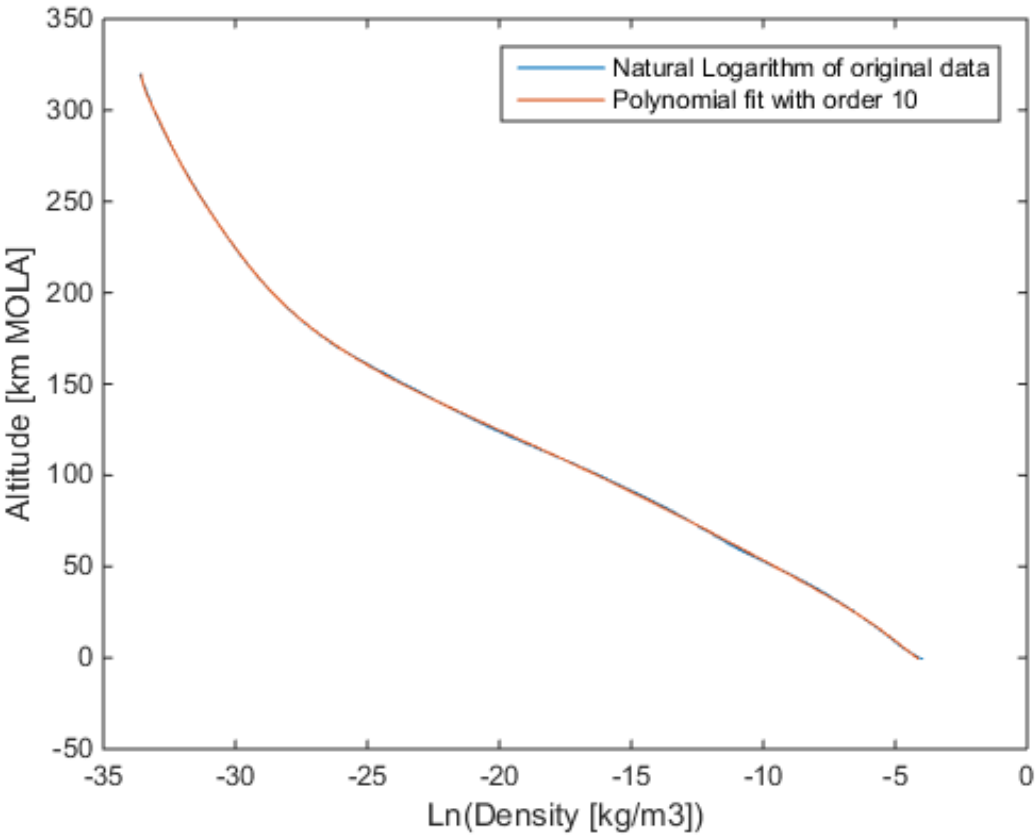
Figure 3.7: Polynomial fit for the launch site density data curve
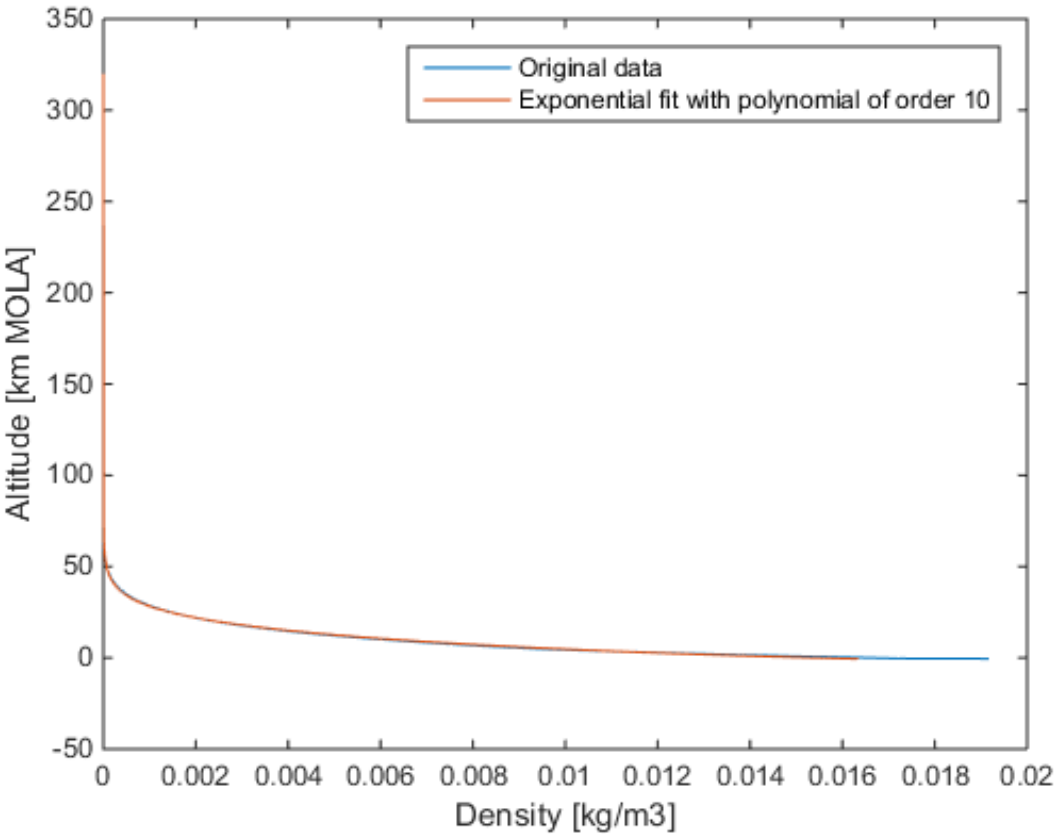
Figure 3.8: Exponential fit for the launch site density data curve
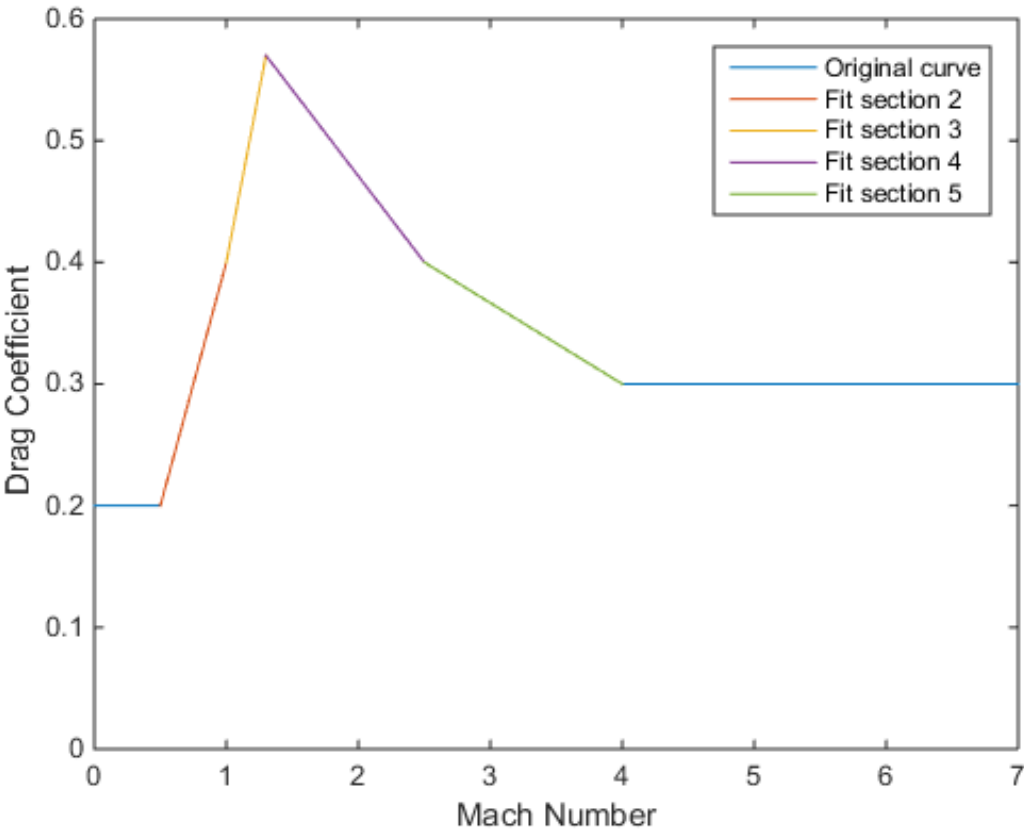
Figure 3.9: All section fits for the drag coefficient - Mach curve

4

STANDARD INTEGRATION METHODS

Propagation refers to the process of modelling/predicting the manner in which an object (for instance) will progress (in time) from a starting point, usually given an initial condition. Such an initial condition could be a constant force or another kind of perturbation. In orbital computations, numerical integration is often used to model this behaviour, because of the irregularities in the dynamic environment (many perturbations) and the absence of analytical solutions. The solution then provides an estimate of the trajectory and the state of the s/c(Hofsteenge, 2013). There are several different types of numerical integrators that all try to predict the s/c behaviour in different ways. These types are described in Section 4.1. In Section 4.2 the method is chosen that will be used in this research to compare the performance of the TSI method with.

Numerical integration methods do have one major drawback compared to analytic methods, and that is the accuracy of the produced result. Numerical methods come close to the actual result but usually do not reach it. Therefore, there will always be a certain error associated with the answer. One of the most important errors is called the local (and total) truncation error, which is caused by the numerical inaccuracy of the method itself, and are usually the largest errors. A second error can be introduced by the round-off properties of the used computer, which then also depends on the number of evaluations required for each of the integration methods (more evaluations means more round-off errors). These round-off errors are due to the fact that computers can only accurately represent a number up until a certain number of decimal figures. According to Milani and Nobili (1987) there are also specific errors that arise when integrating space-related problems. Instability errors can occur if the simulated system is chaotic or if the step-size is too large.

Another, non-method specific and not necessarily integration related, error source is the mistakes made in the physical model representing the problem in the simulation. Such errors can occur when forces and disturbances are not (properly) taken into account in the assumptions made to create the physical model.

Fortunately, many of the standard integration methods already contain functions that approximate these errors and then include those approximations to come up with a better solution, or try to minimize these errors by using multiple approximations. The focus of this chapter will thus be on the different integration methods and not the different methods of determining the different errors.

4.1. DIFFERENT INTEGRATOR TYPES

A number of different numerical integration methods exist, however in this section they will be split based on how they work. In this case they have been split into single-step (Section 4.1.1) and multi-step methods (Section 4.1.2) based on Noomen (2013a). The methods can also be split based on the used step-size; either a fixed step-size that does not change during the integration, or a variable step-size that changes per step (or sometimes even during the step). Finally, the methods can also be categorised by either being explicit or implicit. An explicit method uses the information provided at the start of the integration (the current state $\mathbf{x}_i$ and sometimes previous states) to determine the next state $\mathbf{x}_{i+1}$. Whereas an implicit method uses the same information to determine $\mathbf{x}_{i+1}$, but once this first solution is obtained, it uses this next state as an approximation of the solution and feeds it back into the method in order to determine a more accurate solution. This requires iteration.

The numerical approximation of the next state can be written as the current state plus the change during one time-step. This change is defined as the step-size h times the increment function Φ as shown by Equa-

tion (4.1), which changes depending on the method used. Here, η represents the total numerical approximation.

$$\mathbf{x}(t_0 + h) \approx \mathbf{x}_0 + h\mathbf{\Phi} = \eta(t_0 + h) \tag{4.1}$$

4.1.1. SINGLE-STEP

Single-step methods solely use the information at the current point to determine the approximation of the next state. This means tht the information of the previous points is neglected and usually not saved (Noomen, 2013a). Examples of the most simple explicit, fixed step-size, single-step methods are Euler, Mid-point and Runge-Kutta 4th order (RK4) (Hofsteenge, 2013). Euler uses the information at the current state to directly compute the estimate of the next state. Mid-point already incorporates an extra estimation where it first computes a point at half the step-size and then uses that information to approximate the next state, and RK4 takes 4 points into account and takes the weighted average of those to come up with a solution (the starting point, two mid-points and a final point). Many methods exists that are based on these simple methods, for instance the Mid-point method based high-order extrapolation (a.k.a. DIFEX2) (explicit) method (Deuflhard *et al.*, 1994).

Many more methods however are based on the RK4 principle such as Runge-Kutta-Nyström (RKN, with variations such as RKN7(6)9) (implicit) (Montenbruck, 1992b; Dormand *et al.*, 1987), Runge-Kutta-Nyström 12th order (RKN12) (implicit) (Montenbruck, 1992b) and Runge-Kutta-Fehlberg 4th (5th) order (RKF45) and Runge-Kutta-Fehlberg 7th (8th) order (RKF78) (Fehlberg, 1969, 1968). These last two integrators are slightly different since they are still explicit, but use a variable step-size.

4.1.2. MULTI-STEP

Compared to the single-step method, the multi-step method does use the information of the previous points to estimate the next state. Usually reaching as far back as the previous three points such as the Adams-Bashforth 4th order (AB4) method (Noomen, 2013a), this being the only difference between this method and the RK4 method. Extending this method creates the explicit Adams-Bashforth 6th order (AB6) method. An example of an implicit, fixed step-size, multi-step method is the Adams-Moulton method. It uses a polynomial to interpolate the function values in order to approximate the next state (Noomen, 2013a). Explicit and implicit methods can also be combined to create so-called Predictor-Corrector methods. Here an initial guess is created by the explicit method, which is then fed into the implicit part in order to correct and improve the estimate. Examples of Predictor-Corrector methods are Adams-Bashforth-Moulton 4th order (ABM4) and Adams-Bashforth-Moulton 12th order (ABM12) (Noomen, 2013a; Montenbruck, 1992b).

All previously mentioned multi-step methods use a fixed step-size. Variable step-size methods also exist, such as Shampine-Gordon (SG) (explicit) (Berry, 2004; Meijaard, 1991) and Störmer-Cowell 14th order (SC14) (Predictor-Corrector) (Berry, 2004; Ramos and Vigo-Aguiar, 2005).

4.2. CHOSEN METHOD FOR COMPARISON

In order to choose the method that will be used to compare the performance of TSI to, it was important to understand which methods were readily available. If a method is already validated and available for use a lot of time can be saved. Therefore, an inquiry of available methods is made in Section 4.2.1. Another important criteria is that the performance of TSI should be able to be compared to previous study cases. The easiest way of doing that is to see what methods other researchers used to compare TSI to (see Section 4.2.2. Using the information from Sections 4.2.1 and 4.2.2 a decision could be made on the final comparison method as is described in Section 4.2.3.

4.2.1. TUDAT METHODS

One of the software tools used in this thesis is Tudat (see Section 6.1.1 for more information). It is a computational toolbox that already comes with a number of useful functions. It also contains a number of pre-programmed validated numerical integrators. A list of the available integration methods is provided in Table 4.1.

Most of these methods are very similar except RK4 which is a fixed step-size method, and Dormand-Prince 8th (7th) order (DOPRIN87) which is actually a Runge-Kutta method similar to RKF with an accuracy order 8(7) using the formulations as described by Prince and Dormand (1981) according to Weeks and Thrasher

Table 4.1: Available Tudat integrators (Dirkx *et al.*, 2016)

Method	Kind of method	File	Ready for use
RK4	explicit, fixed step-size, single-step	rungeKutta4Integrator.h	Yes
RKF45	explicit, variable step-size, single-step	numericalIntegrator.h & rungeKuttaVariableStep-SizeIntegrator.h & rungeKuttaCoefficients.h/.cpp	Yes
RKF56	explicit, variable step-size, single-step	numericalIntegrator.h & rungeKuttaVariableStep-SizeIntegrator.h & rungeKuttaCoefficients.h/.cpp	No
RKF78	explicit, variable step-size, single-step	numericalIntegrator.h & rungeKuttaVariableStep-SizeIntegrator.h & rungeKuttaCoefficients.h/.cpp	Yes
DOPRIN87	explicit, variable step-size, single-step	numericalIntegrator.h & rungeKuttaVariableStep-SizeIntegrator.h & rungeKuttaCoefficients.h/.cpp	Yes

(2007). At the time of the research, the Runge-Kutta-Fehlberg 5th $\left(6^{th}\right)$ order (RKF56) method that was pre-programmed into Tudat was unfortunately not available for use.

4.2.2. METHODS USED IN PREVIOUS RESEARCH
Out of the research done on integration methods for space missions, the most relevant is the research that was done on TSI. The research performed by Scott and Martini (2008) focused on orbital trajectories and used RKF8(9) and the researched performed by Bergsma and Mooij (2016) focussed on re-entry cases and used RKF56. Unfortunately, RKF8(9) was not available through Tudat and RKF56 was out of commission at the time of this thesis research. However, it is good to notice that both researchers used higher order RKF methods, which encourages the use of similar methods for this research and fortunately similar methods are available.

4.2.3. CHOSEN METHOD
Considering the available methods and the methods used in previous TSI research it was determined that the RKF methods and DOPRIN87 would be tested in the early phases of the verification process. In this case RK4 would serve as a back-up. During the verification of the standard integrator it was found that RKF78 showed the best performance when dealing with these ascent problems, which is why it was chosen as the integration method to which TSI was later compared.

4.3. WORKINGS OF RKF
The principle behind RKF is perhaps best explained by first looking at a simpler Runge-Kutta method such as RK4. Noomen (2013a) provides a simple explanation of the workings of RK4 that have been adapted here. In this case, use is made of the general formulation for the numerical approximation as was shown in Equation (4.1). The increment function for RK4 is then presented by Equation (4.2). In this case four points are used to approximate the next state as visualised in Figure 4.1.

$$\Phi_{RK4} = \frac{1}{6}\left(k_1 + 2k_2 + 2k_3 + k_4\right) \tag{4.2}$$
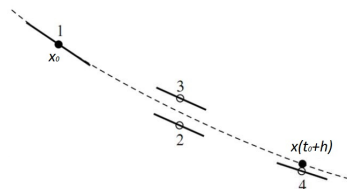
Figure 4.1: Principle of RK4 for a single parameter Noomen (2013a).

Runge-Kutta works with the time-derivatives at those points. The derivative at the first point is called k_1, at the second point k_2 etcetera. These time derivatives are used both in the increment function but also in

the process of determining the derivative of the next intermediate point as shown by Equation (4.3).

$$
\begin{aligned}
k_1 &= f'(t_0, \mathbf{x}_0) \\
k_2 &= f'(t_0 + h/2, \mathbf{x}_0 + h k_1/2) \\
k_3 &= f'(t_0 + h/2, \mathbf{x}_0 + h k_2/2) \\
k_4 &= f'(t_0 + h, \mathbf{x}_0 + h k_3)
\end{aligned}
\tag{4.3}
$$

Equations (4.2) and (4.3) can also be generalized as presented by Equation (4.4). In this case b_i represents the different weights for each of the points with the corresponding step-size weights c_i, n is the order and $a_{i,j}$ are the coefficients of the previous time-derivatives.

$$
\Phi_{RK} = \sum_{i=1}^{n} b_i k_i
$$

$$
\text{with} \quad k_i = f'\left(t + c_n h, y + h \sum_{j=1}^{n-1} a_{i,j} k_j \right)
\tag{4.4}
$$

This general formulation can now also be used to compute the higher order Runge-Kutta approximations given that $a_{i,j}$, b_i and c_i are provided. These sets of numbers can be found in various literature, and different people have come up with different sets. Fehlberg was one of these people. In order to get a more accurate solution he decided to use two different methods. In the case of this research, RKF78 was used, which means that a 7th order and 8th order solution can be computed using Equation (4.4). The 7th order solution is then used as the method solution and the difference between the 8th and the 7th order solution results in an error estimate which can be used to determine the next step-size. This step-size is thus computed such as to minimize this error estimate. This means that the only difference between RKF78 and RKF45 (for instance) is the coefficient set (a, b and c's).

5

TAYLOR SERIES INTEGRATION

Taylor Series integration (TSI) is different from the previously mentioned integrators, because it only uses the information at the current point to predict the next point. However, it does this using higher order derivatives at that point. These higher order derivatives have to be obtained as a function of the current state and the first order state derivatives. As soon as the Kth order derivative as been found, a Taylor Series can be set up to determine the next state as a function of the chosen step-size. This is all explained and described in more detail in Section 5.1. In this thesis, TSI is the main focus of the analysis. The performance with respect to the RKF integrators is tested. In order to be able to do this for the given model, a number of equation sets can be identified which have to be written in such a format that it can be used by TSI. These are described, and where needed derived, in Section 5.2.

5.1. GENERAL THEORY

TSI has been used to solve ordinary differential equations since the early 1960s (Scott and Martini, 2008). However, the first modern implementation of TSI in a space trajectory problem was provided by Montenbruck (1992a). Scott and Martini (2008) were able to implement this TSI method into the SNAP trajectory propagator which is the implementation that is used in this thesis. The method is described in Section 5.1.1 and the used step-size method is discussed in Section 5.1.2.

5.1.1. WORKINGS OF TSI

The formulation used in this thesis is based on the one used by Scott and Martini (2008).

TSI uses the current state and its derivatives to determine the next state by computing its Taylor Series described in Equation (5.1). The state vector is represented by **X** with the corresponding vector for the initial conditions **X**$_0$. Each of the variables can at any point be represented by $x_n(t)$. For a given step-size h and an order $K \in \mathbb{R}$ (chosen by the user) the updated state $x_n(t+h)$ can be represented by the Taylor Series with $n = 1, \ldots, 7$ in this case (7 variables: three position, three velocity and one mass). The exact solution is obtained by adding $T_{n,K}$, which is the truncation error for the nth variable using K terms.

$$x_n(t+h) = \sum_{k=0}^{K} \frac{x_n^{(k)}(t)}{k!}(h)^k \quad + \quad T_{n,K} \tag{5.1}$$

This particular TSI method uses recurrence relations to determine the kth order derivatives and only requires the current state (x_n) and its first derivatives ($x'_n = u_n$). Each recurrence relation describes a certain operation in the state derivative, such as: multiplication, division, power, exponential, sines and cosines. Equation (5.2) shows the recurrence relations for multiplication ($w(t) = f(t)g(t)$) and division ($w(t) = \frac{f(t)}{g(t)}$) respectively (the other operations are described later in this chapter when they are required).

For multiplications $\quad W(k) = \sum_{j=0}^{k} F(j) G(k-j)$

For divisions $\quad W(k) = \dfrac{1}{g(t_0)} \left[F(k) - \sum_{j=1}^{k} G(j) W(k-j) \right]$ $\qquad$ (5.2)

$Both\ with \quad W(k) = \dfrac{w^{(k)}(t_0)}{k!}, \quad F(j) = \dfrac{f^{(j)}(t_0)}{j!} \quad \text{and} \quad G(k-j) = \dfrac{g^{(k-j)}(t_0)}{(k-j)!}$

Here, both $f(t)$ and $g(t)$ are place-holder functions and $w(t)$ is called the auxiliary function which replaces the respective operation. Sometimes, the state derivative functions can be rather complex and have many operations intertwined. One can then choose to introduce extra variables to simplify the derivatives and reduce the number of operations in that particular derivative. These extra variables together with the expression that they replace then form the auxiliary equations. A random example is shown in Equation (5.3).

$$x_4' = u_4 = 2x_1 + \frac{(x_3 x_1 + x_2 x_3)}{x_4}$$

$$x_8 = x_3 x_1 + x_2 x_3$$
$\qquad$ (5.3)

However, now that the extra variable x_8 is introduced, the derivative of the corresponding auxiliary equations has to be described as well (see Equation (5.4)), which in turn will use auxiliary functions to determine the kth derivative of x_8.

$$x_4' = u_4 = 2x_1 + \frac{x_8}{x_4}$$

$$x_8' = u_8 = x_3' x_1 + x_3 x_1' + x_2' x_3 + x_2 x_3' = u_3 x_1 + x_3 u_1 + u_2 x_3 + x_2 u_3$$
$\qquad$ (5.4)

At this point it should be emphasised that using auxiliary equations and derivatives is a choice. It is not required to make TSI work. Sometimes it can be easier to introduce auxiliary equations because it makes the problem more comprehensible but this could introduce errors because all auxiliary equations also require auxiliary derivatives, which might not be easy to find. In those cases it could be more useful to just leave the state derivatives as they are and write more auxiliary functions instead. This all depends on the problem and the preference of the user.

Now let $u_n^{(k-1)} = x_n^k$ for $k = 1, \ldots, K$, then $\dfrac{u_n^{(k-1)}}{(k-1)!} = \dfrac{x_n^k}{(k-1)!}$, and also $\dfrac{x_n^k}{k!} = X_n(k)$. Combining this results in Equation (5.5).

$$U_n(k-1) = k X_n(k) \Rightarrow X_n(k) = \frac{U_n(k-1)}{k}$$
$\qquad$ (5.5)

The $X_n(k)$ are also known as the Taylor Series coefficients of the nth variable for the kth order derivative. Also, $U_n(k)$ are the recurrence relation expressions for the nth variable which consist of all the reduced auxiliary functions ($W(k)$) that form that derivative.

Using the expression described in Equation (5.5) all Taylor Series coefficients can be found. Then Equation (5.1) can be used to determine the next state values at time $t + h$ for the known previous parameter values at time t. The same can then be done to determine the values at the time-step after that using the state values at $t + h$, etc. Going through all these different time-steps results in the final integration.

5.1.2. STEP-SIZE

The step-size used for TSI can be either set as a constant value by the user or determined using a step-size controller, giving it the variable step-size properties, which is done in this thesis. The chosen step-size method was based on the recommendation of both Scott and Martini (2008) and Bergsma (2015) and directly uses the chosen (or preferred) local error tolerance τ to determine the next step size. This method assures that the step-size is small enough such that all variables satisfy the error condition directly. The step-size is determined using a so-called fixed-point iteration performed using Equation (5.6). The initial step-size h_1 can be

chosen to be the current step-size h as an easy estimate. Then the iteration is performed over l until a certain required convergence is reached.

$$h_{l+1} = exp\left(\frac{1}{K-1}ln\left[\frac{\tau}{\left|X_n(K-1)\right| + K\left|X_n(K)\right|h_l}\right]\right)$$ (5.6)

This is then done for all variables and the smallest required step-size is chosen, which is then used to determine the next step-size through $h_{next} = \eta h_{chosen}$, where η is the chosen step multiplication factor which has to be smaller than 1.

5.2. ASSOCIATED EQUATIONS

In order for TSI to be implemented, the state derivatives have to be modelled as a set of continuous functions which are a function of the state only. This can be done in different ways. In this case, three cases were tested: two Cartesian cases and one spherical case. For the Cartesian cases, the initial conditions first have to be transformed into Cartesian coordinates. The Cartesian equations themselves require reference frame transformations, which can be written in two different ways. The first case in described in in Section 5.2.1 and the second in Section 5.2.2. The reason for testing the spherical case is that the initial conditions are provided in spherical coordinates and the intermediate computations can be easily interpreted and checked for errors. However, the equations are highly sensitive to singularities. The spherical equations are described in Section 5.2.3 and already include reference frame transformations.

5.2.1. CARTESIAN EQUATIONS, FIRST CASE

The Cartesian state is described in Equation (5.7), where m_{MAV} is the mass of the MAV and the subscript I refers to the inertial frame.

$$\mathbf{r} = \begin{pmatrix} x_I \\ y_I \\ z_I \end{pmatrix} \qquad\qquad \mathbf{V} = \begin{pmatrix} V_{x_I} \\ V_{y_I} \\ V_{z_I} \end{pmatrix} \qquad\qquad m_{MAV}$$ (5.7)

The corresponding state derivatives are then described by Equation (5.8).

$$\begin{matrix} \dot{x}_I = V_{x_I} \\ \dot{y}_I = V_{y_I} \\ \dot{z}_I = V_{z_I} \end{matrix} \qquad \begin{matrix} \ddot{x}_I = \dot{V}_{x_I} = a_{x_I} \\ \ddot{y}_I = \dot{V}_{y_I} = a_{y_I} \\ \ddot{z}_I = \dot{V}_{z_I} = a_{z_I} \end{matrix} \qquad \dot{m}_{MAV} = -\frac{T}{g_0 I_{sp}}$$ (5.8)

From this point on, the subscript I is omitted, because the state and the state derivatives are always presented in the inertial frame. If variables have to be presented in any other reference frame the corresponding subscripts will be provided and explained. The accelerations in the x-, y- and z-direction have three contributing components: gravitational acceleration, drag and thrust. The gravitational acceleration can be directly expressed in the inertial frame, however the drag is presented in the body frame and the thrust is expressed in the propulsion frame. Therefore, both the drag and thrust contributions have to be transformed to the inertial frame using transformation matrices. This then results in the expression for the acceleration vector as shown by Equation (5.9). The subscript G shows that the parameter is a function of the ground velocity.

$$\begin{pmatrix} a_x \\ a_y \\ a_z \end{pmatrix} = \begin{pmatrix} -\mu_M \frac{x}{r^3} \\ -\mu_M \frac{y}{r^3} \\ -\mu_M \frac{z}{r^3} \end{pmatrix} + \Bigg|_{\mathbf{I}} \mathbb{T}_{\mathbf{z}}(-\Omega_M t_O + \omega_P) \Bigg|_{\mathbf{R}} \mathbb{T}_{\mathbf{z}}(-\tau)\, \mathbb{T}_{\mathbf{y}}\left(\frac{\pi}{2}+\delta\right) \Bigg|_{\mathbf{V}} \mathbb{T}_{\mathbf{z}}(-\chi_G)\, \mathbb{T}_{\mathbf{y}}(-\gamma_G) \Bigg|_{\mathbf{B}} \left[\begin{pmatrix} -\frac{D}{m_{MAV}} \\ 0 \\ 0 \end{pmatrix} + \dots \right.$$

$$\left. \dots \Bigg|_{\mathbf{B}} \mathbb{T}_{\mathbf{z}}(-\psi_T)\, \mathbb{T}_{\mathbf{y}}(-\epsilon_T) \Bigg|_{\mathbf{P}} \begin{pmatrix} \frac{T}{m_{MAV}} \\ 0 \\ 0 \end{pmatrix} \right]$$ (5.9)

It can be seen that this set of equations is a function of the current position and many other parameters. These parameters will all have to be written as a function of the current state. This can be done by writing them into auxiliary equations, forming extra variables that then also require the auxiliary derivatives. This works for certain parameters, such as the gravity, because these equations are already expressed in the inertial frame. However, the transformation angles are defined in different reference frames, which means that finding the proper auxiliary derivatives can be tricky sometimes. Therefore it was decided to directly write these parameters as auxiliary functions. Each of the auxiliary functions performs one simple algebraic operation and the collection of these auxiliary functions then form the complete set of recurrence relations using the recurrence relations for the simple algebraic operations. For the auxiliary equations, a similar notation will be used as shown by Scott and Martini (2008). Here the equations are denoted by x_{number} and the corresponding derivatives x'_{number}. This notation will also be used for the current state and the corresponding state derivatives. This way, Equation (5.7) can be written as Equation (5.10) and the corresponding derivatives can be written as presented by Equation (5.11).

$$
\begin{aligned}
x_1 &= x & x_4 &= \dot{x} = V_x \\
x_2 &= y & x_5 &= \dot{y} = V_y & x_7 &= m_{MAV} \\
x_3 &= z & x_6 &= \dot{z} = V_z
\end{aligned}
\tag{5.10}
$$

$$
\begin{aligned}
x'_1 &= x_4 & x'_4 &= \dot{V}_x = a_x = a_{g,x} + a_{D,x} + a_{T,x} \\
x'_2 &= x_5 & x'_5 &= \dot{V}_y = a_y = a_{g,y} + a_{D,y} + a_{T,y} & x'_7 &= \dot{m}_{MAV} = -\frac{T}{g_0 I_{sp}} \\
x'_3 &= x_6 & x'_6 &= \dot{V}_z = a_z = a_{g,z} + a_{D,z} + a_{T,z}
\end{aligned}
\tag{5.11}
$$

In this case the thrust and specific impulse are constant, which means that x'_7 is constant and any additional derivative will be zero. Also, neither one of the thrust angles is a function of the state, which means that a_T, in the body frame, is only a function of x_7 (also see Equation (5.9)). However, both a_g and a_D are a function of the position and velocity, where a_D is also a function of the MAV mass. Only a_g is rewritten using auxiliary equations as mentioned before.

GRAVITATIONAL ACCELERATION

For the gravitational acceleration two auxiliary equations were required since $r = \sqrt{x^2 + y^2 + z^2}$. The resulting expressions for the gravitational acceleration are shown in Equation (5.12) with the corresponding auxiliary equations and the derivatives defined in Equation (5.13).

$$
\begin{aligned}
a_{g,x} &= -\mu_M \frac{x_1}{r^3} = \frac{x_1}{\left(x_1^2 + x_2^2 + x_3^2\right)^{3/2}} = -\mu_M \frac{x_1}{x_9} \\
a_{g,y} &= -\mu_M \frac{x_2}{r^3} = \frac{x_2}{\left(x_1^2 + x_2^2 + x_3^2\right)^{3/2}} = -\mu_M \frac{x_2}{x_9} \\
a_{g,z} &= -\mu_M \frac{x_3}{r^3} = \frac{x_3}{\left(x_1^2 + x_2^2 + x_3^2\right)^{3/2}} = -\mu_M \frac{x_3}{x_9}
\end{aligned}
\tag{5.12}
$$

$$
\begin{aligned}
x_8 &= x_1^2 + x_2^2 + x_3^2 & x'_8 &= 2x_1 x_4 + 2x_2 x_5 + 2x_3 x_6 \\
x_9 &= x_8^{3/2} & x'_9 &= \frac{3}{2} \frac{x_9 x'_8}{x_8}
\end{aligned}
\tag{5.13}
$$

TRANSFORMATION ANGLES

The angles required for the transformation to go from the body frame to the reference frame all have to be written as a function of the state variables. The required angles are λ, δ, χ_G and γ_G. Here $\lambda = \tau + \Omega_M t_O - \omega_P$. This means that instead of first transforming to the rotating frame completely and then transforming to the inertial frame, an inertial longitude angle λ can be defined to directly transform to the inertial frame. The first two angles are the longitude and latitude and are spherical coordinates. Thus the relations for these angles can be found using the transformation from the Cartesian to the spherical system. However, the angles themselves are not required directly, because they are only used in transformation matrices. These matrices
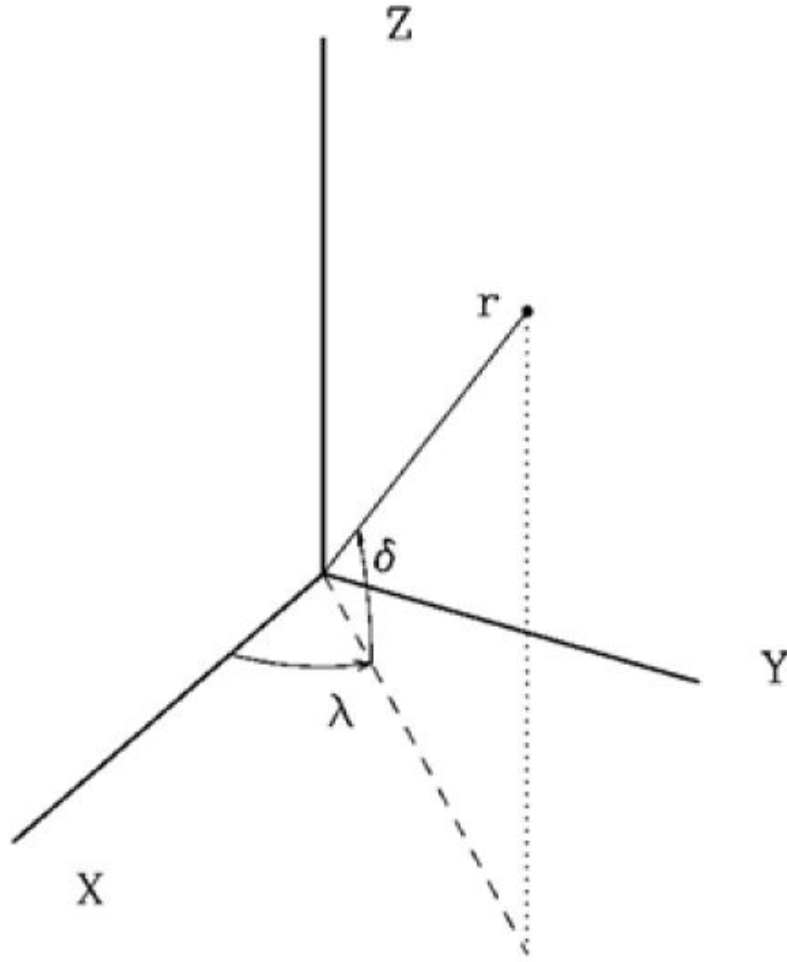
Figure 5.1: Spherical position variables in an inertial Cartesian frame (Noomen, 2013b).

are comprised of the sines and cosines of these angles, which means that a direct relation between the state variables and the sines and cosines of the position angles can be used. These relations can be derived from Figure A.8 and are described in Equation (5.14)

$$
r = \sqrt{x^2 + y^2 + z^2} \qquad
\begin{aligned}
\sin \lambda &= \frac{y}{\sqrt{x^2 + y^2}} \\[2mm]
\cos \lambda &= \frac{x}{\sqrt{x^2 + y^2}}
\end{aligned}
\qquad
\begin{aligned}
\sin \delta &= \frac{z}{r} \\[2mm]
\cos \delta &= \frac{\sqrt{x^2 + y^2}}{r}
\end{aligned}
\qquad (5.14)
$$

The corresponding auxiliary functions can then be described by Equation (5.15) using the definitions provided in Equations (5.10) and (5.11).

$$
\begin{aligned}
w_{4,1} &= x_1^2 + x_2^2 \\
w_{4,2} &= w_{4,1} + x_3^2 \\
w_{4,3} &= r = \sqrt{w_{4,2}} \\
w_{4,4} &= \sqrt{w_{4,1}}
\end{aligned}
\qquad
\begin{aligned}
w_{4,5} &= s\lambda = \frac{x_2}{w_{4,4}} \\[3mm]
w_{4,6} &= c\lambda = \frac{x_1}{w_{4,4}}
\end{aligned}
\qquad
\begin{aligned}
w_{4,7} &= s\delta = \frac{x_3}{w_{4,3}} \\[3mm]
w_{4,8} &= c\delta = \frac{w_{4,4}}{w_{4,3}}
\end{aligned}
\qquad (5.15)
$$

The latitude and longitude could be described using the position vector in the inertial frame, however the transformation from the body frame to the vertical frame is a function of the ground (underscore 'G') velocity in the rotational frame. Since the position and velocity in the inertial frame are known (current state), the ground velocity (V_G) can be written as a function of the inertial velocity (V_I). For this, the velocity components have to be transformed from the inertial frame to the vertical frame (which is the inverse of the first

three transformations described in Equation (5.9)). This transformation is shown in Equation (5.16) and was described in Mooij (1994). Here, c stands for cosine and s stands for sine. This transformation also includes the rotational effect on the velocity due to the rotation of Mars.

$$\mathbf{V_V} = \begin{pmatrix} V_{x_V} \\ V_{y_V} \\ V_{z_V} \end{pmatrix} = \begin{bmatrix} -c\lambda s\delta & -s\lambda s\delta & c\delta \\ -s\lambda & c\lambda & 0 \\ -c\lambda c\delta & -s\lambda c\delta & -s\delta \end{bmatrix} \left\{ \begin{pmatrix} V_x \\ V_y \\ V_z \end{pmatrix} - \begin{pmatrix} 0 \\ 0 \\ \Omega_M \end{pmatrix} \times \begin{pmatrix} x \\ y \\ z \end{pmatrix} \right\} \tag{5.16}$$

The ground velocity can now be computed as the norm of the vertical velocity vector as shown by Equation (5.17). The transformation matrices disappear because the norm of a transformation matrix is simply 1, which means that $V_G = V_V = V_R$.

$$V_G = \|\mathbf{V_V}\| = \left\| \begin{pmatrix} V_x \\ V_y \\ V_z \end{pmatrix} - \begin{pmatrix} 0 \\ 0 \\ \Omega_M \end{pmatrix} \times \begin{pmatrix} x \\ y \\ z \end{pmatrix} \right\| \tag{5.17}$$

Equation (5.17) can be rewritten as Equation (5.18).

$$V_G = \sqrt{\left(V_x + \Omega_M y\right)^2 + \left(V_y - \Omega_M x\right)^2 + V_z^2} \tag{5.18}$$

The corresponding auxiliary functions are provided in Equation (5.19).

$$
\begin{aligned}
w_{4,9} &= V_x + \Omega_M y = x_4 + \Omega_M x_2 & w_{4,11} &= w_{4,9}^2 + w_{4,10}^2 + x_6^2 \\
w_{4,10} &= V_y - \Omega_M x = x_5 - \Omega_M x_1 & w_{4,12} &= V_G = \sqrt{w_{4,11}}
\end{aligned}
\tag{5.19}
$$

The spherical velocity angles can now be derifed from Figure 5.2 as described by Equation (5.20). These were also provided by Mooij (1994).
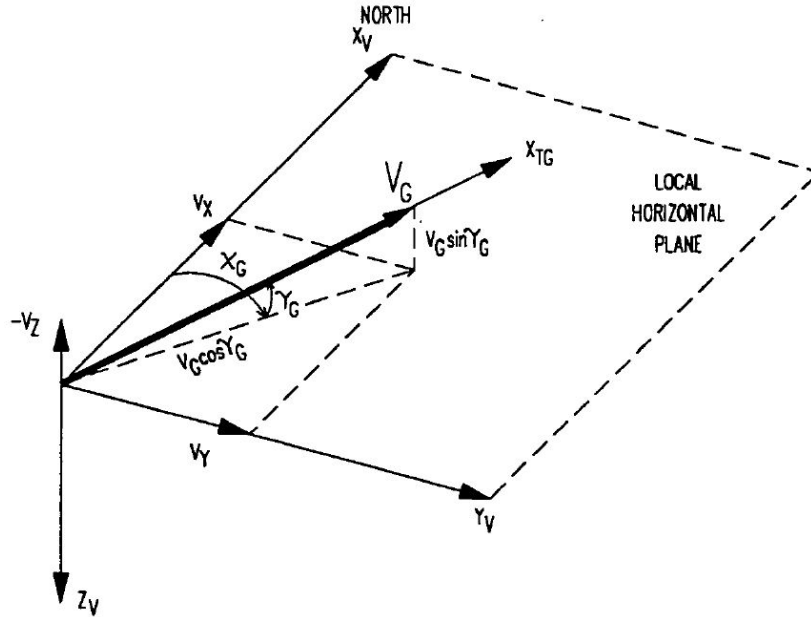

Figure 5.2: Spherical velocity variables in a vertical Cartesian frame (Mooij, 1994).

$$
\begin{aligned}
\sin\chi_G &= \frac{V_{y_V}}{\sqrt{V_{x_V}^2 + V_{y_V}^2}} & \sin\gamma_G &= \frac{-V_{z_V}}{V_G} \\
\cos\chi_G &= \frac{V_{x_V}}{\sqrt{V_{x_V}^2 + V_{y_V}^2}} & \cos\gamma_G &= \frac{\sqrt{V_{x_V}^2 + V_{y_V}^2}}{V_G}
\end{aligned}
\tag{5.20}
$$

Here, V_{x_V}, V_{y_V} and V_{z_V} are the velocities in the vertical frame. Expressions for these variables can be obtained by rewriting Equation (5.16). This then results in Equation (5.22).

$$\begin{aligned}
V_{x_V} &= -\left(V_x + \Omega_M y\right) s\delta\, c\lambda - \left(V_y - \Omega_M x\right) s\delta\, s\lambda + V_z c\delta \\
V_{y_V} &= \left(V_y - \Omega_M x\right) c\lambda - \left(V_x + \Omega_M y\right) s\lambda \\
V_{z_V} &= -\left(V_x + \Omega_M y\right) c\delta\, c\lambda - \left(V_y - \Omega_M x\right) c\delta\, s\lambda - V_z s\delta
\end{aligned} \tag{5.21}$$

The combined auxiliary functions for Equations (5.20) and (5.22) are described in Equation (5.19).

$$\begin{aligned}
w_{4,13} &= -c\lambda\, s\delta = -w_{4,6} w_{4,7} & w_{4,17} &= V_{x_V} = x_6 w_{4,8} + w_{4,9} w_{4,13} + w_{4,10} w_{4,14} & w_{4,22} &= s\chi_G = \frac{w_{4,18}}{w_{4,21}} \\
w_{4,14} &= -s\delta\, s\lambda = -w_{4,7} w_{4,5} & w_{4,18} &= V_{y_V} = w_{4,10} w_{4,6} - w_{4,9} w_{4,5} & w_{4,23} &= c\chi_G = \frac{w_{4,17}}{w_{4,21}} \\
w_{4,15} &= -c\delta\, c\lambda = -w_{4,8} w_{4,6} & w_{4,19} &= V_{z_V} = w_{4,9} w_{4,15} - x_6 w_{4,7} + w_{4,10} w_{4,16} & w_{4,24} &= s\gamma_G = -\frac{w_{4,19}}{w_{4,12}} \\
w_{4,16} &= -c\delta\, s\lambda = w_{4,8} w_{4,5} & w_{4,20} &= V_{x_V}^2 + V_{y_V}^2 = w_{4,17}^2 + w_{4,18}^2 & w_{4,25} &= c\gamma_G = \frac{w_{4,21}}{w_{4,12}} \\
& & w_{4,21} &= \sqrt{w_{4,20}} &
\end{aligned} \tag{5.22}$$

DRAG ACCELERATION

The drag acceleration is determined in the body frame by dividing the drag force (D) by the mass of the MAV (x_7). The drag force itself is a function of the position and velocity. The equations associated with the drag function are described in Equation (5.23) except for the C_D equations. The polynomial coefficients for the density equation are provided in Table 3.4 and are represented in Equation (5.23) by P_ρ.

$$\begin{aligned}
h &= r - R_{MOLA} \\
D &= \frac{1}{2}\rho V_G^2 S C_D \\
\rho &= e^{P_{\rho 10} h^{10} + P_{\rho 9} h^9 + P_{\rho 8} h^8 + P_{\rho 7} h^7 + P_{\rho 6} h^6 + P_{\rho 5} h^5 + P_{\rho 4} h^4 + P_{\rho 3} h^3 + P_{\rho 2} h^2 + P_{\rho 1} h + P_{\rho 0}}
\end{aligned} \tag{5.23}$$

The numbering for the drag auxiliary functions start with 27 because it was added later on and because it used to be an auxiliary equation. The auxiliary functions for the density can then be described by Equation (5.29).

$$\begin{aligned}
w_{27,1} &= h = w_{4,3} - R_{MOLA} & w_{27,7} &= w_{27,1}^7 \\
w_{27,2} &= w_{27,1}^2 & w_{27,8} &= w_{27,1}^8 \\
w_{27,3} &= w_{27,1}^3 & w_{27,9} &= w_{27,1}^9 \\
w_{27,4} &= w_{27,1}^4 & w_{27,10} &= w_{27,1}^{10} \\
w_{27,5} &= w_{27,1}^5 & w_{27,11} &= P_{\rho 10} w_{27,10} + P_{\rho 9} w_{27,9} + \ldots + P_{\rho 1} w_{27,1} + P_{\rho 0} \\
w_{27,6} &= w_{27,1}^6 & w_{27,12} &= \rho = e^{w_{27,11}}
\end{aligned} \tag{5.24}$$

Since the drag coefficient is a function of Mach number as by Figure 2.4 and is not a continuous function, it has to be split into 6 different sections. Each section has a separate $C_D - M$ relation. Before these relations can be described, three additional expressions are required which are described in Equation (5.25).

$$\begin{aligned}
M &= \frac{V_G}{a} \\
a &= \sqrt{\gamma_a R_a^* T_a} \quad \text{where} \quad R_a^* = \frac{R_a}{M_a}
\end{aligned} \tag{5.25}$$

Where the corresponding auxiliary functions can be described by Equation (5.26).

$$w_{27,14} = a = \sqrt{\gamma_a R_a^* w_{27,13}}$$
$$w_{27,15} = M = \frac{w_{4,12}}{w_{27,14}} \tag{5.26}$$

The conditional relations shown in Equation (5.27) describe the different equations that have to be used associated with the different sections of the drag coefficient plot. Here $P_{C_D number,section}$ are the polynomial fit coefficients as provided in Table 3.5.

$$C_D = \begin{cases} 0.2, & \text{for } 0 \le M < 0.5 \\ P_{C_D 1,2} M + P_{C_D 0,2}, & \text{for } 0.5 \le M < 1 \\ P_{C_D 1,3} M + P_{C_D 0,3}, & \text{for } 1 \le M < 1.3 \\ P_{C_D 1,4} M + P_{C_D 0,4}, & \text{for } 1.3 \le M < 2.5 \\ P_{C_D 1,5} M + P_{C_D 0,5}, & \text{for } 2.5 \le M < 4 \\ 0.3, & \text{for } M \ge 4 \end{cases} \tag{5.27}$$

In this case, the auxiliary functions for $C_D \left(= w_{27,16}\right)$ is any of the conditional relations depending on $M \left(= w_{27,15}\right)$.

This only leaves the temperature $T_a \left(= w_{27,13}\right)$, which is a function of the altitude $h \left(= w_{27,1}\right)$ in km, MOLA. But as described in Section 3.4.1, this parameter is split into different sections as well. The equations per section for the temperature is provided in Equation (5.28). Here $P_{T number,section}$ are the polynomial fit coefficients as provided in Table 3.2.

$$T_a = \begin{cases} P_{T1,1} h + P_{T0,1}, & \text{for } -0.6 \le h < 5.04 \\ P_{T3,2} h^3 + P_{T2,2} h^2 + P_{T1,2} h + P_{T0,2}, & \text{for } 5.04 \le h < 35.53 \\ P_{T6,3} h^6 + P_{T5,3} h^5 + P_{T4,3} h^4 + P_{T3,3} h^3 + \ldots \\ \qquad \ldots + P_{T2,3} h^2 + P_{T1,3} h + P_{T0,3}, & \text{for } 35.53 \le h < 75.07 \\ P_{T8,4} h^8 + P_{T7,4} h^7 + P_{T6,4} h^6 + P_{T5,4} h^5 + \ldots \\ \qquad \ldots + P_{T4,4} h^4 + P_{T3,4} h^3 + P_{T2,4} h^2 + P_{T1,4} h + P_{T0,4}, & \text{for } 75.07 \le h < 170.05 \\ 136.5, & \text{for } h \ge 170.05 \end{cases} \tag{5.28}$$

For both the conditional parameters C_D and T_a the required section has to be determined before the evaluation of the equations.

The drag can now also be described as an auxiliary function as shown by Equation (5.29).

$$w_{27,17} = V_G^2 = w_{4,12}^2$$
$$w_{27,18} = V_G^2 C_D = w_{27,17} w_{27,16}$$
$$w_{27,19} = D = \frac{1}{2} S w_{27,18} w_{27,12} \tag{5.29}$$

THRUST ACCELERATION

The only acceleration component still missing is the thrust acceleration. To be able to write the auxiliary functions for the thrust, Equation (5.9) first has to be rewritten such that all the transformations are gathered into two transformation matrices (see Equation (5.30)). The transformation matrices are described by Equations (5.32) and (A.5) for $\mathbb{T}_{\mathbf{BP}}$ and $\mathbb{T}_{\mathbf{IB}}$ respectively.

$$\begin{pmatrix} x_4' \\ x_5' \\ x_6' \end{pmatrix} = \begin{pmatrix} -\mu_M \frac{x_1}{x_9} \\ -\mu_M \frac{x_2}{x_9} \\ -\mu_M \frac{x_3}{x_9} \end{pmatrix} + \mathbb{T}_{\mathbf{IB}} \left[\begin{pmatrix} -\frac{w_{27,19}}{x_7} \\ 0 \\ 0 \end{pmatrix} + \mathbb{T}_{\mathbf{BP}} \begin{pmatrix} \frac{T}{x_7} \\ 0 \\ 0 \end{pmatrix} \right] \tag{5.30}$$

$$\mathbb{T}_{\mathbf{BP}} = \begin{bmatrix} c\psi_T c\epsilon_T & -s\psi_T & c\psi_T s\epsilon_T \\ s\psi_T c\epsilon_T & c\psi_T & s\psi_T s\epsilon_T \\ -s\epsilon_T & 0 & c\epsilon_T \end{bmatrix} \tag{5.31}$$

$$\mathbb{T}_{\mathbf{IB}} = \begin{bmatrix} c\lambda\left(-s\delta c\chi c\gamma + c\delta s\gamma\right) - s\lambda s\chi c\gamma & c\lambda s\delta s\chi - s\lambda c\chi & c\lambda\left(-s\delta c\chi s\gamma - c\delta c\gamma\right) - s\lambda s\chi s\gamma \\ s\lambda\left(-s\delta c\chi c\gamma + c\delta s\gamma\right) + c\lambda s\chi c\gamma & s\lambda s\delta s\chi + c\lambda c\chi & s\lambda\left(-s\delta c\chi s\gamma - c\delta c\gamma\right) + c\lambda s\chi s\gamma \\ c\delta c\chi c\gamma + s\delta s\gamma & -c\delta s\chi & c\delta c\chi s\gamma - s\delta c\gamma \end{bmatrix} \tag{5.32}$$

The thrust accelerations in the x-, y- and z-directions (in the body frame) can now be found by rewriting the last part of Equation (5.30) to Equation (5.33) using Equation (A.5).

$$\mathbb{T}_{\mathbf{BP}} \begin{pmatrix} \dfrac{T}{x_7} \\ 0 \\ 0 \end{pmatrix} = \begin{pmatrix} \dfrac{T}{x_7} c\psi_T c\epsilon_T \\ \dfrac{T}{x_7} s\psi_T c\epsilon_T \\ -\dfrac{T}{x_7} s\epsilon_T \end{pmatrix} \tag{5.33}$$

Equation (5.33) can be expressed as a collection of auxiliary functions as well. These are described in Equation (5.34).

$$\begin{aligned} w_{4,26} &= \cos\psi_T \\ w_{4,27} &= \cos\epsilon_T \\ w_{4,28} &= \sin\psi_T \\ w_{4,29} &= \sin\epsilon_T \\ w_{4,30} &= c\psi_T c\epsilon_T = w_{4,26}\,w_{4,27} \\ w_{4,31} &= c\epsilon_T s\psi_T = w_{4,27}\,w_{4,28} \\ w_{4,32} &= \frac{1}{x_7} \end{aligned} \qquad \begin{aligned} w_{4,33} &= \frac{T}{x_7} = T w_{4,32} \\ w_{4,34} &= \frac{T}{x_7} c\epsilon_T c\psi_T = w_{4,33}\,w_{4,30} \\ w_{4,37} &= \frac{T}{x_7} c\epsilon_T s\psi_T = w_{4,33}\,w_{4,31} \\ w_{4,38} &= \frac{T}{x_7} s\epsilon_T = w_{4,33}\,w_{4,29} \end{aligned} \tag{5.34}$$

The thrust accelerations are now written in the body frame, which means that they can be combined with the drag acceleration in the body frame. This is done in Equation (5.35). Here, $w_{4,35}$ represents the drag acceleration in the body frame and $w_{4,36}$ is the total acceleration in the x-direction in the body frame caused by both the drag and the thrust.

$$\begin{pmatrix} -\dfrac{x_{27}}{x_7} \\ 0 \\ 0 \end{pmatrix} + \begin{pmatrix} w_{4,34} \\ w_{4,37} \\ -w_{4,38} \end{pmatrix} = \begin{pmatrix} w_{4,34} - w_{4,35} \\ w_{4,37} \\ -w_{4,38} \end{pmatrix} = \begin{pmatrix} w_{4,36} \\ w_{4,37} \\ -w_{4,38} \end{pmatrix} \tag{5.35}$$

All accelerations combined

At this point the gravity accelerations are known in the inertial frame and the drag and thrust accelerations in the body frame. In order to get the final acceleration vector in the inertial frame, the drag and thrust accelerations have to be transformed from the body frame to the inertial frame using $\mathbb{T}_{\mathbf{IB}}$ resulting in Equation (5.36).

$$\mathbb{T}_{\mathbf{IB}} \begin{pmatrix} w_{4,36} \\ w_{4,37} \\ -w_{4,38} \end{pmatrix} = \begin{pmatrix} w_{4,36}\left(c\lambda\left(-s\delta c\chi c\gamma + c\delta s\gamma\right) - s\lambda s\chi c\gamma\right) + w_{4,37}\left(c\lambda s\delta s\chi - s\lambda c\chi\right) - w_{4,38}\left(c\lambda\left(-s\delta c\chi s\gamma - c\delta c\gamma\right) - s\lambda s\chi s\gamma\right) \\ w_{4,36}\left(s\lambda\left(-s\delta c\chi c\gamma + c\delta s\gamma\right) + c\lambda s\chi c\gamma\right) + w_{4,37}\left(s\lambda s\delta s\chi + c\lambda c\chi\right) - w_{4,38}\left(s\lambda\left(-s\delta c\chi s\gamma - c\delta c\gamma\right) + c\lambda s\chi s\gamma\right) \\ w_{4,36}\left(c\delta c\chi c\gamma + s\delta s\gamma\right) + w_{4,37}\left(-c\delta s\chi\right) - w_{4,38}\left(c\delta c\chi s\gamma - s\delta c\gamma\right) \end{pmatrix} \tag{5.36}$$

Now including the gravity components as well, the (lengthy) expressions for x_4', x_5' and x_6' become Equations (5.37) to (5.39) respectively.

$$\begin{aligned} x_4' = -\mu_M \frac{x_1}{x_9} &+ w_{4,36}\left(c\lambda\left(-s\delta c\chi c\gamma + c\delta s\gamma\right) - s\lambda s\chi c\gamma\right) + \ldots \\ &\ldots w_{4,37}\left(c\lambda s\delta s\chi - s\lambda c\chi\right) - \ldots \\ &\ldots w_{4,38}\left(c\lambda\left(-s\delta c\chi s\gamma - c\delta c\gamma\right) - s\lambda s\chi s\gamma\right) \end{aligned} \tag{5.37}$$

$$x_5' = -\mu_M \frac{x_2}{x_9} + w_{4,36}\left(s\lambda\left(-s\delta c\chi c\gamma + c\delta s\gamma\right) + c\lambda s\chi c\gamma\right) + \dots$$
$$\dots w_{4,37}\left(s\lambda s\delta s\chi + c\lambda c\chi\right) - \dots \tag{5.38}$$
$$\dots w_{4,38}\left(s\lambda\left(-s\delta c\chi s\gamma - c\delta c\gamma\right) + c\lambda s\chi s\gamma\right)$$

$$x_6' = -\mu_M \frac{x_3}{x_9} + w_{4,36}\left(c\delta c\chi c\gamma + s\delta s\gamma\right) + w_{4,37}\left(-c\delta s\chi\right) - w_{4,38}\left(c\delta c\chi s\gamma - s\delta c\gamma\right) \tag{5.39}$$

These equations now have to be written as a collection of auxiliary functions for the x-, y- and z-direction in the inertial frame. The gravitational acceleration can be written as the vector shown by Equation (5.40).

$$\mathbf{a_g} = \begin{pmatrix} -\mu_M \dfrac{x_1}{x_9} \\ -\mu_M \dfrac{x_2}{x_9} \\ -\mu_M \dfrac{x_3}{x_9} \end{pmatrix} = \begin{pmatrix} w_{4,39} \\ w_{5,1} \\ w_{6,1} \end{pmatrix} \tag{5.40}$$

The auxiliary derivatives ($u = x'$) can now be defined as the collection of auxiliary functions that describe the different transformations for $u_4, u_5\, and\, u_6$. These are shown in Equations (5.41) to (5.43) respectively.

$$
\begin{aligned}
&& w_{4,46} &= w_{4,42}\,c\gamma_G = w_{4,42}\,w_{4,25} \\
w_{4,40} &= -s\delta c\chi_G = -w_{4,7}\,w_{4,23} & w_{4,47} &= -w_{4,13}\,s\chi_G = -w_{4,13}\,w_{4,22} \\
w_{4,41} &= c\delta s\gamma_G = w_{4,8}\,w_{4,24} & w_{4,48} &= w_{4,40}\,s\gamma_G = w_{4,40}\,w_{4,24} \\
w_{4,42} &= -s\lambda s\chi_G = -w_{4,5}\,w_{4,22} & w_{4,49} &= w_{4,42}\,s\gamma_G = w_{4,42}\,w_{4,24} \\
w_{4,43} &= -s\lambda c\chi_G = -w_{4,5}\,w_{4,23} & w_{4,50} &= c\lambda\left(w_{4,45} + w_{4,41}\right) + w_{4,46} = w_{4,6}\left(w_{4,45} + w_{4,41}\right) + w_{4,46} \\
w_{4,44} &= -c\delta c\gamma_G = -w_{4,8}\,w_{4,25} & w_{4,51} &= c\lambda\left(w_{4,48} + w_{4,44}\right) + w_{4,49} = w_{4,6}\left(w_{4,48} + w_{4,44}\right) + w_{4,49} \\
w_{4,45} &= w_{4,40}\,c\gamma_G = w_{4,40}\,w_{4,25} & w_{4,52} &= w_{4,39} + w_{4,36}\,w_{4,50} + w_{4,37}\left(w_{4,47} + w_{4,43}\right) - w_{4,38}\,w_{4,51} \\
&& u_4 &= w_{4,52}
\end{aligned}
\tag{5.41}
$$

$$
\begin{aligned}
w_{5,2} &= c\lambda s\chi_G = w_{4,6}\,w_{4,22} \\
w_{5,3} &= s\lambda\left(w_{4,45} + w_{4,41}\right) + w_{5,2}\,c\gamma_G = w_{4,5}\left(w_{4,45} + w_{4,41}\right) + w_{5,2}\,w_{4,25} \\
w_{5,4} &= -w_{4,14}\,s\chi_G + c\lambda c\chi_G = -w_{4,14}\,w_{4,22} + w_{4,6}\,w_{4,23} \\
w_{5,5} &= s\lambda\left(w_{4,48} + w_{4,44}\right) + w_{5,2}\,s\gamma_G = w_{4,5}\left(w_{4,48} + w_{4,44}\right) + w_{5,2}\,w_{4,24} \\
w_{5,6} &= w_{5,1} + w_{4,36}\,w_{5,3} + w_{4,37}\,w_{5,4} - w_{4,38}\,w_{5,5} \\
u_5 &= w_{5,6}
\end{aligned}
\tag{5.42}
$$

$$
\begin{aligned}
&& w_{6,5} &= -w_{4,44}\,c\chi_G + w_{6,2} = -w_{4,44}\,w_{4,23} + w_{6,2} \\
w_{6,2} &= s\delta s\gamma_G = w_{4,7}\,w_{4,24} & w_{6,6} &= w_{4,41}\,c\chi_G + w_{6,4} = w_{4,41}\,w_{4,23} + w_{6,4} \\
w_{6,3} &= c\delta s\chi_G = w_{4,8}\,w_{4,22} & w_{6,7} &= w_{6,1} + w_{4,36}\,w_{6,5} - w_{4,37}\,w_{6,3} - w_{4,38}\,w_{6,6} \\
w_{6,4} &= -s\delta c\gamma_G = -w_{4,7}\,w_{4,25} & u_6 &= w_{6,7}
\end{aligned}
\tag{5.43}
$$

Also, because auxiliary equations were used for the gravitational acceleration. The corresponding auxiliary derivatives can be written as a collection of auxiliary functions as shown in Equation (5.44).

$$
\begin{aligned}
w_{8,1} &= x_1 x_4 & w_{9,0} &= x_9 u_8 \\
w_{8,2} &= x_2 x_5 & w_{9,1} &= \frac{w_{9,0}}{x_8} \\
w_{8,3} &= x_3 x_6 & \\
u_8 &= 2\left(w_{8,1} + w_{8,2} + w_{8,3}\right) & u_9 &= 1.5\,w_{9,1}
\end{aligned}
\tag{5.44}
$$

Then the equations in Equation (5.45) complete the whole set of auxiliary derivatives.

$$
\begin{aligned}
u_1 &= x_4 & u_3 &= x_6 \\
u_2 &= x_5 & u_7 &= -\frac{T}{g_0 I_{sp}}
\end{aligned}
\tag{5.45}
$$

5.2.2. CARTESIAN EQUATIONS, SECOND CASE

The second case (based on a method described by (Bergsma, 2015)) is similar to the first case in terms of set-up of the dynamic equations, the gravitational acceleration, and the drag and thrust accelerations in the body frame. The only difference lies in the formulation of $\mathbb{T}_{\mathbf{IB}}$. Instead of using Euler angles and rotation transformation matrices, $\mathbb{T}_{\mathbf{IB}}$ can be set-up as one single matrix performing a direct transformation. This matrix is described in Equation (5.46), where C stands for transformation matrix coefficient.

$$
\mathbb{T}_{\mathbf{IB}} = \begin{bmatrix} C_1 & C_4 & C_7 \\ C_2 & C_5 & C_8 \\ C_3 & C_6 & C_9 \end{bmatrix}
\tag{5.46}
$$

As was seen in Section 5.2.1 the rotation from the vertical to the inertial frame is purely a function of the radius in the inertial frame ($\mathbf{r}$ or $\mathbf{r_I}$) Also, the transformation from the body frame to the vertical frame was purely a function of the ground velocity in the vertical frame ($\mathbf{V_V}$ or $\mathbf{V_{G_V}}$). Therefore, if this transformation is to be done in one transformation, the ground velocity in the inertial frame is required ($\mathbf{V_{G_I}}$), because it would transform directly to the inertial frame. This means that the coefficients in Equation (5.46) will have to be a function of $\mathbf{r_I}$ and $\mathbf{V_{G_I}}$, where $\mathbf{V_{G_I}}$ is given by Equation (5.47).

$$
\mathbf{V_{G_I}} = \begin{pmatrix} V_x \\ V_y \\ V_z \end{pmatrix} - \begin{pmatrix} 0 \\ 0 \\ \Omega_M \end{pmatrix} \times \begin{pmatrix} x \\ y \\ z \end{pmatrix} = \begin{pmatrix} V_x + \Omega_M y \\ V_y - \Omega_M x \\ V_z \end{pmatrix}
\tag{5.47}
$$

BODY FRAME UNIT VECTORS

So when looking from the inertial frame, there are two state vectors: position and ground velocity. The state changes part due to the accelerations in the body frame $\mathbf{a_B}$, which is a vector comprised of the drag and thrust accelerations. This vector has the same length and direction in the body frame and the inertial frame. Also, any vector is simply a multiplication of the corresponding unit vector. The same holds for the velocity, which means that because the velocity in the body frame is defined through the x-axis of that frame, the unit vector of the ground velocity can be described as the unit vector in the x-direction $\hat{\mathbf{i}}$ as shown by Equation (5.48).

$$
\hat{\mathbf{i}} = \frac{\mathbf{V_{G_I}}}{\|\mathbf{V_{G_I}}\|}
\tag{5.48}
$$

This unit vector is also shown in Figure 5.3.

In Figure 5.3 it can be seen that the z-axis unit vector $\hat{\mathbf{k}}$ is defined in the same plane as $\hat{\mathbf{i}}$, $\mathbf{V_{G_I}}$ and $\mathbf{r_I}$ perpendicular to $\hat{\mathbf{i}}$. As a matter of fact, if the flight path angle is zero degrees, $\hat{\mathbf{k}}$ points in the same direction as the radius vector. In that case, the y-axis unit vector $\hat{\mathbf{j}}$ completes the unit frame. Since $\hat{\mathbf{j}}$ is perpendicular to the $\hat{\mathbf{i}}$-$\hat{\mathbf{k}}$ plane, it is also perpendicular to $\mathbf{V_{G_I}}$ and $\mathbf{r_I}$. Now because the radius vector is pointing through the centre of the body away from the centre of the inertial frame, the Right-hand-rule (RHR) gives Equation (5.49).

$$
\hat{\mathbf{j}} = \frac{\mathbf{r_I} \times \mathbf{V_{G_I}}}{\|\mathbf{r_I} \times \mathbf{V_{G_I}}\|}
\tag{5.49}
$$

Now $\hat{\mathbf{k}}$ can be computed by applying the RHR to $\hat{\mathbf{i}}$ and $\hat{\mathbf{j}}$. This results in Equation (5.50).

$$
\hat{\mathbf{k}} = \hat{\mathbf{i}} \times \hat{\mathbf{j}}
\tag{5.50}
$$

This leaves us with the unit vectors in the body frame defined as a function of the state in the inertial frame.
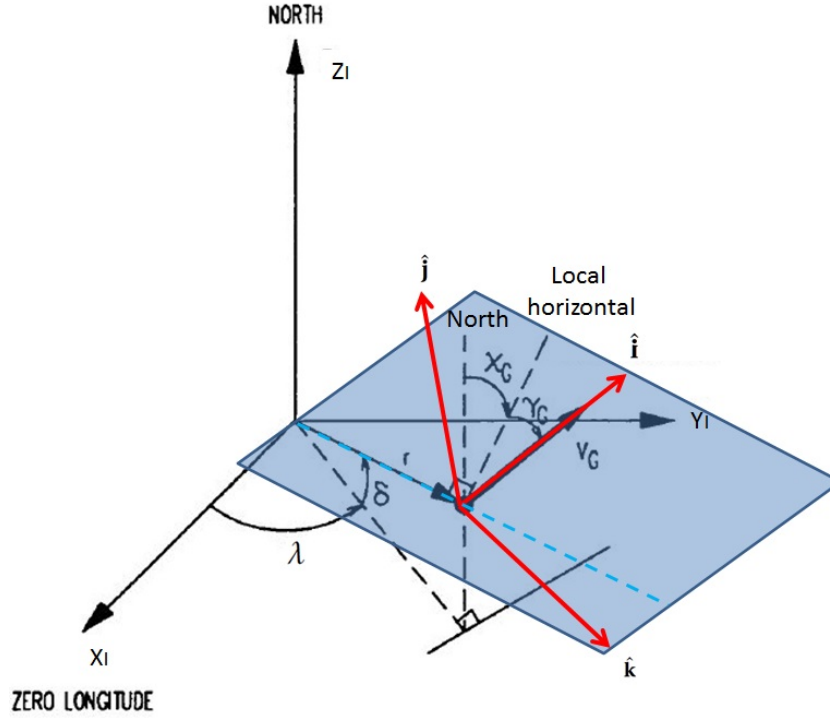
Figure 5.3: Definition of the body frame unit vectors based on the radius and ground velocity expressed in the inertial frame.

DEFINING THE TRANSFORMATION MATRIX COEFFICIENTS

Now, if the acceleration in the x-direction in the body frame is multiplied with $\hat{\mathbf{i}}$ this a_{x_B} is redefined in the inertial frame by providing a contribution in the x-, y- and z-direction. A similar multiplication can be done for a_{y_B} and $\hat{\mathbf{j}}$, and a_{z_B} and $\hat{\mathbf{k}}$. In matrix form this can be represented by Equation (5.51).

$$\begin{bmatrix} \hat{\mathbf{i}} & \hat{\mathbf{j}} & \hat{\mathbf{k}} \end{bmatrix} \cdot \begin{pmatrix} a_{x_B} \\ a_{y_B} \\ a_{z_B} \end{pmatrix} \tag{5.51}$$

Comparing Equation (5.51) to the expression for the transformation matrix provided by Equation (5.46) it can be seen that the coefficients can now be expressed as Equation (5.52).

$$\begin{pmatrix} C_1 \\ C_2 \\ C_3 \end{pmatrix} = \hat{\mathbf{i}} \qquad\qquad \begin{pmatrix} C_4 \\ C_5 \\ C_6 \end{pmatrix} = \hat{\mathbf{j}} \qquad\qquad \begin{pmatrix} C_7 \\ C_8 \\ C_9 \end{pmatrix} = \hat{\mathbf{k}} \tag{5.52}$$

Given these definitions, the corresponding auxiliary functions can now be defined.

AUXILIARY FUNCTIONS FOR THE SECOND CASE

With the transformation matrix now defined, Equation (5.9) can be written as Equation (5.53).

$$\begin{pmatrix} a_x \\ a_y \\ a_z \end{pmatrix} = \begin{pmatrix} -\mu_M \dfrac{x}{r^3} \\ -\mu_M \dfrac{y}{r^3} \\ -\mu_M \dfrac{z}{r^3} \end{pmatrix} + \begin{bmatrix} \hat{\mathbf{i}} & \hat{\mathbf{j}} & \hat{\mathbf{k}} \end{bmatrix} \cdot \left[\begin{pmatrix} -\dfrac{D}{m_{MAV}} \\ 0 \\ 0 \end{pmatrix} + \dots\dots \bigg|_{\mathbf{B}} \mathbb{T}_{\mathbf{z}}\left(-\psi_T\right) \mathbb{T}_{\mathbf{y}}\left(-\epsilon_T\right) \bigg|_{\mathbf{P}} \begin{pmatrix} \dfrac{T}{m_{MAV}} \\ 0 \\ 0 \end{pmatrix} \right] \tag{5.53}$$

In this case, all the auxiliary functions involving the rotation angles and the transformations ($w_{4,5} - w_{4,8}$, $w_{4,13} - w_{4,25}$, $w_{4,40} - w_{4,52}$, $w_{5,2} - w_{5,6}$ and $w_{6,2} - w_{6,7}$) can be discarded and instead new auxiliary functions have to be defined for the new transformation matrix. Please note that the discarded numbers will be reused but now with different function definitions for the second case!

The first auxiliary functions can found by rewriting Equation (5.48) as a function of the non-discarded auxiliary functions described in Section 5.2.1 and are shown in Equation (5.54).

$$w_{4,13} = C_1 = \frac{V_x + \Omega_M y}{V_G} = \frac{w_{4,9}}{w_{4,12}} \qquad w_{4,14} = C_2 = \frac{V_y - \Omega_M x}{V_G} = \frac{w_{4,10}}{w_{4,12}} \qquad w_{4,15} = C_3 = \frac{V_z}{V_G} = \frac{x_6}{w_{4,12}} \tag{5.54}$$

In case of the auxiliary functions for $\hat{\mathbf{j}}$ first the cross product has to be computed and the norm of that cross product. This is done in Equation (5.55).

$$
\begin{aligned}
w_{4,16} &= x_6 x_2 - w_{4,10} x_3 \\
w_{4,17} &= w_{4,9} x_3 - x_6 x_1 \\
w_{4,18} &= w_{4,10} x_1 - w_{4,9} x_2
\end{aligned}
\qquad
\begin{aligned}
w_{4,19} &= w_{4,16}^2 + w_{4,17}^2 + w_{4,18}^2 \\
w_{4,20} &= \sqrt{w_{4,19}}
\end{aligned}
\qquad
\begin{aligned}
w_{4,21} &= C_4 = \frac{w_{4,16}}{w_{4,20}} \\
w_{4,22} &= C_5 = \frac{w_{4,17}}{w_{4,20}} \\
w_{4,23} &= C_6 = \frac{w_{4,18}}{w_{4,20}}
\end{aligned}
\tag{5.55}
$$

These auxiliary functions can now be used to describe the $\hat{\mathbf{k}}$ functions as shown by Equation (5.56). In this case, the last auxiliary functions was named 40 because 26 is already taken up by an auxiliary function for the thrust acceleration.

$$
\begin{aligned}
w_{4,24} &= C_7 = C_2 C_6 - C_3 C_5 = w_{4,14} w_{4,23} - w_{4,15} w_{4,22} \\
w_{4,25} &= C_8 = C_3 C_4 - C_1 C_6 = w_{4,15} w_{4,21} - w_{4,13} w_{4,23} \\
w_{4,40} &= C_9 = C_1 C_5 - C_2 C_4 = w_{4,13} w_{4,22} - w_{4,14} w_{4,21}
\end{aligned}
\tag{5.56}
$$

Then combining everything results in the expression presented in Equation (5.57) for u_4, u_5 and u_6.

$$
\begin{aligned}
u_4 &= w_{4,39} + w_{4,36} w_{4,13} + w_{4,37} w_{4,21} - w_{4,38} w_{4,24} \\
u_5 &= w_{5,1} + w_{4,36} w_{4,14} + w_{4,37} w_{4,22} - w_{4,38} w_{4,25} \\
u_6 &= w_{6,1} + w_{4,36} w_{4,15} + w_{4,37} w_{4,23} - w_{4,38} w_{4,40}
\end{aligned}
\tag{5.57}
$$

5.2.3. Spherical equations

For the Spherical case, the initial conditions are readily provided. The position comes directly from the chosen launch site and the velocity comes from the initial MAV conditions. These are all defined in the rotating frame as depicted in Figure 5.4 and Equation (5.58).

$$
\mathbf{R} = \begin{pmatrix} r \\ \delta \\ \tau \end{pmatrix}
\qquad
\mathbf{V} = \begin{pmatrix} V_G \\ \gamma_G \\ \chi_G \end{pmatrix}
\qquad
m_{MAV}
\tag{5.58}
$$

The different variables are now defined as shown by Equation (5.59) and the derivatives by Equation (5.60). The numbers that were given to the variables are a result of the early derivations.

$$
\begin{aligned}
x_{16} &= r = h + R_{MOLA} \\
x_{12} &= \delta \\
x_{11} &= \tau
\end{aligned}
\qquad
\begin{aligned}
x_{15} &= V_G \\
x_{14} &= \gamma_G \\
x_{13} &= \chi_G
\end{aligned}
\qquad
x_7 = m_{MAV}
\tag{5.59}
$$

$$
\begin{aligned}
x_{16}' &= \dot{r} \\
x_{12}' &= \dot{\delta} \\
x_{11}' &= \dot{\tau}
\end{aligned}
\qquad
\begin{aligned}
x_{15}' &= \dot{V}_G \\
x_{14}' &= \dot{\gamma}_G \\
x_{13}' &= \dot{\chi}_G
\end{aligned}
\qquad
x_7' = \dot{m}_{MAV} = -\frac{T}{g_0 I_{sp}}
\tag{5.60}
$$

The derivatives given in Equation (5.60) are already provided by Mooij (1994) in the rotating frame and include the rotational effects. A simplified form can be seen in Equations (5.61) and (5.62). This is why it
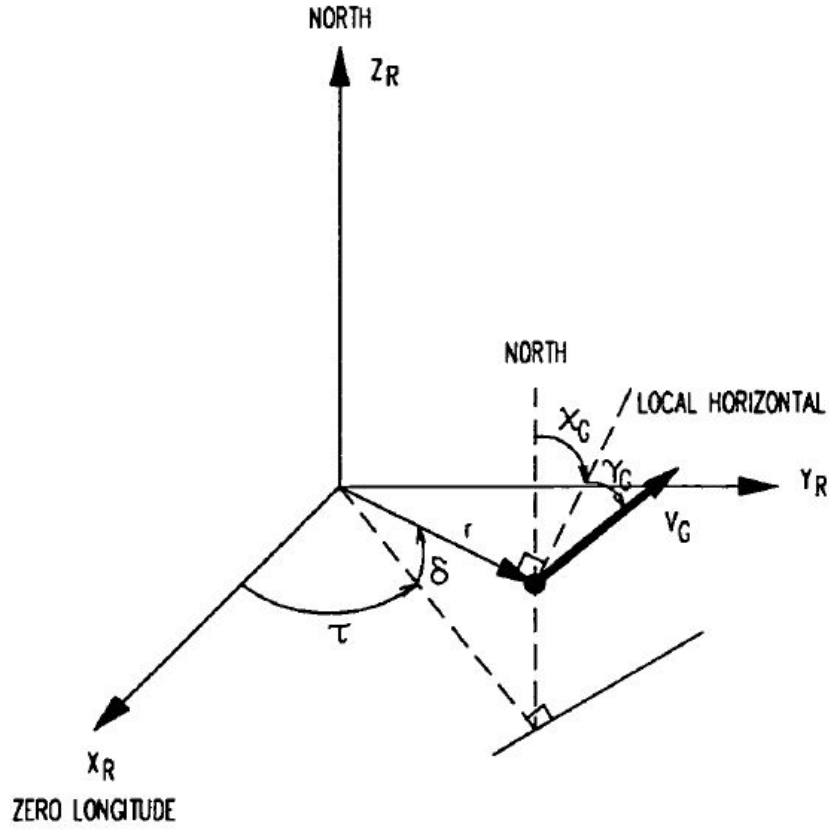
Figure 5.4: Definition of the Spherical coordinates (Mooij, 1994).

was decided to perform the TSI for the Spherical case in the rotating frame. At the end of the integration the variables can then be transformed to the inertial frame for comparison.

$$x'_{16} = \dot{r} = V_G s\gamma_G \qquad x'_{12} = \dot{\delta} = \frac{V_G c\chi_G c\gamma_G}{r} \qquad x'_{11} = \dot{\tau} = \frac{V_G s\chi_G c\gamma_G}{rc\delta} \qquad (5.61)$$

$$x'_{15} = \dot{V}_G = \Omega_M^2 rc\delta \left(s\gamma_G c\delta - c\gamma_G s\delta c\chi_G\right) + \frac{Tc\psi_T c\epsilon_T}{m} - \frac{D}{m} - \frac{\mu_M}{r^2} s\gamma_G$$

$$x'_{14} = \dot{\gamma}_G = 2\Omega_M c\delta s\chi_G + \frac{V_G}{r} c\gamma_G + \frac{\Omega_M^2 rc\delta}{V_G} \left(c\delta c\gamma_G + s\gamma_G s\delta c\chi_G\right) + \frac{Ts\epsilon_T}{V_G m} - \frac{\mu_M}{V_G r^2} c\gamma_G \qquad (5.62)$$

$$x'_{13} = \dot{\chi}_G = 2\Omega_M \left(s\delta - \frac{c\delta s\gamma_G c\chi_G}{c\gamma_G}\right) + \frac{V_G}{r} c\gamma_G \frac{s\delta}{c\delta} s\chi_G + \frac{\Omega_M^2 rc\delta s\delta s\chi_G}{V_G c\gamma_G} + \frac{Ts\psi_T c\epsilon_T}{V_G m c\gamma_G}$$

The last term in the first two expressions of Equation (5.62) correspond to the acceleration contribution of the gravity. The first expression has a drag component and all three have a thrust component similar to the Cartesian cases. The rest of the terms come from the rotational effects. In this case it was decided to define the drag as an auxiliary equation x_{27}, which will be discussed in more detail later in this section.

AUXILIARY FUNCTIONS FOR THE SPHERICAL CASE
Before the auxiliary functions for Equations (5.61) and (5.61) can be written, some standard auxiliary functions have to be defined first. These include δ, γ_G and χ_G. The numbering is based on early derivations and do not correspond to the definitions provided for the Cartesian cases! The angle auxiliary functions are defined in Equation (5.63).

$$w_{4,4} = s\delta = sx_{12} \qquad\qquad w_{4,7} = s\gamma_G = sx_{14}$$
$$w_{4,5} = c\chi_G = cx_{13} \qquad\qquad w_{4,8} = c\gamma_G = cx_{14} \qquad\qquad (5.63)$$
$$w_{4,6} = c\delta = cx_{12} \qquad\qquad w_{4,9} = s\chi_G = sx_{13}$$

Some expression for the thrust are also required. These are similar to the equations defined in Section 5.2.1 but are repeated in Equation (5.64) for convenience.

$$w_{4,26} = \cos\psi_T \qquad\qquad w_{4,28} = \sin\psi_T$$
$$w_{4,27} = \cos\epsilon_T \qquad\qquad w_{4,29} = \sin\epsilon_T \qquad\qquad w_{4,32} = \frac{1}{x_7} \qquad (5.64)$$

Now the auxiliary functions can be written for $x'_{11} = u_{11}$ till $x'_{16} = u_{16}$ and are shown in Equations (5.65) to (5.70) respectively.

$$w_{11,0} = V_G c\gamma_G = x_{15} w_{4,8} \qquad w_{11,2} = w_{11,1} s\chi_G = w_{11,1} w_{4,9}$$
$$w_{11,1} = \frac{w_{11,0}}{r} = \frac{w_{11,0}}{x_{16}} \qquad w_{11,3} = \frac{w_{11,2}}{c\delta} = \frac{w_{11,2}}{w_{4,6}} \qquad u_{11} = w_{11,3} \qquad (5.65)$$

$$w_{12,1} = w_{11,1} c\chi_G = w_{11,1} w_{4,5} \qquad\qquad u_{12} = w_{12,1} \qquad (5.66)$$

$$w_{13,0} = s\psi_T c\epsilon_T = w_{4,28} w_{4,27} \qquad w_{13,5} = w_{13,3} s\chi_G + w_{13,4} = w_{13,3} w_{4,9} + w_{13,4}$$
$$w_{13,1} = s\gamma_G c\chi_G = w_{4,7} w_{4,5} \qquad w_{13,6} = \frac{w_{13,5}}{V_G} = \frac{w_{13,5}}{x_{15}}$$
$$w_{13,2} = \Omega_M^2 r c\delta = \Omega_M^2 x_{16} w_{4,6} \qquad w_{13,7} = -2\Omega_M c\delta w_{13,1} + w_{13,6} = -2\Omega_M w_{4,6} w_{13,1} + w_{13,6} \qquad u_{13} = w_{13,9}$$
$$w_{13,3} = w_{13,2} s\delta = w_{13,2} w_{4,4} \qquad w_{13,8} = \frac{w_{13,7}}{c\gamma_G} = \frac{w_{13,7}}{w_{4,8}}$$
$$w_{13,4} = \frac{T w_{13,0}}{x_7} = T w_{13,0} w_{4,32} \qquad w_{13,9} = \left(2\Omega_M + w_{11,3}\right) s\delta + w_{13,8} = \left(2\Omega_M + w_{11,3}\right) w_{4,4} + w_{13,8}$$
$$\qquad (5.67)$$

$$w_{14,0} = \frac{T s\epsilon_T}{x_7} = T w_{4,29} w_{4,32} \qquad\qquad w_{14,5} = w_{14,4} + w_{13,2} w_{14,1} + w_{14,0}$$
$$w_{14,1} = c\delta c\gamma_G + w_{13,1} s\delta = w_{4,6} w_{4,8} + w_{13,1} w_{4,4} \qquad w_{14,6} = \frac{w_{14,5}}{V_G} = \frac{w_{14,5}}{x_{15}}$$
$$w_{14,2} = -\mu_M c\gamma_G = -\mu_M w_{4,8}$$
$$w_{14,3} = r^2 = x_{16}^2 \qquad\qquad w_{14,7} = 2\Omega_M c\delta s\chi_G + w_{11,1} + w_{14,6} = 2\Omega_M w_{4,6} w_{4,9} + w_{11,1} + w_{14,6}$$
$$w_{14,4} = \frac{w_{14,2}}{w_{14,3}} \qquad\qquad u_{14} = w_{14,7}$$
$$\qquad (5.68)$$

$$w_{15,0} = T c\psi_T c\epsilon_T - D = T w_{4,26} w_{4,27} - x_{27} \qquad w_{15,4} = c\gamma_G c\chi_G = w_{4,8} w_{4,5}$$
$$w_{15,1} = \frac{w_{15,0}}{m} = \frac{w_{15,0}}{x_7} \qquad\qquad w_{15,5} = s\gamma_G c\delta - w_{15,4} s\delta = w_{4,7} w_{4,6} - w_{15,4} w_{4,4}$$
$$\qquad\qquad w_{15,6} = w_{13,2} w_{15,5} + w_{15,1} + w_{15,3} \qquad (5.69)$$
$$w_{15,2} = -\mu_M s\gamma_G = -\mu_M w_{4,7}$$
$$w_{15,3} = \frac{w_{15,2}}{w_{14,3}} \qquad\qquad u_{15} = w_{15,6}$$

$$w_{16,1} = V_G s\gamma_G = x_{15} w_{4,7} \qquad\qquad u_{16} = w_{16,1} \qquad (5.70)$$

Drag acceleration as auxiliary variable

The drag acceleration for the Spherical case is similar to the Cartesian case, except this time it was chosen to use auxiliary variables to describe the drag. This means that auxiliary equations have to be defined as is shown in Equation (5.71). Also, this means that auxiliary derivatives are required for each of these equations. Equation (5.72) shows the different derivatives corresponding to the equations.

$$
\begin{aligned}
x_{27} &= D = \frac{1}{2}\rho V_G^2 S C_D = \frac{1}{2} S x_{28} x_{15}^2 x_{29} \\
x_{28} &= \rho = e^{x_{30}} \\
x_{29} &= C_D \\
x_{30} &= P_{\rho 10} x_{31}^{10} + P_{\rho 9} x_{31}^9 + P_{\rho 8} x_{31}^8 + P_{\rho 7} x_{31}^7 + P_{\rho 6} x_{31}^6 + P_{\rho 5} x_{31}^5 + P_{\rho 4} x_{31}^4 + P_{\rho 3} x_{31}^3 + P_{\rho 2} x_{31}^2 + P_{\rho 1} x_{31} + P_{\rho 0} \\
x_{31} &= h = r - R_{MOLA} = x_{16} - R_{MOLA}
\end{aligned}
\tag{5.71}
$$

$$
\begin{aligned}
x_{27}' &= \frac{1}{2} S x_{15} \left(x_{15} \left(x_{29} x_{28}' + x_{28} x_{29}' \right) + 2 x_{28} x_{29} x_{15}' \right) \\
x_{28}' &= x_{30}' x_{28} \\
x_{30}' &= x_{31}' \left(10 P_{\rho 10} x_{31}^9 + 9 P_{\rho 9} x_{31}^8 + 8 P_{\rho 8} x_{31}^7 + 7 P_{\rho 7} x_{31}^6 + 6 P_{\rho 6} x_{31}^5 + \ldots \right. \\
&\qquad \left. \ldots + 5 P_{\rho 5} x_{31}^4 + 4 P_{\rho 4} x_{31}^3 + 3 P_{\rho 3} x_{31}^2 + 2 P_{\rho 2} x_{31} + P_{\rho 1} \right) \\
x_{31}' &= x_{16}'
\end{aligned}
\tag{5.72}
$$

The auxiliary derivatives described in Equation (5.72) can now be used to define the auxiliary functions. These are described in Equations (5.73) to (5.75) for u_{27}, u_{28} and u_{30} respectively. In this case $u_{31} = u_{16}$.

$$
\begin{array}{lll}
w_{27,1} = C_D \dot{\rho} = x_{29} u_{28} & w_{27,4} = V_G \left(w_{27,1} + w_{27,2} \right) = x_{15} \left(w_{27,1} + w_{27,2} \right) & \\
w_{27,2} = \rho \dot{C}_D = x_{28} u_{29} & w_{27,5} = w_{27,3} \dot{V}_G = w_{27,3} u_{15} & u_{27} = \frac{1}{2} S w_{27,6} \\
w_{27,3} = \rho C_D = x_{28} x_{29} & w_{27,6} = V_G \left(w_{27,4} + w_{27,5} \right) = x_{15} \left(w_{27,4} + w_{27,5} \right) &
\end{array}
\tag{5.73}
$$

$$
w_{28,1} = u_{30} \rho = u_{30} x_{28} \qquad\qquad u_{28} = w_{28,1}
\tag{5.74}
$$

$$
\begin{array}{ll}
w_{30,1} = h^9 = x_{31}^9 & w_{30,6} = h^4 = x_{31}^4 \\
w_{30,2} = h^8 = x_{31}^8 & w_{30,7} = h^3 = x_{31}^3 \\
w_{30,3} = h^7 = x_{31}^7 & w_{30,8} = h^2 = x_{31}^2 \\
w_{30,4} = h^6 = x_{31}^6 & w_{30,9} = u_{31} \left(10 P_{\rho 10} w_{30,1} + \cdots + 3 P_{\rho 3} w_{30,8} + 2 P_{\rho 2} x_{31} + P_{\rho 1} \right) \\
w_{30,5} = h^5 = x_{31}^5 & \\
& u_{30} = w_{30,9}
\end{array}
\tag{5.75}
$$

Again, three additional auxiliary equations are required for the $C_D - M$ relation (see Figure 2.4) and are presented in Equation (5.76).

$$
\begin{aligned}
x_{32} &= M = \frac{V_G}{a} = \frac{x_{15}}{x_{33}} \\
x_{33} &= a = \sqrt{\gamma_a R_a^* T_a} = \sqrt{\gamma_a R_a^* x_{34}} \quad \text{where} \quad R_a^* = \frac{R_a}{M_a} \\
x_{34} &= T_a
\end{aligned}
\tag{5.76}
$$

In this case the conditional relations shown in Equation (5.77) are not used directly in the recurrence relations, but only serve as initial conditions. Again, the $P_{C_D number, section}$ are the polynomial fit coefficients as provided in Table 3.5.

$$x_{29} = C_D = \begin{cases} x_{29,1} = 0.2, & \text{for } 0 \le x_{32} < 0.5 \\ x_{29,2} = P_{C_D 1,2} x_{32} + P_{C_D 0,2}, & \text{for } 0.5 \le x_{32} < 1 \\ x_{29,3} = P_{C_D 1,3} x_{32} + P_{C_D 0,3}, & \text{for } 1 \le x_{32} < 1.3 \\ x_{29,4} = P_{C_D 1,4} x_{32} + P_{C_D 0,4}, & \text{for } 1.3 \le x_{32} < 2.5 \\ x_{29,5} = P_{C_D 1,5} x_{32} + P_{C_D 0,5}, & \text{for } 2.5 \le x_{32} < 4 \\ x_{29,6} = 0.3, & \text{for } x_{32} \ge 4 \end{cases} \tag{5.77}$$

The corresponding derivatives that will have to be used for the recurrence relations are presented in Equation (5.78).

$$x'_{29} = \begin{cases} x'_{29,1} = 0, & \text{for } 0 \le x_{32} < 0.5 \\ x'_{29,2} = P_{C_D 1,2} x'_{32}, & \text{for } 0.5 \le x_{32} < 1 \\ x'_{29,3} = P_{C_D 1,3} x'_{32}, & \text{for } 1 \le x_{32} < 1.3 \\ x'_{29,4} = P_{C_D 1,4} x'_{32}, & \text{for } 1.3 \le x_{32} < 2.5 \\ x'_{29,5} = P_{C_D 1,5} x'_{32}, & \text{for } 2.5 \le x_{32} < 4 \\ x'_{29,6} = 0, & \text{for } x_{32} \ge 4 \end{cases} \tag{5.78}$$

The Mach derivative and corresponding speed of sound derivative are then described in Equation (5.79).

$$x'_{32} = \frac{x_{33} x'_{15} - x_{15} x'_{33}}{x_{33}^2}$$
$$x'_{33} = \frac{\gamma_a R_a^*}{2 x_{33}} x'_{34} \tag{5.79}$$

For the drag coefficient, there are no auxiliary functions required. That is why x' in Equation (5.78) can simply be replaced by u. The Mach number and the speed of sound do require auxiliary functions and are described in Equations (5.80) and (5.81) respectively.

$$\begin{aligned} w_{32,1} = a\dot{V}_G = x_{33} u_{15} \qquad & w_{32,3} = a^2 = x_{33}^2 \\ w_{32,2} = V_G \dot{a} = x_{15} u_{33} \qquad & w_{32,4} = \frac{w_{32,1} - w_{32,2}}{w_{32,3}} \qquad u_{32} = w_{32,4} \end{aligned} \tag{5.80}$$

$$w_{33,1} = \frac{\dot{T}_a}{a} = \frac{u_{34}}{x_{33}} \qquad\qquad u_{33} = w_{33,1} \tag{5.81}$$

The last relations that still need to be described are the ones for the temperature T_a. Similar to C_D the corresponding auxiliary equations, shown by Equation (5.82) are only used for the initial conditions. Again, $P_{T number, section}$ are the polynomial fit coefficients as provided in Table 3.2.

$$x_{34} = T_a = \begin{cases} x_{34,1} = P_{T 1,1} x_{31} + P_{T 0,1}, & \text{for } -0.6 \le x_{31} < 5.04 \\ x_{34,2} = P_{T 3,2} x_{31}^3 + P_{T 2,2} x_{31}^2 + P_{T 1,2} x_{31} + P_{T 0,2}, & \text{for } 5.04 \le x_{31} < 35.53 \\ x_{34,3} = P_{T 6,3} x_{31}^6 + P_{T 5,3} x_{31}^5 + P_{T 4,3} x_{31}^4 + P_{T 3,3} x_{31}^3 + \ldots \\ \qquad \ldots + P_{T 2,3} x_{31}^2 + P_{T 1,3} x_{31} + P_{T 0,3}, & \text{for } 35.53 \le x_{31} < 75.07 \\ x_{34,4} = P_{T 8,4} x_{31}^8 + P_{T 7,4} x_{31}^7 + P_{T 6,4} x_{31}^6 + P_{T 5,4} x_{31}^5 \\ \qquad + P_{T 4,4} x_{31}^4 + P_{T 3,4} x_{31}^3 + P_{T 2,4} x_{31}^2 + P_{T 1,4} x_{31} + P_{T 0,4}, & \text{for } 75.07 \le x_{31} < 170.05 \\ x_{34,5} = 136.5, & \text{for } x_{31} \ge 170.05 \end{cases} \tag{5.82}$$

The corresponding derivatives that are used for the recurrence relations are presented in Equation (5.83).

$$x'_{34} = \begin{cases} x'_{34,1} = P_{T1,1}\,x'_{31}, & \text{for } -0.6 \le x_{31} < 5.04 \\ x'_{34,2} = \left(3P_{T3,2}\,x_{31}^2 + 2P_{T2,2}\,x_{31} + P_{T1,2}\right)x'_{31}, & \text{for } 5.04 \le x_{31} < 35.53 \\ x'_{34,3} = \left(6P_{T6,3}\,x_{31}^5 + 5P_{T5,3}\,x_{31}^4 + 4P_{T4,3}\,x_{31}^3 + \dots \right. \\ \qquad \left. \dots + 3P_{T3,3}\,x_{31}^2 + 2P_{T2,3}\,x_{31} + P_{T1,3}\right)x'_{31}, & \text{for } 35.53 \le x_{31} < 75.07 \\ x'_{34,4} = \left(8P_{T8,4}\,x_{31}^7 + 7P_{T7,4}\,x_{31}^6 + 6P_{T6,4}\,x_{31}^5 + 5P_{T5,4}\,x_{31}^4 + \dots \right. \\ \qquad \left. \dots + 4P_{T4,4}\,x_{31}^3 + 3P_{T3,4}\,x_{31}^2 + 2P_{T2,4}\,x_{31} + P_{T1,4}\right)x'_{31}, & \text{for } 75.07 \le x_{31} < 170.05 \\ x'_{34,5} = 0, & \text{for } x_{31} \ge 170.05 \end{cases} \tag{5.83}$$

All the power relations in Equation (5.83) were already described in auxiliary functions in Equation (5.75). Therefore, depending on the section, the equations presented in Equation (5.83) can be rewritten by simply replacing x' by u and the auxiliary functions. This is shown in Equation (5.84).

$$u_{34} = \begin{cases} u_{34,1} = P_{T1,1}\,u_{31}, & \text{for } -0.6 \le x_{31} < 5.04 \\ u_{34,2} = \left(3P_{T3,2}\,w_{30,2} + 2P_{T2,2}\,x_{31}\right)u_{31} + P_{T1,2}\,u_{31}, & \text{for } 5.04 \le x_{31} < 35.53 \\ u_{34,3} = \left(6P_{T6,3}\,w_{30,5} + 5P_{T5,3}\,w_{30,4} + 4P_{T4,3}\,w_{30,3} + \dots \right. \\ \qquad \left. \dots + 3P_{T3,3}\,w_{30,2} + 2P_{T2,3}\,x_{31}\right)u_{31} + P_{T1,3}\,u_{31}, & \text{for } 35.53 \le x_{31} < 75.07 \\ u_{34,4} = \left(8P_{T8,4}\,w_{30,7} + 7P_{T7,4}\,w_{30,6} + 6P_{T6,4}\,w_{30,5} + 5P_{T5,4}\,w_{30,4} + \dots \right. \\ \qquad \left. \dots + 4P_{T4,4}\,w_{30,3} + 3P_{T3,4}\,w_{30,2} + 2P_{T2,4}\,x_{31}\right)u_{31} + P_{T1,4}\,u_{31}, & \text{for } 75.07 \le x_{31} < 170.05 \\ u_{34,5} = 0, & \text{for } x_{31} \ge 170.05 \end{cases} \tag{5.84}$$

Now all the information that is required to compute the recurrence relation for the drag is available. Please note that there is a certain order in which these equations have to be computed, since they depend on each other. Table 5.1 shows this order.

Table 5.1: Order of auxiliary equations and derivatives computations

Auxiliary equations				Auxiliary derivatives			
Order	x_n	Order	x_n	Order	u_n	Order	u_n
0	$x_7, x_{11}, x_{12}, x_{13}, x_{14}, x_{15}, x_{16}$	4	x_{32}	7	$u_7, u_{11}, u_{12}, u_{16}$	11	u_{32}
1	x_{31}	5	x_{29}	8	u_{31}	12	u_{29}
2	x_{30}, x_{34}	6	x_{27}	9	u_{30}, u_{34}	13	u_{27}
3	x_{33}, x_{28}			10	u_{28}, u_{33}	14	u_{13}, u_{14}, u_{15}

5.2.4. Recurrence relations

Now that all the auxiliary functions are known, they can be used to determine the required recurrence relations. In order to write these concisely and following the same convention as used by Scott and Martini (2008), a number of extra parameters will have to be introduced. The Taylor series coefficients can be written as described by Equation (5.85). Where n is the variable number and k is the order of the derivative.

$$\frac{x_n^{(k)}}{k!} \triangleq X_n(k) \quad \text{where} \quad k \ge 1 \tag{5.85}$$

A similar expression is defined for u_n and w_n as well as the place-holder functions f_n and g_n which are all shown in Equation (5.86).

$$U_n(k) \triangleq \frac{u_n^{(k)}}{k!} \qquad W_n(k) \triangleq \frac{w_n^{(k)}}{k!} \qquad F_n(k) \triangleq \frac{f_n^{(k)}}{k!} \qquad G_n(k) \triangleq \frac{g_n^{(k)}}{k!} \tag{5.86}$$

Then remembering that $u_n = x'_n$ and using Equation (5.85) a relation can be described between X_n and U_n as shown in Equation (5.87) (Scott and Martini, 2008).

$$u_n^{(k-1)} = x_n^{(k)} \quad \Rightarrow \quad \frac{u_n^{(k-1)}}{(k-1)!} = \frac{x_n^{(k)}}{(k-1)!} \quad \Rightarrow$$
$$U_n(k-1) = kX_n(k) \quad \Rightarrow \quad X_n(k) = \frac{U_n(k-1)}{k} \tag{5.87}$$

Using these definitions, the auxiliary functions can be written into reduced auxiliary functions $W(k)$ for the three cases. The equations stay the same, but the lower-case letters are replaced by their upper-case counterparts. A complete list of the reduced auxiliary functions (starting at $k = 2$, or the second derivative u') for the three cases is presented in Appendix E. As was mentioned before, all the auxiliary functions have been defined such that they incorporate one of the following operations: multiplication, division, power, exponential or trigonometric. This has been done because recurrence relations exist for these simple operations as provided by Jorba and Zou (2005). These recurrence relations are written using the definitions from Equation (5.86) and are described in Equations (5.88) to (5.94).

$$\text{for} \quad f_n \pm g_n \quad \Rightarrow \quad W_{n,\pm}(k) = F_n(k) \pm G_n(k) \tag{5.88}$$

$$\text{for} \quad f_n g_n \quad \Rightarrow \quad W_{n,mult}(k) = \sum_{j=0}^{k} F_n(j) G_n(k-j) \tag{5.89}$$

$$\text{for} \quad \frac{f_n}{g_n} \quad \Rightarrow \quad W_{n,div}(k) = \frac{1}{G_n(0)} \left[F_n(k) - \sum_{j=1}^{k} G_n(j) W_{n,div}(k-j) \right] \tag{5.90}$$

$$\text{for} \quad f_n^{\alpha} \quad \Rightarrow \quad W_{n,pow}(k) = \frac{1}{kF_n(0)} \sum_{j=0}^{k-1} \left[k\alpha - j(\alpha+1) \right] F_n(k-j) W_{n,pow}(j) \tag{5.91}$$

$$\text{for} \quad e^{f_n} \quad \Rightarrow \quad W_{n,exp}(k) = \frac{1}{k} \sum_{j=0}^{k-1} (k-j) W_{n,exp}(j) F_n(k-j) \tag{5.92}$$

$$\text{for} \quad \cos f_n \quad \Rightarrow \quad W_{n,cos}(k) = -\frac{1}{k} \sum_{j=1}^{k} j W_{n,sin}(k-j) F_n(j) \tag{5.93}$$

$$\text{for} \quad \sin f_n \quad \Rightarrow \quad W_{n,sin}(k) = \frac{1}{k} \sum_{j=1}^{k} j W_{n,cos}(k-j) F_n(j) \tag{5.94}$$

Checking the presented equations it can be seen that Equations (5.93) and (5.94) are interdependent. This means that whenever a cosine recurrence relation has to be computed, the same recurrence relation for sine (with at least order $k-1$) has to be computed at the same time (and vice versa). All these equations have been derived by Jorba and Zou (2005) using the general Leibniz rule for the kth derivative of a multiplication as portrayed in Equation (5.95).

$$(f_n g_n)^{(k)} = \sum_{j=0}^{k} \binom{k}{j} f_n^{(j)} g_n^{(k-j)} \tag{5.95}$$

Combining Equation (5.95) and the definition of the reduced derivative for the auxiliary function (see Equation (5.86)) results in Equation (5.96). This equation, when rewritten to include the reduced derivatives for f_n and g_n, results in Equation (5.89).

$$W_{n,mult}(k) = \frac{1}{k!} \sum_{j=0}^{k} \binom{k}{j} f_n^{(j)} g_n^{(k-j)} \tag{5.96}$$

With all the recurrence relations now known, and using the definition of Equation (5.87) the updated state can be described using the Taylor series expansion as described in Equation (5.97).

$$x_n(t+h) = \sum_{k=0}^{K} \frac{x_n^{(k)}(t)}{k!} h^k + T_{n,K} = \sum_{k=0}^{K} X_n(k) h^k + T_{n,K} \quad \text{with } n = 1, \ldots, 7 \tag{5.97}$$

Here K is the order of the series to which it has to be evaluated and $T_{n,K}$ is the truncation error. Please note that all the Taylor series coefficients computed for the auxiliary equations are only needed to determine the Taylor series coefficients of the state variables (which is why they are auxiliary).

6

PROGRAM SIMULATION TOOL

To perform the analysis associated with this thesis, a simulation program has been written. This tool is comprised of both existing (Section 6.1) and newly developed software (Section 6.2). It is written in C++ and is based on the Tudat structure. The purpose of the software is to simulate the trajectory of the MAV using RKF and TSI. This tool is written such that the performance of both integrators can be compared. The final workings of the complete tool is described in Section 6.3.

6.1. EXISTING SOFTWARE

The use of existing software can greatly improve the performance of the final tool and save time as well. Another important reason to use existing software is that this will make it easier for other people to use and incorporate into their own software as well. The existing software used for this thesis is software that is currently being used by the space department of the TU Delft and (in case of Mars-GRAM) by the mission design section at JPL.

6.1.1. TUDAT

Tudat is, as the name suggests, a toolbox that can be used to solve numerous astrodynamic problems (Dirkx *et al.*, 2016). It was, and still is, being developed by students and staff of the Delft University of Technology. Specifically by the section Astrodynamics and Space missions of the Aerospace Engineering faculty. It is programmed in C++ and consists of a number of libraries. These libraries can be called upon by the user to invoke different Tudat functionalities such as standard reference frame transformations or often used integrators. The available software is completely validated and comes with its own tests to make sure that everything is working properly. It itself uses two external libraries: Eigen and Boost. Both these libraries will be discussed in Sections 6.1.2 and 6.1.3 respectively. Figure 6.1 shows Tudat with the different libraries that are used within the Tudat Bundle including the core functions (Tudat Core). In this thesis, the Tudat libraries are used for all standard mathematical and astrodynamic operations.

Figure 6.1: Tudat structure

6.1.2. Eigen

Eigen is an external C++ library that was written to perform linear algebra computations [1]. The software is free and easy to use, which is why it is widely used by the C++ community and thus also within Tudat (Dirkx *et al.*, 2016). Another advantage is that because it does not use any source files, it does not need to be build before using it. The Eigen libraries contain a number of standardized matrices and vectors, each with its own characteristics. An example of an often used vector is *Vector3d* (or *Eigen::Vector3d*), which can for instance be used to store the Cartesian position of a satellite. Here the *3* shows that it can store 3 values/parameters and the *d* shows that these are of the type *double*. It is mentioned on the Tudat wiki (Dirkx *et al.*, 2016) that these Eigen vectors and matrices should only be used if required for linear algebra computations. For ordinary storage, the C++ arrays, vectors and matrices should be used to save both storage and computation time.

6.1.3. Boost

Boost is a slightly more complicated set of C++ libraries, where compared to the Eigen library, Boost first has to be compiled before being able to use all of its functionalities. Fortunately, this compiling is performed by Tudat automatically when setting it up for the first time. Boost is described as an addition to the standard C++ libraries, thus adding more functionalities (Dirkx *et al.*, 2016) [2]. Within Tudat, Boost is used to pass free and class functions as an argument to another object and also for dynamic allocation using so-called pointers. Four libraries that are often used within Tudat are *boost::function*, *boost::bind*, *boost::shared_ptr* and *boost::make_shared*. The first two libraries are used to pass functions (a function is pointed to by *function* and called by *bind*) and the last two are used in case of dynamic allocation (*shared_ptr* is the pointer and *make_shared* is the object creator that returns a shared pointer to the created object).

6.1.4. Mars-GRAM

Mars-GRAM is a high-fidelity atmospheric model developed by NASA to simulate the global atmospheric conditions on Mars (Justh and Justus, 2008) [3]. The model is based on NASA Ames Mars General Circulation Model (for altitudes between 0-80 km) and Mars Thermospheric General Circulation model (for altitudes above 80 km). It can provide density, temperature and pressure data (among other data) with respect to the current altitude, latitude and longitude on Mars. Seasonal variations are taken into account in the model as well, which is why different calender dates will result in different atmospheric compositions. The tool can be used within a simulation tool or as a separate executable. Unfortunately, because it is so detailed, each computation requires a lot of CPU time. This is why it was decided to use the stand-alone Mars-GRAM executable to generate a detailed table with atmospheric data as a function of altitude, latitude and longitude at the start of the optimisation. Even generating this table required a lot of CPU time (on average a single computation using the stand-alone executable took 67.9 seconds to complete). The starting altitude was set at -0.6 km MOLA and advanced with a step-size of 0.1 km to 320 km altitude to cover the entire range that the MAV would have to cover. Also, the latitude and longitude were varied within 10 degrees from the launch site with a step-size of 1 degree. A Matlab script was written to extract the relevant atmospheric data from the Mars-GRAM output files and write them into a .csv file, thus creating the required atmospheric data table. The atmospheric data in this table was then interpolated to provide an estimate of the atmospheric characteristics at every point along the ascent trajectory, which is required to compute the drag at each time step. Some of the earlier versions of Mars-GRAM are available for free (such as the Mars-GRAM 2005 version used in this thesis), however, the latests versions (such as the Mars-GRAM 2010 version used as a back-up in this thesis) require a licence agreement.

6.2. Developed software

This section of the software chapter describes the software that either had to be developed around existing software/libraries or had to be developed from scratch (the TSI propagator). Each piece of software is accompanied by the corresponding software architecture. Every next piece of software then indirectly incorporates the previous architecture through the use of the completed tool.

---

[1] More documentation on Eigen can be found on eigen.tuxfamily.org/dox/ [Accessed 8 March 2016]

[2] More documentation on Boost can be found on http://www.boost.org/ [Accessed 8 March 2016]

[3] NASA website: https://see.msfc.nasa.gov/model-Marsgram [Accessed 9 March 2016]

6.2.1. RKF PROPAGATOR

The RKF (or traditional) propagator architecture is described in Figure 6.2. It starts with the current state, which is then passed on to the state derivative function. The state derivative function is used by the RKF integrators to determine the next state by calling the function a number of times depending on the used method. Both RK4 and RKF45 (and higher order RKF integrators) are already available through the Tudat libraries. RK4 can be called by including the rungeKutta4Integrator.h header file, and RKF methods can be called by including the rungeKuttaVariableStepSizeIntegrator.h header file. This integration process is repeated until the final condition is met. Within the state derivative function all the sate derivatives are updated and stored. The current position is used to update the gravitational acceleration on the MAV, the current mass is used to determine the accelerations caused by the thrust and finally the complete state is required to determine the accelerations caused by the drag. Both the drag and thrust accelerations have to be transformed to the inertial frame using the updated angles from the current state. The function also computes the current mass flow rate, however since the thrust is constant, this does not change over time. In the state derivative function, all the transformations are governed by pre-developed functions within the Tudat library, which includes the state transformations and the frame transformation from the body frame to the inertial frame. The transformation from the propulsion frame to the body frame is however not included in Tudat and had to be written.

All blocks represent a different action. These actions might be performed in classes, header files and/or source files. More information on the classification of the different blocks can be found in Appendix D.

6.2.2. TSI PROPAGATOR

The TSI propagator has a significantly different architecture compared to the traditional propagator as can be seen in Figure 6.3. TSI requires an initial order and step-size to start the integration process. In this thesis it has been decided to keep the order the same throughout the entire integration. The step-size will change during the integration depending on the Taylor series evaluations. The initial state is set as the current state and is fed into the TSI block. Within this block, first the auxiliary equations and functions are called, which were set-up for this particular problem. They are evaluated using the current state. These auxiliary equations and functions already include all the reference frame and coordinate transformations, as well as approximate atmospheric parameter functions. This is required to set-up the recurrence relations, which is where TSI differs from the traditional propagator. Once the auxiliary equations and functions have been computed they are used to compute the Taylor coefficients through the recurrence relations set-up for the thesis problem. These coefficients are then stored for later use and are also passed to the block creating the Taylor series expansion for every state variable thus creating the updated state. The last two coefficients are then used to determine the next step-size. This continues until the final integration condition has been met.

6.3. COMPLETED SIMULATION TOOL

The final simulation tool combined the integration software in such a way that a complete trajectory propagation could be simulated. It consists of different phases: initialisation, initial propagation, integrator burn phase, integrator coast phase, final circularisation and comparison. A brief description of each phase is provided in this section. It should be noted that in the actual program, the TSI propagation (burn and coast phase) supersedes the RKF propagation. Also, three different RKF methods can be chosen: Runge-Kutta-Fehlberg 4th (5th) order (RKF45), RKF78 and DOPRIN87.

6.3.1. INITIALISATION

During the initialisation phase, all the input values are loaded into the program. This is done by calling the input .txt files and assigning all the proper values to the corresponding parameters. Then, the Mars celestial body class and the MAV class are initialised, providing the Mars atmospheric and planetary data and the MAV system characteristics respectively. At this point, any values that differ from the pre-set default values are updated in both classes. The next step is to convert the initial spherical state into the initial Cartesian state and both states are saved in the respective output files for both TSI and RKF. Finally, the StateAndTime class is initialised for the TSI.

6.3.2. INITIAL PROPAGATION

As will be described in Chapter 7, during the verification process it was found that TSI had trouble dealing with initial conditions close to its singular values during the initial second(s), both for velocity and flight-path angle. This is why it was decided to slightly shift the initial conditions at which the actual integration

for TSI would start. Because RKF did not have similar issues with the first second(s), it was chosen to use an RKF method to propagate the first second. For this initial integration, the default integrator is RKF78 with a tolerance of $1 \cdot 10^{-15}$. The output of this initial propagation is then used as the initial state for both TSI and RKF for the remainder of the integration. This way, both methods can still be compared properly.

6.3.3. INTEGRATOR BURN PHASE
At the start of the burn phase the final state of the initial propagation is taken as the initial state input for the integrators. During the burn phase, both TSI and RKF are initiated and run until the end of the first burn phase occurs. Within this phase, TSI stops at every altitude and Mach section of the atmospheric graphs to make sure that no errors occur in the model. Provided that the atmospheric graphs are piecewise continuous, such stops are not required for RKF. The end of the first burn phase can either be based on a set time or a set altitude. Of course, extra cut-off criteria can be added. During the propagation, all intermediate states are stored in the output files for both methods.

6.3.4. INTEGRATOR COAST PHASE
After the first burn phase, the MAV enters a coasting phase. This is simulated by setting the thrust equal to zero. For TSI this can simply be done by setting the thrust in the MAV class zero within the propagation do-loop. This means that when the set burn-out condition is met, the class is updated, and the loop is continued. However, it is not possible to do this within one loop for the RKF, because of the manner in which RKF is initialised. In Tudat it is described that in order to use the build in RKF functions, a separate state derivative class has to be build first. This class is initialised using the initial state classes, and therefore does not change when updating the initial state classes in the loop directly. This means that when the thrust changes to zero, the state derivative class has to be re-initialised, creating the need for a second separate do-loop. This also means that the integrator class has to be re-initialised as well, which means that a separate integrator has to be defined (one with a different name from the first one). Both the TSI and RKF coasting phases are terminated whenever the desired altitude is reached, or after a certain limit time. Again, all the intermediate states are stored in the output files during the coasting phase.

6.3.5. FINAL CIRCULARISATION
Once the final condition is met, both the RKF and the TSI final state are used to determine the required final circularisation burn in order to reach the desired final orbit. For this computation, the states are first converted into Kepler elements using the Tudat library. Then the required ΔV is computed using the methods described by Wakker (2010). In this case, an instantaneous burn to change the inclination, flight-path angle and orbital velocity to match the desired orbit is assumed. From the ΔV for both methods, it can be determined, using the Tsiolkovsky rocket equation what the required propellant mass is. This then results in a final mass estimate for both the RKF and the TSI propagations.

6.3.6. COMPARISON
Finally, the end states of both TSI and RKF are compared to each other. The program provides the numeric difference between the position, velocity and mass as well as the quotient between those values. This quotient, or difference fraction, is the TSI state divided by the RKF state and the numeric difference is the TSI state minus the RKF state. These values were used in the verification and validation phase and are used during the thesis analysis as well to show the behaviour of TSI compared to RKF.
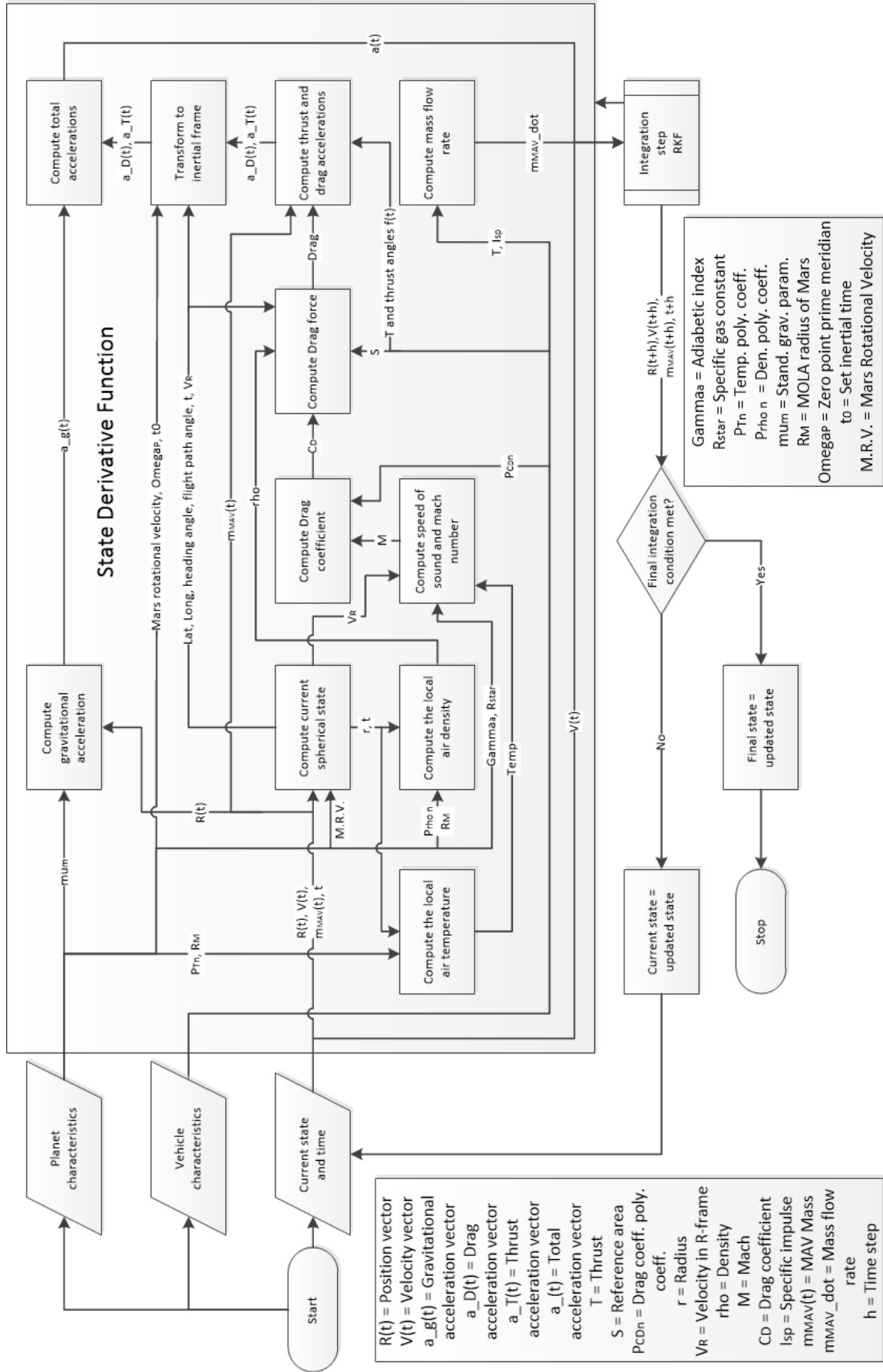
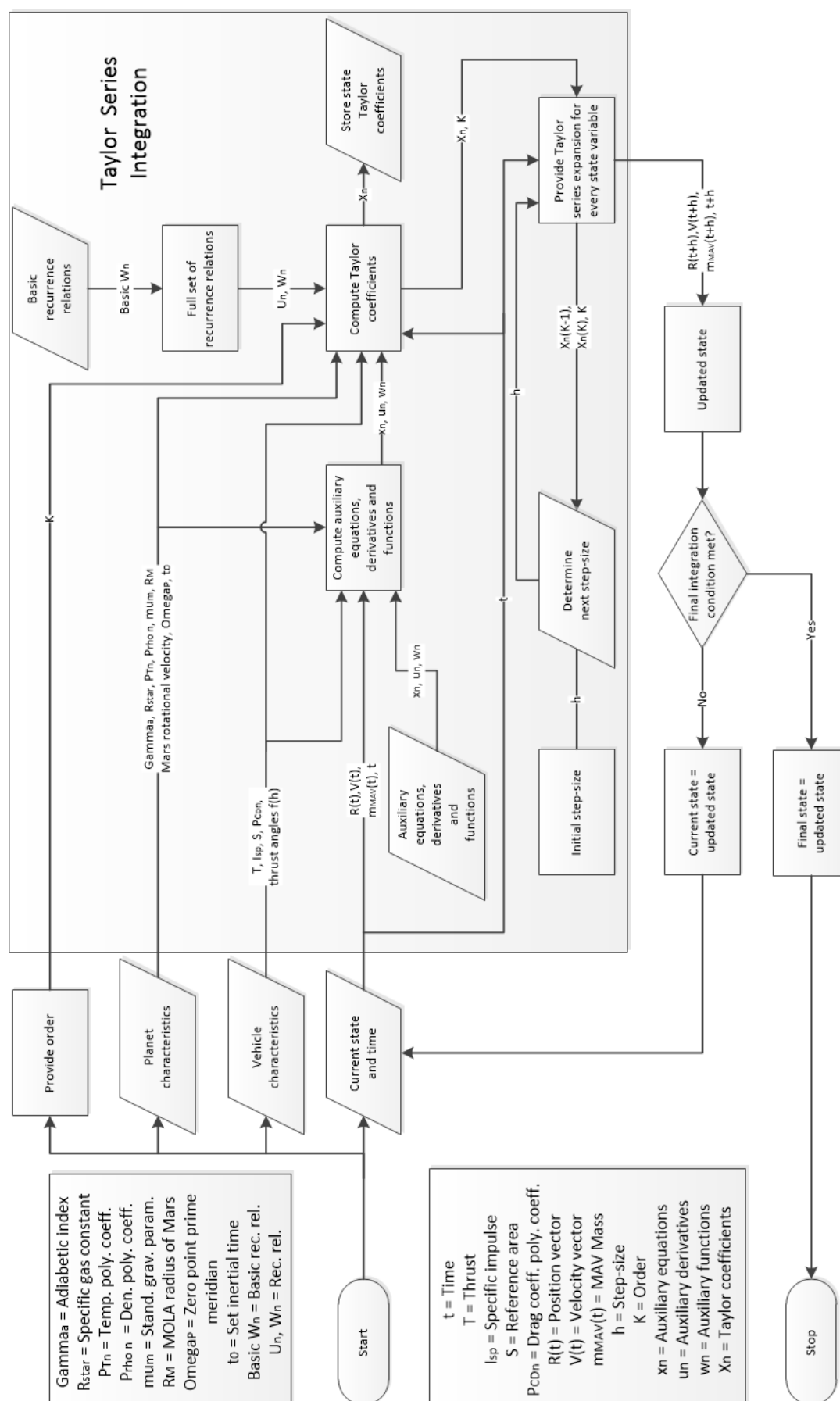Figure 6.2: RKF interface architecture

Figure 6.3: TSI architecture

7

VERIFICATION AND VALIDATION

Verification is the process of determining whether a program meets the requirements or not. Is it working the way it is suppose to? As soon as it works and produces output (verified), these outputs can be compared to other data from which it is known that it is correct. This is called validation. If a program is verified and validated, the outputs should be correct. Fortunately, all the existing software has already been validated, which means that they only still have to be verified to make sure everything is working properly on the simulation computer. Each of the software packages comes with tests which can be used to do this. If all the tests are passed it means that the software is verified for the computer and ready to use. Since Tudat shipped with Eigen and Boost, the Tudat test files also test these libraries. All the tests were passed, which means that the Tudat, Eigen and Boost libraries are working properly. However, because the integrators are an intricate part of this thesis, it was decided to perform a separate verification for the Runge-Kutta integrators. This verification is described in Section 7.1.

Mars-GRAM also came with its own verification test, where three delivered output files had to be replicated. These verification tests were also successful.

7.1. RK4 AND RKF INTEGRATORS

The tutorial page of the Tudat website (Dirkx *et al.*, 2016) offers two integration tutorials: one involving RK4 and another involving variable step-size Runge-Kutta methods including RKF. The objective of the tutorial is to get familiar with the different integration methods available in Tudat. At the same time, a small data table has to be reproduced, which also serves as a verification test. For each of the integrators the same problem was addressed: the computation of the velocity of a falling body after a certain amount of time assuming no drag. The results that had to be reproduced are presented in Table 7.1.

Table 7.1: Verification data for the standard integrators

End time [s]	1.0	5.0	15.0	25.0
Velocity [m/s]	-9.81	-49.05	-147.15	-245.25

The first script was written using the instructions from the tutorial and is called numericalintegrators.cpp. This script uses the rungeKutta4Integrator.h header file and the RungeKutta4IntegratorXd function from this header file. This function requires three inputs: the state derivative function (problem specific), the initial time and the initial state. Using the .integrateTo extension the end state at a certain end time can be computed. This requires the end time and the step-size. For RK4 the step-size is constant. This resulted in the same values as presented in Table 7.1.

The second script was used to test the variable step-size integrators RKF. This script is called rungekuttavariable.cpp and uses the rungeKuttaCoefficients.h and rungeKuttaVariableStepSizeIntegrator.h header files. In this case the RungeKuttaVariableStepSizeIntegratorXd function was used which requires the Runge-Kutta coefficients (from the respective header file), the state derivative function (problem specific), the initial time,

initial state, zero minimum step-size, infinite maximum step-size, relative tolerance and the absolute tolerance as inputs. In this case the integration can be done in individual steps using .performIntegrationStep with the current step-size as the only input. The current step-size is computed in the integration method itself, but in this case it is checked to make sure that the step-size does not take the function beyond the specified end time. The integration steps are then repeated until the end time is met. Running this script resulted in the same results as presented in Table 7.1 as well.

These results, combined with the fact that the test files for these two methods produced no errors is proof that they are working accordingly. Thus it can be said that the standard integration methods used in this thesis are verified and ready for use in the simulation tool. However, during the development of the trajectory propagation tools, the entire tool (including the integrators) will be verified again to determine the performance of the integrators.

For the actual propagation tool, the RKF method required the state derivative function associated with this particular ascent problem. The state derivative class was constructed using the state derivative functions as described in this thesis in the Cartesian coordinate system based on equations provided by Mooij (1994). The state is used to compute the required transformation angles first and then both the thrust and drag accelerations are transformed to the inertial frame. There they are combined with the gravitational acceleration resulting in the accelerations in the x-, y- and z-direction. This class was tested by itself by inputting certain values which would result in known outcomes. And those simple values by themselves provided the expected results. Later the state derivative function was combined with the RKF integrator in the trajectory propagation tool and verified again as will be described in Section 7.3.

The verification of the state derivative class took approximately one day.

7.2. TAYLOR SERIES INTEGRATION

In this section, the verification and validation of the TSI header and source file is described. This was done for each of the blocks shown in Figure 6.3. For the verification it was important that the running of the different classes and header/source files did not produce any obvious errors. For the validation, the results were often checked against manual calculations and expected behaviour. The verification and validation of TSI was a very lengthy process and required many rewrites of the used equations because of mistakes in the model or mistakes in the derivations. Section 7.3 talks a bit more about the model mistakes. This section has been divided into several subsections which showed similar issues during the verification and validation.

7.2.1. AUXILIARY EQUATIONS, DERIVATIVES AND FUNCTIONS

As shown by Figure 6.3 the first step in the TSI is to compute the auxiliary equations, derivatives and functions. The computations, in theory, are fairly straightforward, however it is really easy to make a mistake. During the initial verification of these different classes the outcomes were checked against simple manual solutions. Thus, provided a certain input, the output was known. This was an easy way to check any coding errors. Since the early versions of the code required a lot of equations, it took a long time to go through all the equations and find all the errors and mistakes. This was initially done with the combination of Cartesian coordinates and spherical transformation angles, however, later on more efficient equations were used for separate Cartesian and spherical cases. This also made it easier to identify mistakes in the equations and understand certain issues found during the validation process.

7.2.2. COMPUTING THE TAYLOR SERIES COEFFICIENTS AND THE UPDATED STATE

Once the auxiliary classes were verified, the Taylor Series coefficients could be computed using the basic recurrence relations and the full set of recurrence relations. For the Taylor Series coefficients it is important that they show a decreasing number series for each of the coefficients. This was the desired outcome that was used for the verification of the full set of recurrence relations. The basic recurrence relations were all checked by hand calculations to determine if they indeed worked the way that they were suppose to. The verified basic recurrence relations were used to verify the full set of recurrence relations. This class consists of the equations mentioned in Appendix E. When writing the full set of recurrence relations, it is really easy to make mistakes and there are a lot of rules that have to be taken into account as mentioned in Chapter 5. Therefore, a lot of time was spend on rewriting these equations in such a way that the outcomes were what was expected. Also, a number of these recurrence relations were checked by manual calculations. An often recurring problem was that the Taylor Series coefficients would show a diverging behaviour where the coef-

ficient would keep increasing to infinity (theoretically). This was often an indication that a writing mistake was made when setting up the full set of recurrence relations. Another easy way to identify mistakes during the validation process was to compute the next state. Should an error occur in the computation of the Taylor Series coefficients, this would usually result in very large increases in the state even if the coefficient itself would be relatively small. Then following the trail back to the largest change in Taylor Series coefficient, often a coding or writing mistake could be identified in the full set of recurrence relations.

7.2.3. NEXT STEP-SIZE

Fortunately, the step-size class was not a very large class and took less time to verify and validate. Provided a set of Taylor Series coefficients, the step-size class could be tested separately from the other files. The verification process was rather straight forward; the class should be able to provide a step-size estimate given the different input values. Also, when similar sets of Taylor Series coefficients were used, the output step-sizes should be rather similar. This was then also part of the validation process. A pure validation process was difficult because there were no reference Taylor series coefficients available, however an estimate for the order of the next step-size could be used. This can however still be improved. Two different step-size determination methods were tested, but in the end it was found that the direct method described by Scott and Martini (2008) and Bergsma (2015) showed more reasonable results and was easier to implement. Also, during the verification process, the iteration method failed to work properly which led to unusable results and the program failing. But the direct method worked very well.

7.3. COMPLETE TRAJECTORY PROPAGATION

For the complete trajectory propagation it was important to have the integrator method as the only difference between the RKF and the TSI propagation. First the initial values were provided and transformed into the proper coordinate system. These would then be fed into the integrator and at the end of the integration, the results would be printed. The verification and validation of the complete trajectory propagation have been split up into several phases.

7.3.1. PHASE 1: RKF PROPAGATION

This was first done for RKF because this method was already validated. Therefore, any mistakes or problems found would lead back to a mistake in the state derivative functions or the model itself. During this phase, a number of problems were identified; certain singularities were found, a limit to the tolerance value was determined for each of the RKF methods (DOPRIN87 does not converge fast enough in many cases for a value of 10^{-15}) and a mistake in the model was found where the wrong velocity was used to determine the drag acceleration. This meant that some of the model equations had to be rewritten for both RKF and TSI.

7.3.2. PHASE 2: BOTH RKF AND TSI

During the second phase of the verification, both RKF and TSI were tested at the same time and the outcomes were compared. Since the RKF method was verified and validated at this point, the outcome of the RKF propagation could be used to verify TSI. This was done using different test cases that focussed on different elements of the code.

Each element was tested separately by activating (or deactivating) the gravity, thrust and drag as well as the rotation of Mars. In each case, simple test cases were used to verify the class, such as: vertical drops from a certain altitude, thrusting in a known direction and flying parabolic trajectories. This was all done in each of the axis directions first and then combining the different axes. First the gravity was tested, then the thrust, then a combination of these two, followed by the drag all in the non-rotating case. The same was then done for the rotating case as well. This was initially done for a zero thrust elevation and thrust azimuth angle, such that the trust was acting directly through the x-axis of the body frame. Also, because the drag by definition works through the x-axis of the body frame, there should not be any accelerations in the y- and z-direction in the body frame. This simplified the problem and meant that some of the equations could be tested without involving all the other equations just yet.

During this phase it was discovered that there was an inconsistency in the manner in which the different accelerations were computed. Basically, the rotational angles were being computed using spherical equations which already incorporated the accelerations and then those angles were then used to transform the Cartesian coordinates and incorporate the accelerations again. Therefore it was decided to rewrite all the equations and actually come up with three different sets: two Cartesian models and one spherical model for

TSI. The associated equations were already described in Chapter 5.

7.3.3. Phase 3: three different models for TSI
The third phase consisted of verifying each of these three models in a similar manner as was done during the second phase. During this phase, it was discovered that a starting ground velocity too close to zero would cause singularities in both the Cartesian as well as the spherical model. This is why a small initial ground velocity was introduced, which seemed to work for the second Cartesian case (unit vector transformations) and the spherical case, however, the first Cartesian case (Euler angles) still did not work. At this point it was decided to focus on the other two methods instead because of time constraints. It was also found that the initial flight path angle could not be equal to (or close to) 90 degrees for the spherical case due to singularities in the model. This is why a value of 89 degrees was chosen for the test cases of that particular model. This worked well for gravity and thrust for the spherical and second Cartesian case. But not always.

7.3.4. Phase 4: one final TSI model
As it turned out, setting an initial ground velocity for the TSI models (Cartesian and spherical) was only a temporary solution and did not solve the problem. Apparently the initial second is vital for TSI and when the velocity is too small, the Taylor Series coefficients tend to increase in value. The solution was to off-set the initial conditions to a later point in the trajectory. This off-set was achieved by having the first second of the trajectory be integrated by RKF78 with a set tolerance of 10^{-15} (if the method and the tolerance was not set constant, the results of the integration would be inconsistent). When this was applied to the propagation involving TSI the Taylor Series coefficients dropped to an acceptable number again which could then be used to determine the next state. This worked really well for the spherical case, however the second Cartesian case still had some bugs (either in the model or in the coding). Again, due to time constraints it was decided to solely continue with the spherical model and use that for the rest of the thesis work. This is the reason that an initial propagation phase was needed as was described in Section 6.3. At the end of the phase, the TSI code was deemed verified, since it showed similar results to the RKF propagation.

7.3.5. Phase 5: coasting and circularisation
Once the TSI method was verified, the rest of the trajectory propagation could be added. For the coasting phase this meant that the thrust had to be set equal to zero at the point of main engine cut-off. Fortunately, this was a simple change in class value for the TSI method, however this did not work for RKF. Instead it was discovered that because of the manner in which the state derivative class is set-up and used in the integrator itself, the class had to be re-initialized if anything in the state derivative class changed. Therefore, a new integration had to be started for RKF at main engine cut-off.

Because the circularisation is treated as an instantaneous burn, this only affected the total propellant mass and velocity of the MAV. Therefore, it could be treated with simple circularisation equations described by Wakker (2010). The velocity required to reach a perfect desired circular orbit can be computed. Then because the equations are simple and can be solved by hand, the code could be verified (and validated) by using simple cases computed using the program and then compared to the hand written solutions.

7.3.6. Phase 6: tool validation
The most important part of this thesis is the comparison between RKF and TSI, therefore these two methods should produce results that can be compared and where the only difference is the manner in which they were computed. Provided that the RKF method is verified and validated, TSI could be validated using RKF with this purpose as mentioned before. However, besides this validation, it should also be checked if these solutions represent a real-life solution to the problem. This means validating both methods against other validated simulations outcomes from other people. Unfortunately, no flight data is available for a Mars Ascent case yet. Two JPL internal sources were found that could potentially be used to validate the software: Woolley (2015) and Benito and Johnson (2016). Woolley used an analytical model to approximate an ascent trajectory for different launch cases and conditions, one of which was a SSTO launcher which was used for validation. Benito on the other hand used a high-fidelity simulation program to simulate the ascent trajectory of some of the newer concept MAV designs numerically. Some of the latest data was provided and was also used for the validation.

In Table 7.2 are the validation numbers provided associated with the simulated trajectory of the case as presented by Woolley. The left columns show the inputs that were provided and the inputs that were used in the program. The right columns show the results of the simulation as provided and as computed by the program. The thrust angles in that column represent the required thrust angles that were needed as input to get the desired outcome.

Table 7.2: Validation case 1: SSTO Woolley

Provided parameters	Given	Used	Provided parameters	Given	Computed
Thrust [kN]	3.56	3.56	Propellant mass [kg]	202.2	202.07
I$_{sp}$ [s]	256	256	Burn-out angle [deg]	6	5.344
Burn Time [s]	142.6	142.5	Circularisation ΔV [m/s]	181	159.6
MAV GLOM [kg]	267.4	267.4	Ascent time [s]	1757	1796.27
Launch altitude [km MOLA]	-	-0.6	Thrust azimuth [deg]	-	-0.299
Launch latitude [deg]	0.0	0.0	Thrust elevation [deg]	-	-0.184
Launch longitude [deg]	-	74.5			
Launch ground velocity [km/s]	-	$1 \cdot 10^{-5}$			
Launch Flight-path angle (FPA) [deg]	90	89			
Launch Azimuth [deg]	90	90			
Desired altitude [km MOLA]	390	390			
Desired inclination [deg]	45	45			

It can be seen that there are some differences, however in this case the validation is to prove that the trajectory computed by the simulation program is indeed a viable trajectory (so close to a reference trajectory). This is because that is enough to compare the RKF and TSI methods. The plotted trajectories are shown in Figures 7.1 to 7.4.
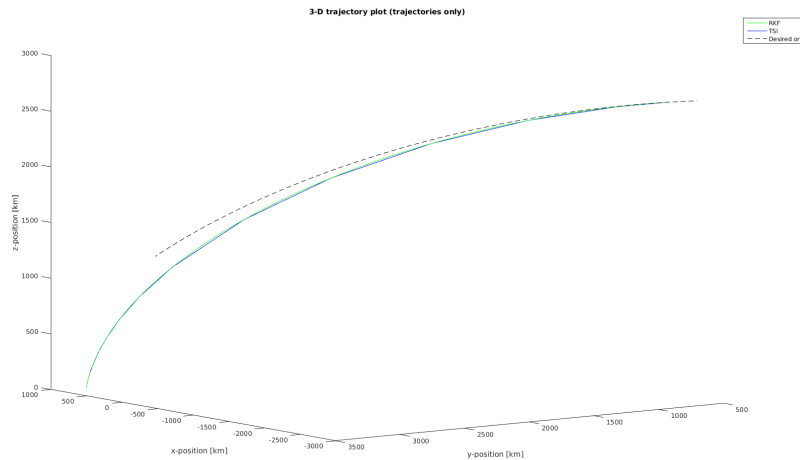
Figure 7.1: Case 1 3-D trajectory

A similar validation was done using the second case. However, in this case the reference trajectory was provided. But the main difference here was that the simulation program still was only able to use a constant thrust elevation and azimuth angle. Therefore, the exact profile could not be matched. Benito also included extra perturbing effects creating another difference. However, it was possible to get a trajectory close to the one provided, which is enough for all current purposes. Table 7.3 shows the used values and computed parameter values for case 2 (similar to case 1).

Again, the trajectory was visualised, however, this time the reference trajectory was also known. In the figures this is represented by a red line. These are shown in Figures 7.5 to 7.8.

The difference in trajectory can mainly be explained by the thrust elevation and thrust azimuth angle

Figure 7.2: Case 1 2-D trajectory as seen from the x-axis
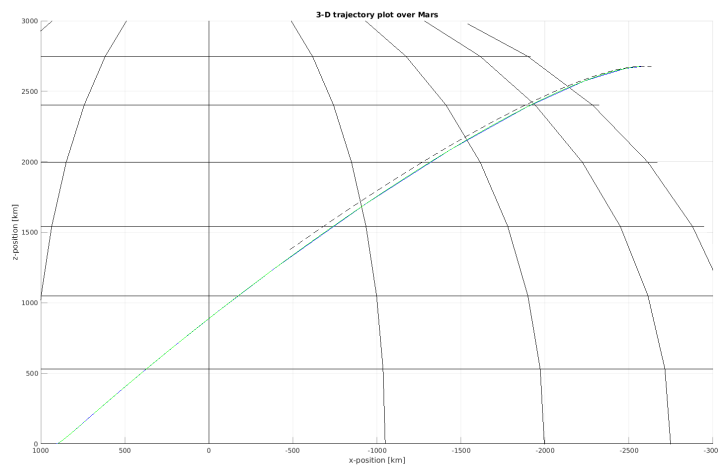
Figure 7.3: Case 1 2-D trajectory as seen from the y-axis

Table 7.3: Validation case 2: SSTO Benito

Provided parameters	Given	Used	Provided parameters	Given	Computed
Thrust [kN]	6.1087	6.0187	Propellant mass [kg]	213.85	213.85
I_{sp} [s]	315.9	315.9	Burn-out angle [deg]	-	15.644
Burn Time [s]	99.362	99.362	Circularisation ΔV [m/s]	757.57	594.74
MAV GLOM [kg]	288.96	288.96	Ascent time [s]	949.12	876.09
Launch altitude [km MOLA]	-0.8	-0.6	Thrust azimuth [deg]	-	-0.7273
Launch latitude [deg]	0.0	0.0	Thrust elevation [deg]	-	-0.674
Launch longitude [deg]	90	90			
Launch ground velocity [km/s]	$1 \cdot 10^{-6}$	$1 \cdot 10^{-6}$			
Launch FPA [deg]	90	89			
Launch Azimuth [deg]	90	90			
Desired altitude [km MOLA]	479.19	479.19			
Desired inclination [deg]	92.69	92.69			
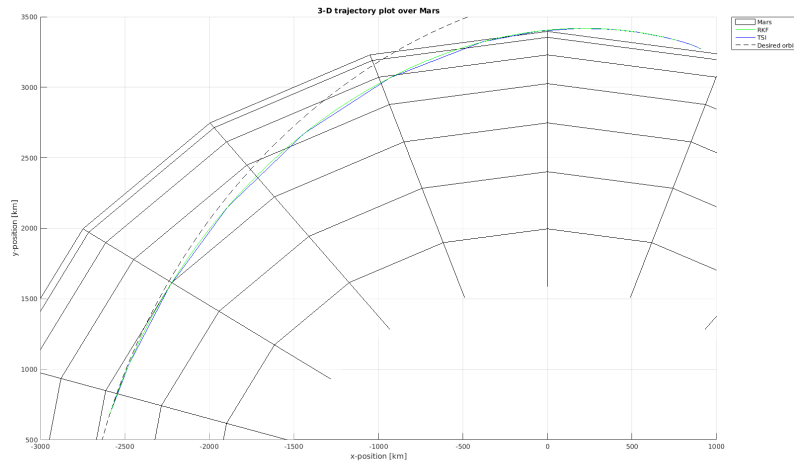
Figure 7.4: Case 1 2-D trajectory as seen from the z-axis
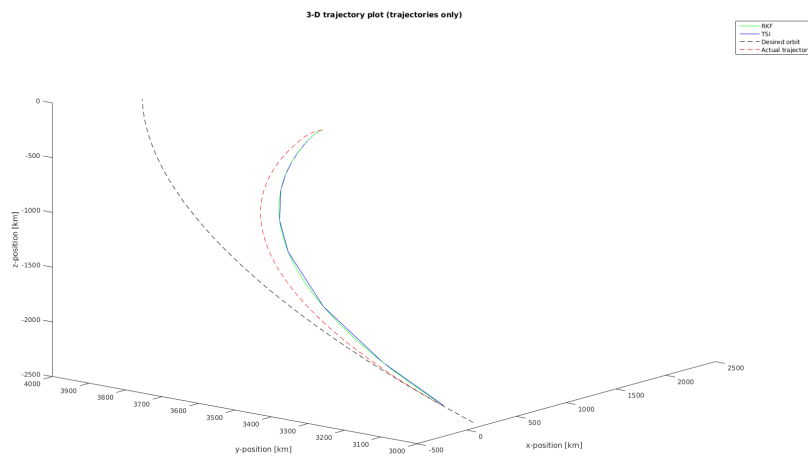
Figure 7.5: Case 2 3-D trajectory

curve of the reference trajectory. This curve was derived from the thrust data provided by Benito. This curve is shown in Figure 7.9.
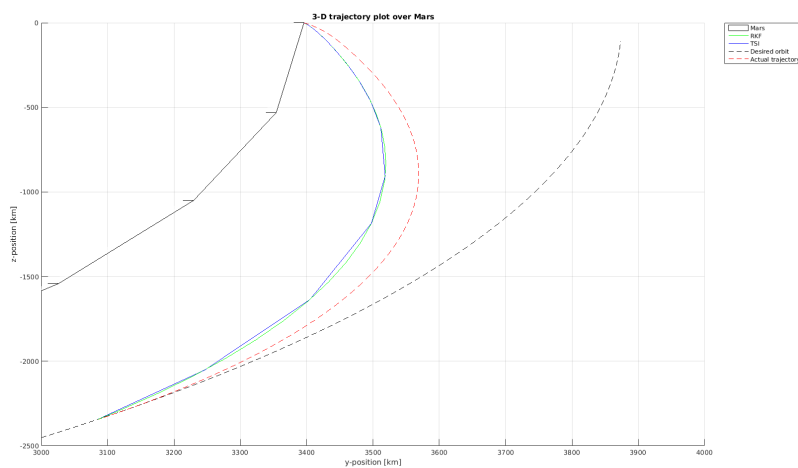
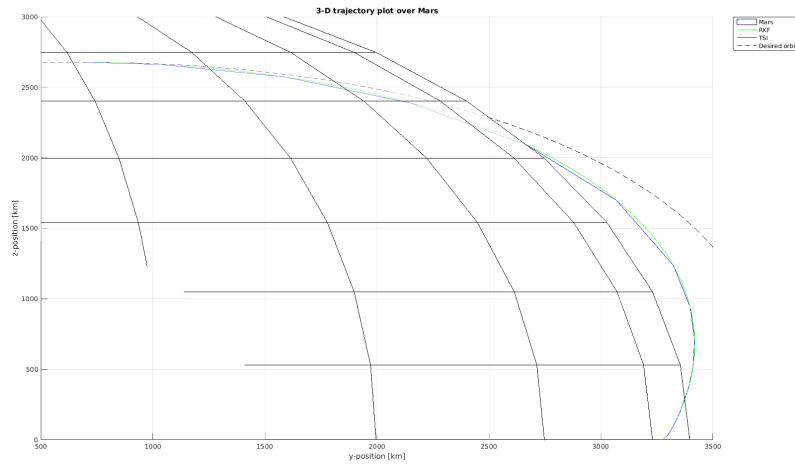Figure 7.6: Case 2 2-D trajectory as seen from the x-axis
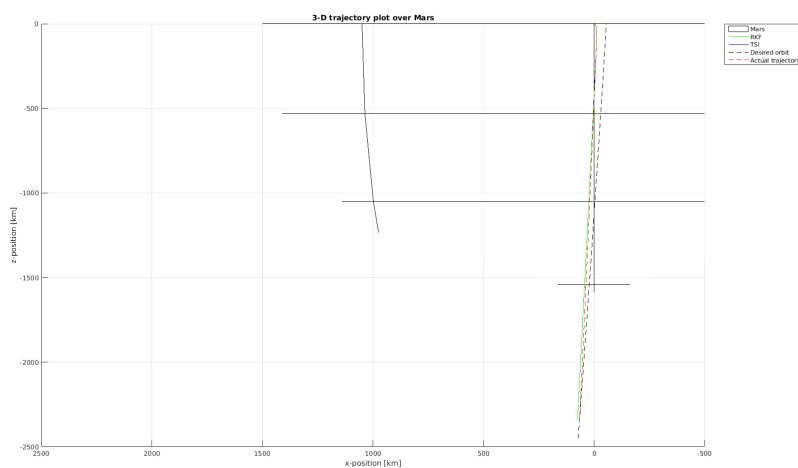
Figure 7.7: Case 2 2-D trajectory as seen from the y-axis
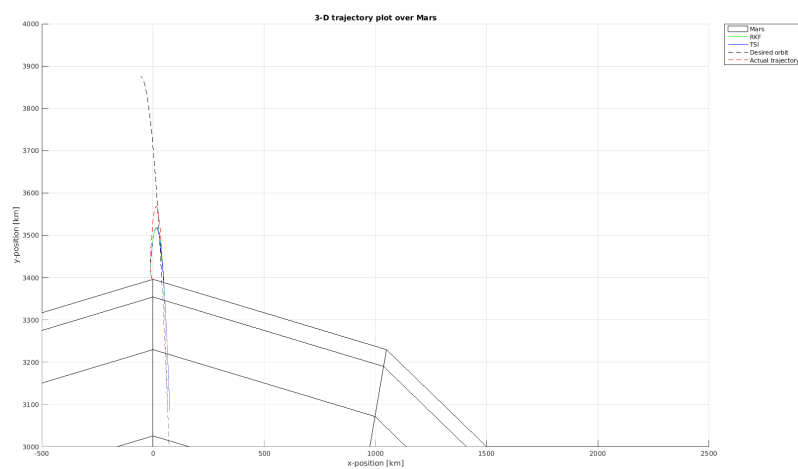
Figure 7.8: Case 2 2-D trajectory as seen from the z-axis
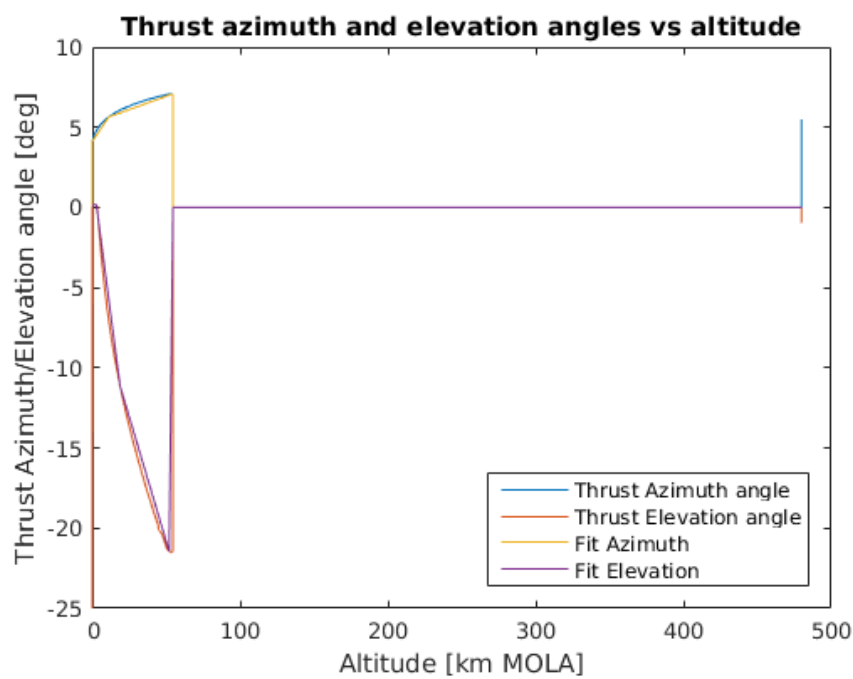
Figure 7.9: Case 2 thrust elevation and azimuth angle curve.

8

RESULTS

9
ANALYSIS

10

CONCLUSIONS AND RECOMMENDATIONS

BIBLIOGRAPHY

R. Shotwell, J. Benito, A. Karp, and J. Dankanich, *Drivers, developments and options under consideration for a Mars ascent vehicle,* in *Aerospace Conference, 2016 IEEE* (IEEE, 2016) pp. 1–14.

R. C. Woolley, R. L. Mattingly, J. E. Riedel, and E. J. Sturm, *Mars Sample Return - Launch and Detection Strategies for Orbital Rendezvous,* in *AAS/AIAA Astrodynamics Specialist Conference,* Vol. 142 (Univelt, Inc., 2011).

J. Fanning and B. Pierson, *A model comparison for optimal Mars ascent trajectories,* in *Engineering Optimization,* Vol. 26 (1996) pp. 271–285.

P. Desai, R. Braun, W. Engelund, F. Cheatwood, and J. Kangas, *Mars Ascent Vehicle Flight Analysis,* in *7th AIAA/ASME Joint Thermophysics and Heat Transfer Conference* (1998).

J. C. Whitehead, *Mars Ascent Propulsion Trades with Trajectory Analysis,* in *40th AIAA/ASME/SAE/ASEE Joint Propulsion Conference and Exhibit* (American Institude of Aeronautics and Astronautics, 2004).

J. C. Whitehead, *Trajectory analysis and staging trades for smaller Mars ascent vehicles,* in *Journal of spacecraft and rockets,* Vol. 42 (2005) pp. 1039–1046.

E. Di Sotto, J. C. Bastante, and R. Drai, *System and GNC concept for RendezVous into elliptical Orbit for Mars Sample Return mission,* in *AIAA Guidance, Navigation, and Control Conference and Exhibit, Colorado* (2007).

M. Trinidad, E. Zabrensky, and A. Sengupta, *Mars Ascent Vehicle system studies and baseline conceptual design,* in *Aerospace Conference, 2012 IEEE* (IEEE, 2012) pp. 1–13.

E. Dumont, *Design of a Modular Transportation System for Future Lunar Robotic Missions,* in *30th ISTS/34th IEPC/6th NSAT Joint Conference, Kobe, Japan* (2015).

R. C. Woolley, *A simple analytic model for estimating Mars Ascent Vehicle mass and performance,* in *2015 IEEE Aerospace Conference* (2015).

J. Benito and B. J. Johnson, *Trajectory Optimization for a Mars Ascent Vehicle,* in *AIAA/AAS Astrodynamics SPecialist Conference* (2016).

O. Montenbruck, *Numerical integration of orbital motion using Taylor series,* in *Spaceflight mechanics* (1992) pp. 1217–1231, available at JPL library.

J. R. Scott and M. C. Martini, *High speed solution of spacecraft trajectory problems using Taylor series integration,* in *AIAA/AAS Astrodynamics Specialist Conference and Exhibit, Honolulu, Hawaii* (2008).

M. Bergsma and E. Mooij, *Application of Taylor-Series Integration to Reentry Problems with Wind,* in *Journal of Guidance, Control, and Dynamics* (American Institute of Aeronautics and Astronautics, 2016) pp. 2324–2335.

J. Whitehead, *Mars ascent propulsion options for small sample return vehicles,* in *33rd AIAA/ASME/SAE/ASEE Joint Propulsion Conference and Exhibit* (AIAA Joint Propulsion Conference and Exhibit, 1997).

C. S. Guernsey, *Mars Ascent Propulsion System (MAPS) Technology Program: Plans and Progress,* in *34th AIAA/ASME/SAE/ASEE Joint Propulsion Conference and Exhibit* (1998).

C. Stone, *Rice Mars,* presentation/website (1999), [online database], URL: http://www.slideshare.net/cliffordstone/rice-mars-nov99 [cited 25 October 2015].

D. Stephenson, *Mars ascent vehicle - Concept development,* in *38th Joint Propulsion Conference and Exhibit, Indianapolos, Indiana,* Vol. 4318 (AIAA, 2002).

D. D. Stephenson and H. J. Willenberg, *Mars ascent vehicle key elements of a Mars Sample Return mission,* in *Aerospace Conference, 2006 IEEE* (IEEE, 2006) p. 11.

A. Sengupta, A. Kennett, M. Pauken, M. Trinidad, and E. Zabrensky, *Systems Engineering and Technology Considerations of a Mars Ascent Vehicle,* in *2011 IEEE Aerospace Conference* (2012).

G. Mungas, D. Fisher, J. Vozoff, and M. Villa, *NOFBX Single Stage to Orbit Mars Ascent Vehicle,* in *Aerospace Conference, 2012 IEEE* (IEEE, 2012) pp. 1–11.

Mars Program Planning Group, *Summary of the Final Report,* (2012), [online database], URL: http://www.nasa.gov//sites/default/files/files/ [cited 14 October 2015].

D. Vaughan, B. Nakazono, A. Karp, R. Shotwell, A. London, A. Mehra, and F. Mechentel, *Technology development and design of liquid bi-propellant mars ascent vehicles,* in *Aerospace Conference, 2016 IEEE* (IEEE, 2016) pp. 1–12.

A. C. Karp, M. Redmond, B. Nakazono, D. Vaughan, R. Shotwell, G. Story, D. Jackson, and D. Young, *Technology development and design of a hybrid Mars ascent vehicle concept,* in *Aerospace Conference, 2016 IEEE* (IEEE, 2016) pp. 1–10.

R. Shotwell, *History of Mars Ascent Vehicle development over the last 20 years,* in *Aerospace Conference, 2016 IEEE* (IEEE, 2016) pp. 1–11.

E. Mooij, *The motion of a vehicle in a planetary atmosphere* (Delft University Press, Delft, 1994).

C. Ho, N. Golshan, and A. Kliore, *Radio Wave Propagation Handbook for Communication on and Around Mars,* 1st ed. (NASA Jet Propulsion Laboratory, Pasadena, CA, 2002) handbook JPL Publication 02-5.

D. Williams, *Mars Fact Sheet,* website (2015), [online database], URL: http://nssdc.gsfc.nasa.gov/planetary/factsheet/marsfact.h [cited 1 November 2015].

R. Hofsteenge, *Computational Methods for the Long-Term Propagation of Space Debris Orbits,* Master's thesis, Delft University of Technology (2013).

A. Milani and A. M. Nobili, *Integration error over very long time spans,* in *Celestial mechanics,* Vol. 43 (Springer, 1987) pp. 1–34.

R. Noomen, *ae4-878.integrators.v4-3,* Lecture slides, Delft University of Technology (2013a), [Internal publication] Course: Mission Geometry and Orbit Design.

P. Deuflhard, U. Nowak, and U. Poehle, *Program Descriptions of ELib,* (1994), [online database], URL: http://elib.zib.de/pub/elib/codelib/difex2/readme [cited 30 October 2015].

O. Montenbruck, *Numerical integration methods for orbital motion,* in *Celestial Mechanics and Dynamical Astronomy,* Vol. 53 (1992) pp. 59–69.

J. Dormand, M. El-Mikkawy, and P. Prince, *Families of Runge-Kutta-Nystrom formulae,* in *IMA Journal of Numerical Analysis,* Vol. 7 (1987) pp. 235–250.

E. Fehlberg, *Low order classical Runge-Kutta formulas with stepwise control,* Tech. Rep. (Marschall Space Flight Center, NASA, 1969) : NASA TR R-316.

E. Fehlberg, *Classical fifth-, sixth-, seventh-, and eighth-order Runge-Kutta formulas with stepsize control,* Tech. Rep. (Marschall Space Flight Center, NASA, 1968) : NASA TR R-287.

M. M. Berry, *A Variable-Step Double-Integration Multi-Step Integrator,* Ph.D. thesis, Virginia Polytechnic Institute and State University (2004).

J. Meijaard, *A Comparison of Numerical Integration Methods with a View to Fast Simulation of Mechanical Dynamical Systems,* in *Real-Time Integration Methods for Mechanical System Simulation,* Vol. 69 (Springer, 1991) pp. 329–343.

H. Ramos and J. Vigo-Aguiar, *Variable stepsize Störmer-Cowell methods,* in *Mathematical and Computer Modelling,* Vol. 42 (2005) pp. 837–846.

D. Dirkx, K. Kumar, E. Doornbos, E. Mooij, and R. Noomen, *TUDAT,* (2016), [online database], URL: tudat.tudelft.nl [cited 8 March 2016].

P. Prince and J. Dormand, *High order embedded Runge-Kutta formulae,* in *Journal of Computational and Applied Mathematics*, Vol. 7 (Elsevier, 1981) pp. 67–75.

M. Weeks and S. Thrasher, *Comparison of Fixed and Variable Time Step Trajectory Integration Methods for Cislunar Trajectories,* in *AAS/AIAA Space Flight Mechanics Meeting* (2007).

M. C. W. Bergsma, *Application of Taylor Series Integration to Reentry Problems,* Master's thesis, Delft University of Technology (2015).

R. Noomen, *ae4-878.basics.v4-14,* Lecture slides, Delft University of Technology (2013b), [Internal publication] Course: Mission Geometry and Orbit Design.

A. Jorba and M. Zou, *A Software Package for the Numerical Integration of ODEs by Means of High-Order Taylor Methods,* in *Experimental Mathematics*, Vol. 14 (Taylor & Francis, 2005) pp. 99–117.

H. L. Justh and C. G. Justus, *Utilizing Mars global reference atmospheric model (Mars-GRAM 2005) to evaluate entry probe mission sites,* Presentation (2008), [online database], URL: https://smartech.gatech.edu/bitstream/handle/1853/26375/34-186-1-PB.pdf?sequence=1 [cited 10 December 2015].

K. Wakker, *Astrodynamics-II Course AE4874, part 2,* Reader, Delft University of Technology (2010), [Internal publication] Course: Astrodynamics-II.

A

REFERENCE SYSTEM TRANSFORMATIONS

When considering the position, velocity and acceleration of a space vehicle, different reference frames are usually used. Why there are different frames, which frames are required, what they are used for and how to transfer from one frame to the other will be discussed in Appendices A.1 and A.2. In case of, for instance, a car travelling on the road, a certain coordinate system has to be used to measure the velocity in a certain direction. For the car it can be said that a Cartesian system is used with x in the direction of motion, z pointing towards the ground and y then pointing to the right if looking in the direction of motion (using the so-called RHR to complete the frame). The speed is then measured and expressed in the x-direction. This works well when a vehicle is travelling in a straight line or on a flat plane, but in orbital mechanics the motion usually has to be described just above or in an orbit around a (spherical) body. Therefore it is important to know which coordinate system is used and how to change between these coordinate systems should the other system become more convenient to use at a certain point. In Appendix A.3 the difference between these coordinate systems and how to transfer from one to the other is explained.

A.1. REQUIRED REFERENCE SYSTEMS

In the example of the car, the Frame of Reference (RF) is fixed to the Earth. However, when considering two cars driving on the same road, one might like to investigate the difference in velocity between both vehicles. In that case an RF is chosen that is fixed to one of the two cars. This makes it easier to determine the relative velocity of one car with respect to the other. The same can be done for s/c (think of formation flying). There are therefore a number of different RFs that can be used. In this section the required RFs and their application will be presented.

A.1.1. MARS-CENTRED INERTIAL RF (I-FRAME)

The Mars-centred inertial (MCI) reference frame is an RF that is, as the name implies, fixed to the centre of mass of Mars (**?**). It is a frame in which Mars still rotates with respect to that frame, or in other words it is an inertial frame with respect to Mars. The x-axis is defined through a certain point which can be set by the user. This means that the user can determine his or her own inertial frame. A frame that is often used (and which is based on J2000[1]) is the MARSIAU frame **??**. This is a Mars inertial frame that is translated from the Earth J2000 frame. For the translation of J2000 a point through the mean equator of Mars is specified where the equator ascends through the mean equator of Earth. The x-axis is defined through this point. The z-axis is then defined through the rotational axis of Mars and the y-axis completes the frame through the RHR. The translation is described in **??** using the J2000 numbers from **?**. The generic inertial frame is shown in Figure A.1. The centre of the frame is represented by the letter 'A'. The MARSIAU frame is required if certain data from outside sources will have to be incorporated into the simulation, however for the actual simulation and optimisation it will be easier and much more straightforward to define a custom Mars inertial reference frame.

This reference system is very useful if the motion of the s/c with respect to the ground-track is not important.

---

[1] J2000 is an Earth referenced inertial frame that was set through the rotational axis of Earth (z-axis) and through the vernal equinox (x-axis). The reference was set on the Julian date of 2451545.0 or 01-01-2000 at 12:00 Greenwich Mean Time (GMT).
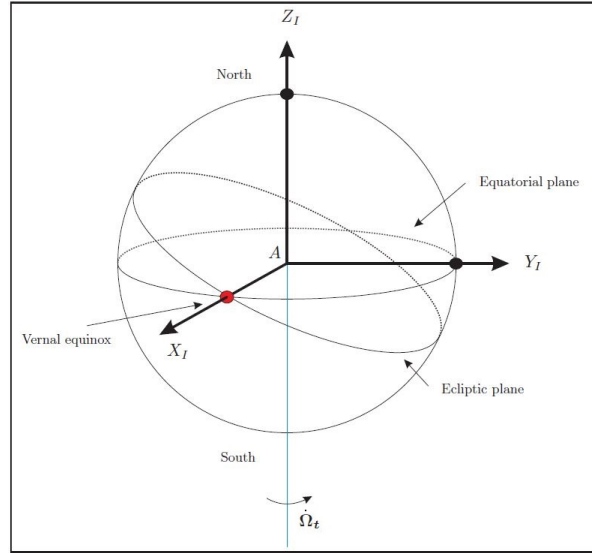
Figure A.1: Graphical definition of the Mars-centred inertial reference frame **?**.

A.1.2. MARS-CENTRED MARS-FIXED RF (R-FRAME)

The Mars-centred Mars-fixed (MCMF) frame is the same as the MCI frame except for one distinct difference. The x-axis of the MCMF frame (x_R) is defined through the 0.5 km wide Airy-0 crater **?** which has a latitude of 5.07829°S **?**. The associated meridian is called the prime meridian. On 1 January 2000 at 12:00 the prime meridian of Mars was 176.630° east of the x-axis in the MARSIAU frame (which is important when transforming from the MARSIAU frame to the current MCMF frame)**??**. Because the Airy-0 crater is fixed to the surface of Mars and rotates around the Martian rotational axis (in both MCI and MCMF the z-axis), the MCMF is also a rotational frame. This frame rotates with Mars and can therefore be very useful for ground observation purposes. In the case of the MAV it is important to take the rotational velocity of Mars into account, since Mars will be rotating underneath the MAV causing rotational effects. A graphical representation of the MCMF frame is provided in Figure A.2. An angle Ω_P is defined as the relative angle between the prime meridian and the x-axis of the MCI frame at the time that the inertial frame was defined.
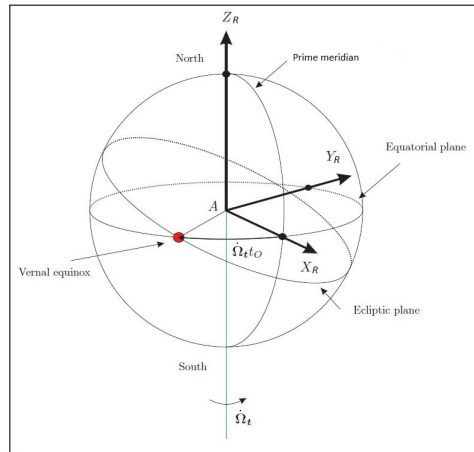
Figure A.2: Graphical definition of the Mars-centred Mars-fixed reference frame **?**. Source: NASA

A.1.3. VERTICAL RF (V-FRAME)

This next RF can be used to describe the motion of an s/c in orbit around a planet. The centre of the vertical frame is defined in the centre of gravity of the s/c **?** but is not rotationally fixed to it. This means that the frame can rotate with respect to the s/c itself. This is because the x-axis is set to point to the north pole of Mars. The z-axis is perpendicular to Mars' surface (or points to the centre of Mars assuming Mars is a sphere)

and the y-axis then points due east. The x-y plane is tangent to Mars' geoid. Figure A.3 shows the vertical frame denoted by the letter 'V' at an arbitrary position around Mars compared to the MCI frame. The centre of the frame is defined by the letter 'G'. The vertical frame relates to the Mars rotational frame through the latitude and longitude.
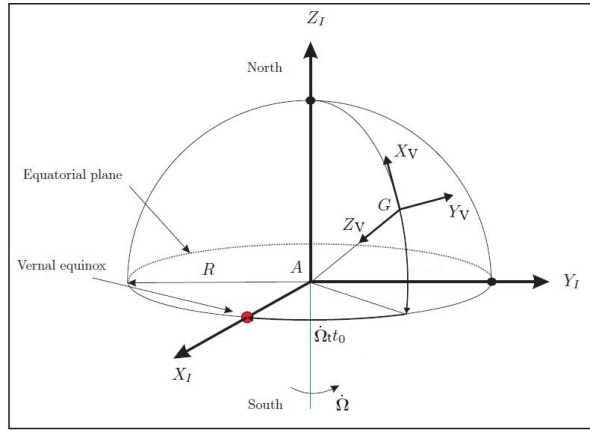
Figure A.3: Graphical definition of the Vertical reference frame compared to the Mars-centred inertial frame **?**.

A.1.4. BODY-FIXED RF (B-FRAME)

The body-fixed BF frame is fixed to the s/c body and therefore rotates with the s/c as well. The origin of the BF RF can be defined in the centre of symmetry (or the middle of the s/c). The axis orientation can be chosen to be in any direction. In this case the x-axis is defined through the vehicle-centre line and goes through the "nose" of the s/c, the z-axis is defined towards the orbiting body (when assuming an orbiting vehicle) and the y-axis completes the frame through the RHR. An example of a body frame that can be applied to the MAV is provided in Figure A.4.
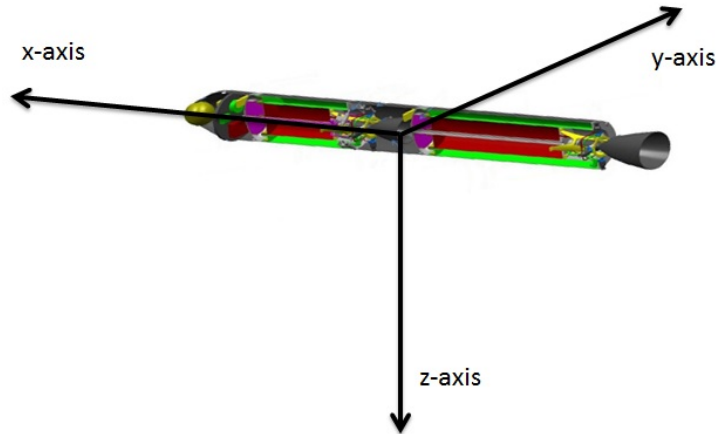
Figure A.4: Graphical example of a Body-fixed reference frame for the MAV Trinidad *et al.* (2012).

The axes of the body frame are denoted by a 'B' in this report. In the thesis problem the body frame relates directly to the vertical frame through the flight-path angle γ and the heading (or azimuth) angle χ, because the x-axis of the body frame coincides with the velocity vector of the s/c.

A.1.5. PROPULSION RF (P-FRAME)

The propulsion or thrust frame is a body frame where the x-axis is defined by the thrust vector. The y-axis is defined in the same plane as the x and y-axes of the B-frame. Then the z-axis completes the frame through the RHR as depicted in Figure A.5.

The B-frame and P-frame are related through the thrust elevation gimbal angle ϵ_T and the thrust azimuth gimbal angle ψ_T.
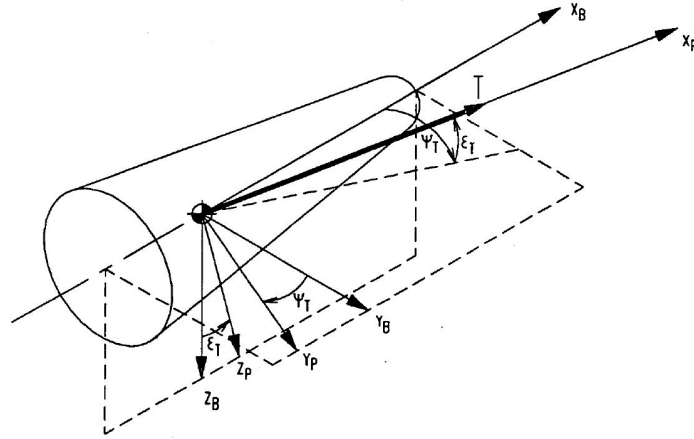
Figure A.5: Propulsion frame relative to the body frame Mooij (1994).

A.2. TRANSFORMATION BETWEEN REFERENCE FRAMES

Because different problems and situations are easier to understand and to formulate in different RFs, it is important to understand how to transform from one RF to the other. In this case only transformations for a set point in time, called static transformations, are required for the described thesis problem. The necessary transformations for this thesis problem are described in this section.

For a transformation between two RFs, a correlation has to exist. This correlation (orientation) can be described using a set of angles, called the Euler angles, between the different RFs **?**. In a 3-dimensional space, there are three axes. So to get from one RF to the other, a maximum of 3 rotations (translations/transformations) have to take place; one over each axis. However, often fewer rotations are necessary because some of the axes are already properly aligned. Sometimes two reference frames are not directly related through known angles, which means that other (intermediate) RFs will have to be used. In this case more than 3 rotations are possible, but again a maximum of three rotations are needed to go from one RF to an intermediate RF given the known angles. Since a 3-dimensional space is described, 3-dimensional coordinates have to be translated to the next reference frame. For this, Cartesian coordinates are used. A rotation around the x-axis can be described by the change in the y- and z-coordinates over an angle ϕ in the yz-plane as visualized in Figure A.6. The rotation around the x-axis follows the RHR of rotation, which states that if the thumb of your right hand is pointed in the axis direction, then the rest of your fingers show the direction of positive orientation. Therefore the described rotation is positive. Should the rotation have been in the other direction (clockwise around the x-axis as seen in Figure A.6), the angle would have been negative. This is very important in transformations, and its usefulness becomes more obvious when more transformations are performed after each other. But first a system of equations is required to transform from the 'i' frame to the 'j' frame.

From Figure A.6 a relation can be described between the coordinates in the 'i' frame and the 'j' frame in matrix form. This relation (convention as by **?**) is shown by Equation (A.1). Here, $\mathbf{r}$ is the position vector and $\mathbb{T}_{\mathbf{x}}(\phi)$ represents the x-axis transformation matrix and is the standard matrix to be used if a transformation around an x-axis is performed. The only parameter that changes is the angle.

$$\begin{pmatrix} x \\ y \\ z \end{pmatrix}_j = \begin{bmatrix} 1 & 0 & 0 \\ 0 & \cos\phi & \sin\phi \\ 0 & -\sin\phi & \cos\phi \end{bmatrix} \begin{pmatrix} x \\ y \\ z \end{pmatrix}_i \Rightarrow \mathbf{r}_j = \mathbb{T}_{\mathbf{x}}(\phi)\mathbf{r}_i \tag{A.1}$$

This rotation described by Figure A.6 and Equation (A.1) can also be described for rotations around the y-axis and the z-axis. The complete set of axis transformation matrices is then presented in Equation (A.2).

$$\mathbb{T}_{\mathbf{x}}(\phi) = \begin{bmatrix} 1 & 0 & 0 \\ 0 & \cos\phi & \sin\phi \\ 0 & -\sin\phi & \cos\phi \end{bmatrix}, \mathbb{T}_{\mathbf{y}}(\phi) = \begin{bmatrix} \cos\phi & 0 & -\sin\phi \\ 0 & 1 & 0 \\ \sin\phi & 0 & \cos\phi \end{bmatrix}, \mathbb{T}_{\mathbf{z}}(\phi) = \begin{bmatrix} \cos\phi & \sin\phi & 0 \\ -\sin\phi & \cos\phi & 0 \\ 0 & 0 & 1 \end{bmatrix} \tag{A.2}$$

From now on, the cosine notation will be shortened to 'c' and the sine notation will be shortened to 's' to make the transformation matrices more comprehensive. Also, because the matrices are orthogonal, the
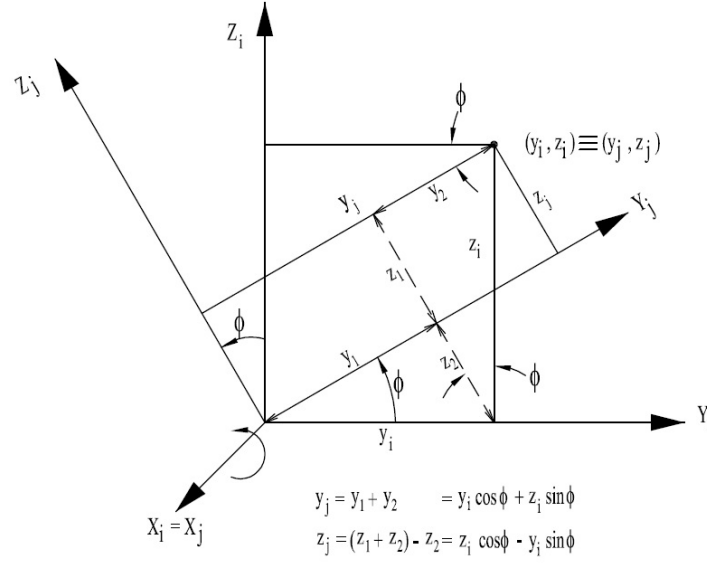
Figure A.6: General rotation around the x-axis **?**.

inverse of the matrix is simply the transpose of the matrix. The inverse of a rotation matrix is the rotation in the other direction.

The order, or sequence, in which these transformations are performed is very important. This is because the sequence results in a matrix multiplication equation, and from linear algebra it is known that $\mathbf{A} \cdot \mathbf{B} \neq \mathbf{B} \cdot \mathbf{A}$. Therefore, if the sequence of transformations is not correct, the resulting RF will not be the desired RF. Also, as mentioned before, it is not always possible or easy to transform from one RF directly into the other. So usually one of the afore mentioned RF is used as an intermediate RF. It is therefore possible to transform from the P-frame all the way to the I-frame using all the other mentioned RFs with a maximum of three rotations between each frame. For convenience it has been chosen to adopt the convention mentioned in **?** and **?** to describe the transformations. Therefore the I-frame, R-frame, V-frame, B-frame and P-frame will be known as F_I, F_R, F_V, F_B and F_P respectively when used to indicate the RFs in equations. And because these equations involve matrix multiplications, they have to be executed from right to left. Therefore it can be said that the transformation matrix to go from $F_B \rightarrow F_R$ is $\mathbb{T}_{\mathbf{RB}} = \mathbb{T}_{\mathbf{RV}}\mathbb{T}_{\mathbf{VB}}$. This is one of the transformations required for the MAV trajectory. The other two transformations are more straightforward: $F_P \rightarrow F_B$ is $\mathbb{T}_{\mathbf{BP}}$ and $F_R \rightarrow F_I$ is $\mathbb{T}_{\mathbf{IR}}$. For the $\mathbb{T}_{\mathbf{IR}}$ matrix , a transition is performed from $F_R \rightarrow F_I$. This is done over the angle $\dot{\Omega}_t t_O$ as defined in Figure A.2. $\dot{\Omega}_t$ is the rotational velocity of Mars and t_O is the time from the set inertial frame. This is also where Ω_{P0} is required (not depicted) since this angle describes the position of the prime meridian at the time that the inertial frame was set. Because the angle is defined east of the x_I-axis, it has to be subtracted from $\dot{\Omega}_t t_O$ since Ω_{P0} is defined positive in the same direction as $\dot{\Omega}_t t_O$ which is defined to be positive going from x_I to x_R. The rotation around the z-axis is positive in the same direction according to the RHR for rotation. In this case the rotation is performed in the negative direction around the z-axis with an angle $-\dot{\Omega}_M t_O + \Omega_P$. The complete RF transformation with the written out matrix for this rotation is given by Equation (A.3). Please note that the signs of the angles changed in the matrix due to the sine and cosine functions.

$$\mathbb{T}_{\mathbf{IR}} = \left.\begin{matrix} \\ \end{matrix}\right|_{\mathbf{I}} \mathbb{T}_{\mathbf{z}}\left(-\dot{\Omega}_M t_O + \Omega_P\right)\left.\begin{matrix} \\ \end{matrix}\right|_{\mathbf{R}} = \begin{bmatrix} c\left(\dot{\Omega}_M t_O - \Omega_P\right) & -s\left(\dot{\Omega}_M t_O - \Omega_P\right) & 0 \\ s\left(\dot{\Omega}_M t_O - \Omega_P\right) & c\left(\dot{\Omega}_M t_O - \Omega_P\right) & 0 \\ 0 & 0 & 1 \end{bmatrix} \tag{A.3}$$

Here the vertical lines with the letter designations depict when a certain reference frame is reached. The transformations for $\mathbb{T}_{\mathbf{RB}}$ and $\mathbb{T}_{\mathbf{BP}}$ can now be written in a similar manner and are described in Equations (A.4) and (A.5) respectively.

$$\mathbb{T}_{\mathbf{RB}} = \left.\begin{matrix} \\ \end{matrix}\right|_{\mathbf{R}} \mathbb{T}_{\mathbf{z}}\left(-\tau\right)\mathbb{T}_{\mathbf{y}}\left(\frac{\pi}{2} + \delta\right)\left.\begin{matrix} \\ \end{matrix}\right|_{\mathbf{V}} \mathbb{T}_{\mathbf{z}}\left(-\chi\right)\mathbb{T}_{\mathbf{y}}\left(-\gamma\right)\left.\begin{matrix} \\ \end{matrix}\right|_{\mathbf{B}}$$

$$
= \begin{bmatrix} c\tau\left(-s\delta c\chi c\gamma + c\delta s\gamma\right) - s\tau s\chi c\gamma & c\tau s\delta s\chi - s\tau c\chi & c\tau\left(-s\delta c\chi s\gamma - c\delta c\gamma\right) - s\tau s\chi s\gamma \\ s\tau\left(-s\delta c\chi c\gamma + c\delta s\gamma\right) + c\tau s\chi c\gamma & s\tau s\delta s\chi + c\tau c\chi & s\tau\left(-s\delta c\chi s\gamma - c\delta c\gamma\right) + c\tau s\chi s\gamma \\ c\delta c\chi c\gamma - c\delta s\gamma & -c\delta s\chi & c\delta c\chi s\gamma - s\delta c\gamma \end{bmatrix} \quad \text{(A.4)}
$$

$$
\mathbb{T}_{\mathbf{BP}} = \left.\left|\, \mathbb{T}_{\mathbf{z}}\left(-\psi_T\right)\mathbb{T}_{\mathbf{y}}\left(-\epsilon_T\right)\right.\right|_{\mathbf{P}} = \begin{bmatrix} c\psi_T c\epsilon_T & -s\psi_T & c\psi_T s\epsilon_T \\ s\psi_T c\epsilon_T & c\psi_T & s\psi_T s\epsilon_T \\ -s\epsilon_T & 0 & c\epsilon_T \end{bmatrix} \quad \text{(A.5)}
$$

Occasionally transformation matrices can become rather complex and it is easy to make mistakes. Fortunately the motion of the orbiter is already known in Kepler (or Modified Equinoctial) elements. This means that for the gravitational accelerations caused by the Sun described in **??**, which are in the MCI RF, they can be directly transformed to the body-fixed f_S, f_N and f_W RF. From now on this RF is referred to as the Gaussian frame or F_G, which can be similar to the F_V frame but does not have to be. The transformation from $F_I \rightarrow F_G$ follows from Figure A.7 and is provided by the transformation convention and matrices described by Equation (A.6). In this case an intermediate reference frame is required which will be called $F_{I''}$, because two z-axis rotations are needed, but they are not in the same plane. It can also be seen that the position of the Prime meridian on the 1st of January 2000 at 12:00 is not important in this direct transformation and will only have to be taken into account in the transformation from $F_R \leftrightarrow F_I$ for the MAV.
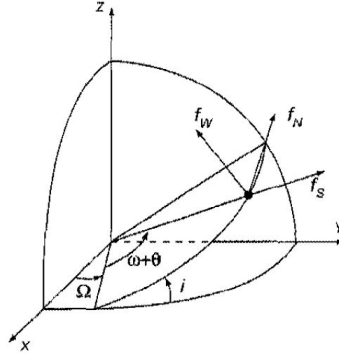
Figure A.7: Relation between the MCI and the Gaussian body frame Wakker (2010).

$$
\mathbb{T}_{\mathbf{GI}} = \mathbb{T}_{\mathbf{GI''}}\mathbb{T}_{\mathbf{I''I}} = \left.\left|\, \mathbb{T}_{\mathbf{z}}(\omega+\theta)\right.\right|_{\mathbf{G}} \left.\left|\, \mathbb{T}_{\mathbf{x}}(i)\mathbb{T}_{\mathbf{z}}(\Omega)\right.\right|_{\mathbf{I}}
$$

$$
= \begin{bmatrix} c(\omega+\theta)c\Omega - s(\omega+\theta)cis\Omega & c(\omega+\theta)s\Omega + s(\omega+\theta)cic\Omega & s(\omega+\theta)si \\ -s(\omega+\theta)c\Omega - c(\omega+\theta)cis\Omega & c(\omega+\theta)cic\Omega - s(\omega+\theta)s\Omega & c(\omega+\theta)si \\ sis\Omega & -sic\Omega & ci \end{bmatrix} \quad \text{(A.6)}
$$

A.3. TRANSFORMATION BETWEEN DIFFERENT COORDINATE SYSTEMS

In the previous sections the different RF and transformations were expressed using x, y and z-axes. These x, y and z-coordinates belong to the Cartesian coordinate system. However, during an integration, simulation or analysis it might be more useful and meaningful to express position (and velocity) in a different coordinate system. Two other systems are the spherical and Keplerian coordinate systems. How to transform back and forth from the Cartesian system to these other two systems will be explained in Appendices A.3.1 and A.3.2 respectively and are based on Noomen (2013b). The transformation from the spherical coordinate system to Kepler elements is described in Appendix A.3.3. Kepler elements are very useful for orbit computations, unfortunately singularities can occur if this coordinate system is used for certain situations. Therefore Appendix A.3.4 will discuss a non-singular form of the Kepler elements.

A.3.1. SPHERICAL AND CARTESIAN

Spherical coordinates can be useful to determine the location of a satellite above Mars assuming that Mars is a perfect sphere. In this thesis problem, however, spherical coordinates are used during the MAV ascent simulation. The coordinate relation between spherical and Cartesian coordinates is shown in Figure A.8.

Based on this diagram, the relations to go from the spherical system to the Cartesian system are derived and are provided in Equation (A.7). Please note that $\lambda \neq \tau$ except for a transformation to (or from) the R-frame.
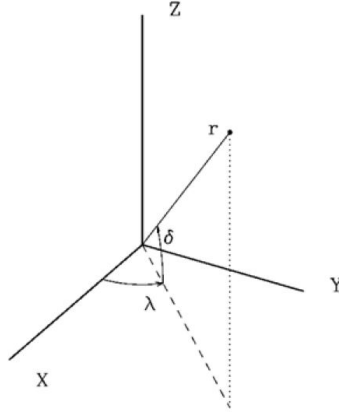
Figure A.8: Relation between spherical position coordinates and Cartesian position coordinates Noomen (2013b).

$$
\begin{aligned}
x &= r \cos \delta \cos(\lambda \\
y &= r \cos \delta \sin(\lambda \\
z &= r \sin \delta
\end{aligned}
\tag{A.7}
$$

The velocities can be obtained by taking the time derivatives of these functions, resulting in the velocity expressions in x-, y- and z-direction given by Equation (A.8). Differentiating those expressions again will result in the accelerations.

$$
\begin{aligned}
\dot{x} &= \dot{r} \cos \delta \cos(\lambda - r \dot{\delta} \sin \delta \cos(\lambda - r \dot{\lambda} \cos \delta \sin(\lambda \\
\dot{y} &= \dot{r} \cos \delta \sin(\lambda - r \dot{\delta} \sin \delta \sin(\lambda + r \dot{\lambda} \cos \delta \cos(\lambda \\
\dot{z} &= \dot{r} \sin \delta + r \dot{\delta} \cos \delta
\end{aligned}
\tag{A.8}
$$

The transformation from Cartesian coordinates to spherical coordinates can again be derived from Figure A.8, resulting in the expressions presented in Equation (A.9).

$$
\begin{aligned}
r &= \sqrt{x^2 + y^2 + z^2} \\
\delta &= \arcsin(\frac{z}{r}) \\
\lambda &= \arctan(\frac{y}{x})
\end{aligned}
\tag{A.9}
$$

However, the expression for λ only results in a value between $-\pi/2$ and $\pi/2$. Also, if x = 0, a singularity occurs. To solve this issue, the so-called 'atan2' function can be used. This function incorporates both sin and cosine values to provide a value for λ between 0 and 2π Noomen (2013b). λ can then be expressed by Equation (A.10) where atan2 is defined by Figure A.9[2].

$$
\lambda = \text{atan2}(y, x)
\tag{A.10}
$$

The time derivatives of these functions can be taken to find the velocity expressions. The resulting velocity expressions are shown in Equation (A.11). The left expressions in this equation define the velocity characteristics as often expressed in the spherical coordinate system required for transformations.

---

[2]Online blog: http://guihaire.com/code/?p=1168 [Accessed 13 November 2015]

$$
\text{atan2}(y,x) = \begin{cases} \text{atan}\left(\dfrac{y}{x}\right) & x > 0 \\[2mm] \pi + \text{atan}\left(\dfrac{y}{x}\right) & y \geq 0, x < 0 \\[2mm] -\pi + \text{atan}\left(\dfrac{y}{x}\right) & y < 0, x < 0 \\[2mm] \dfrac{\pi}{2} & y > 0, x = 0 \\[2mm] -\dfrac{\pi}{2} & y < 0, x = 0 \\[2mm] \text{Undefined} & y = 0, x = 0 \end{cases}
$$

Figure A.9: atan2 function evaluation conditions.

$$
\dot{r} = \frac{x\dot{x} + y\dot{y} + z\dot{z}}{\sqrt{x^2 + y^2 + z^2}}
$$

$$
\dot{\delta} = \frac{x\dot{y} - y\dot{x}}{x^2 + y^2}
$$

$$
\dot{\lambda} = \frac{r\dot{z} - z\dot{r}}{r^2 \sqrt{1 - \left(\dfrac{z}{r}\right)^2}}
$$

$$
V = \sqrt{\dot{x}^2 + \dot{y}^2 + \dot{z}^2}
$$

$$
\gamma = \arcsin\left[\frac{\dot{r}}{V}\right]
$$

$$
\chi = \arccos\left[\frac{r\dot{\delta}}{V \cos\gamma}\right] \tag{A.11}
$$

A.3.2. KEPLERIAN AND CARTESIAN

The relation between the Keplerian and Cartesian systems is slightly more complex. Figure A.10 shows the Kepler elements: a (semi-major axis), e (eccentricity, not shown but is a ratio that determines the elliptic properties of an orbit), i (inclination), ω (argument of perigee), Ω (right ascension of the ascending node) and θ (true anomaly). Often, however, the mean anomaly M is used instead of the true anomaly. The mean anomaly is defined to be the angle between the semi-major axis and the line between the centre of the orbit and an imaginary point (S_M) on the auxiliary circle that can be drawn around the orbit. This point is determined by assuming a constant rotational velocity in this circular orbit with the same orbital time as the actual (elliptical) orbit.
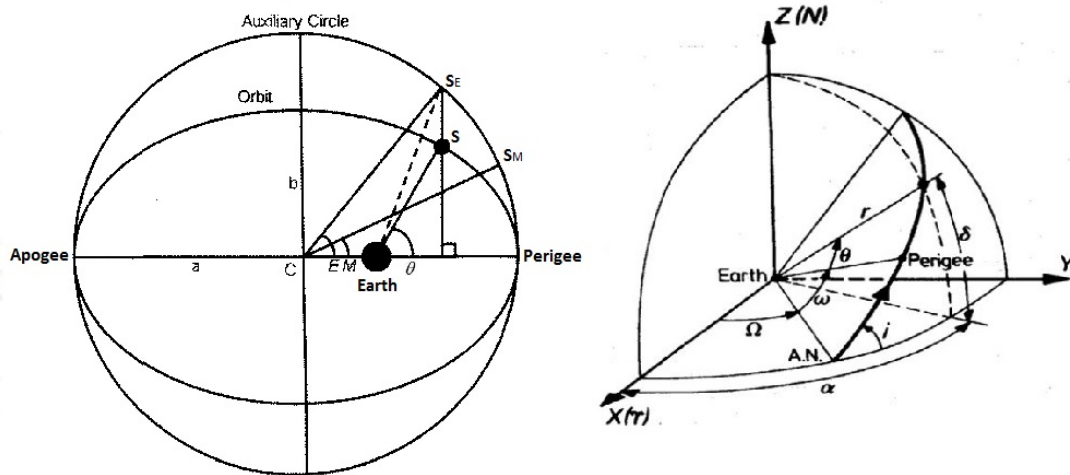

Figure A.10: Definition of the Kepler elements in 2D (left) and 3D (right) Noomen (2013b); **?**.

The transformation from Kepler elements to Cartesian coordinates consists of a number of steps starting with the mean anomaly and eccentricity. Both these values have to be used to determine the eccentric

anomaly E and in turn the true anomaly θ. The eccentric anomaly is computed by rewriting the first expression of Equation (A.12) into the second expression Noomen (2013b).

$$
\begin{aligned}
M &= E - e \cdot \sin E \\
E_{i+1} &= E_i + \frac{M - E_i - e \cdot \sin E_i}{1 - e \cdot \cos(E_i)}
\end{aligned}
\tag{A.12}
$$

The determination of E is an iterative process. First a reasonable estimate of E has to be provided (it is best to use the value for M for this) and then a new E can be computed. This has to be done until the desired level of precision is reached. Then the true anomaly can be computed using this E as shown by Equation (A.13).

$$
\theta = 2 \cdot \arctan\left[\tan\left(\frac{E}{2}\right)\sqrt{\frac{1+e}{1-e}} \right]
\tag{A.13}
$$

With the true anomaly known, the radial distance from the orbiting body to the centre of Mars r can be determined using Equation (A.14)

$$
r = \frac{a \cdot (1 - e^2)}{1 + e\cos\theta}
\tag{A.14}
$$

The Cartesian coordinates can now be computed using the expression in Equation (A.15) with the matrix entries provided by Equation (A.16)Noomen (2013b).

$$
\begin{pmatrix} x \\ y \\ z \end{pmatrix} =
\begin{bmatrix} l_1 & l_2 \\ m_1 & m_2 \\ n_1 & n_2 \end{bmatrix}
\begin{pmatrix} r\cos\theta \\ r\sin\theta \end{pmatrix}
\tag{A.15}
$$

$$
\begin{aligned}
l_1 &= \cos\Omega\cos\omega - \sin\Omega\sin\omega\cos i \\
l_2 &= -\cos\Omega\sin\omega - \sin\Omega\cos\omega\cos i \\
m_1 &= \sin\Omega\cos\omega + \cos\Omega\sin\omega\cos i \\
m_2 &= -\sin\Omega\sin\omega + \cos\Omega\cos\omega\cos i \\
n_1 &= \sin\omega\sin i \\
n_2 &= \cos\Omega\sin i
\end{aligned}
\tag{A.16}
$$

Equation (A.17) then provides the expressions for x, y and z.

$$
\begin{aligned}
x &= r \cdot [\cos\Omega\cos(\omega + \theta) - \sin\Omega\sin(\omega + \theta)\cos i] \\
y &= r \cdot [\sin\Omega\cos(\omega + \theta) - \cos\Omega\sin(\omega + \theta)\cos i] \\
z &= r\sin i\sin(\omega + \theta)
\end{aligned}
\tag{A.17}
$$

For the velocity values, an extra parameter is required. This parameter is called the specific relative angular momentum h. Assuming that the mass of the orbiting body can be neglected with respect to the planet (or other celestial body) it is orbiting, h can be expressed as a function of the standard gravitational parameter of that planet μ, a and e as shown by Equation (A.18).

$$
h = \sqrt{\mu a \cdot (1 - e^2)}
\tag{A.18}
$$

Then with h and the expression from Equation (A.16), the velocities can be expressed by Equation (A.19).

$$
\begin{aligned}
\dot{x} &= \frac{\mu}{h}[-l_1\sin\theta + l_2 \cdot (e + \cos\theta)] \\
\dot{y} &= \frac{\mu}{h}[-m_1\sin\theta + m_2 \cdot (e + \cos\theta)] \\
\dot{z} &= \frac{\mu}{h}[-n_1\sin\theta + n_2 \cdot (e + \cos\theta)]
\end{aligned}
\tag{A.19}
$$

It is also possible to convert from the Cartesian system back to the Kepler system, however, this requires more steps and intermediate expressions. First, it is convenient to express the position and velocity both in one vector each as shown by Equation (A.20).

$$
\begin{aligned}
\mathbf{r} &= \begin{bmatrix} x & y & z \end{bmatrix} \\
\mathbf{V} &= \begin{bmatrix} \dot{x} & \dot{y} & \dot{z} \end{bmatrix}
\end{aligned}
\tag{A.20}
$$

The cross product of these two ($\mathbf{r} \times \mathbf{V}$) will result in the specific relative angular momentum vector $\mathbf{h}$ and the scalar values, or lengths, can then be represented by $r = \|\mathbf{r}\|$, $V = \|\mathbf{V}\|$ and $h = \|\mathbf{h}\|$. Also, a vector $\mathbf{N}$ can be defined as shown by Equation (A.21)Noomen (2013b).

$$
\mathbf{N} = \begin{pmatrix} 0 \\ 0 \\ 1 \end{pmatrix} \times \mathbf{h}
\tag{A.21}
$$

With these parameters set, the first four Kepler elements (a, e, i and Ω) can be computed as shown by Equation (A.22). Here, the value for the eccentricity can be obtained by taking the length of the vector: $e = \|\mathbf{e}\|$. Also, $\mathbf{h}(3)$ is the third value of the specific relative angular momentum vector, so the value in the z-direction. The same principle holds for the values from $\mathbf{N}$.

$$
\begin{aligned}
a &= \left(\frac{2}{r} - \frac{V^2}{\mu} \right)^{-1} \\
\mathbf{e} &= \frac{\mathbf{V} \times \mathbf{h}}{\mu} - \frac{\mathbf{r}}{r} \\
i &= \arccos\left(\frac{\mathbf{h}(3)}{h} \right) \\
\Omega &= \operatorname{atan2}\left(\mathbf{N}(2), \mathbf{N}(1) \right)
\end{aligned}
\tag{A.22}
$$

For the computation of the values for ω and θ, three unit vectors are needed: $\hat{\mathbf{N}} = \dfrac{\mathbf{N}}{\|\mathbf{N}\|}$, $\hat{\mathbf{e}} = \dfrac{\mathbf{e}}{\|\mathbf{e}\|}$ and $\hat{\mathbf{r}} = \dfrac{\mathbf{r}}{\|\mathbf{r}\|}$. This leads to the conditional expressions seen in Equation (A.23).

$$
\begin{aligned}
\omega &= \begin{cases} \arccos\left(\hat{\mathbf{e}} \cdot \hat{\mathbf{N}} \right), & \text{if } \left(\hat{\mathbf{N}} \times \mathbf{e} \right) \cdot \mathbf{h} > 0 \\ -\arccos\left(\hat{\mathbf{e}} \cdot \hat{\mathbf{N}} \right), & \text{otherwise} \end{cases} \\
\theta &= \begin{cases} \arccos\left(\hat{\mathbf{r}} \cdot \hat{\mathbf{e}} \right), & \text{if } \left(\mathbf{e} \times \mathbf{r} \right) \cdot \mathbf{h} > 0 \\ -\arccos\left(\hat{\mathbf{r}} \cdot \hat{\mathbf{e}} \right), & \text{otherwise} \end{cases}
\end{aligned}
\tag{A.23}
$$

The eccentric anomaly can now be computed using θ and e as shown by Equation (A.24), which is the rewritten form of Equation (A.13).

$$
E = 2 \cdot \arctan\left[\tan\left(\frac{\theta}{2} \right) \sqrt{\frac{1-e}{1+e}} \right]
\tag{A.24}
$$

And finally, the mean anomaly can be found using Equation (A.12)Noomen (2013b).

A.3.3. Spherical and Keplerian

Often it is required to transform the spherical coordinates into Kepler elements. Wakker **?** provides this direct transformation through the relations provided in Equation (A.25). In this case the expressions are written explicitly for Mars by using μ_M.

$$a = \cfrac{r}{2 - \cfrac{rV^2}{\mu_M}}$$

$$e = \sqrt{1 - \frac{rV^2}{\mu_M}\left(2 - \frac{rV^2}{\mu_M}\right)\cos^2\gamma}$$

$$i = \arccos\left(\cos\delta\sin\chi\right)$$

$$\theta = 2\arctan\left[\sqrt{\frac{1+e}{1-e}}\tan\left(\frac{E}{2}\right)\right], \qquad \text{where} \qquad E = \arctan\left[\sqrt{\frac{a}{\mu_M}}\frac{rV\sin\gamma}{a-r}\right]$$

$$\omega = \frac{\sin\delta}{\sin(i)} - \theta$$

$$\Omega = \lambda - \arccos\left[\frac{\cos\chi}{\sin(i)}\right]$$

(A.25)

Then the spherical coordinates can be computed by rewriting the expressions provided in Equation (A.25) to the spherical coordinates. These rewritten expressions are shown in Equation (A.26).

$$r = a\left(1 - e\cos(E)\right), \qquad \text{where} \qquad E = 2\arctan\left[\sqrt{\frac{1-e}{1+e}}\tan\left(\frac{\theta}{2}\right)\right]$$

$$V = \sqrt{\mu_M\left(\frac{2}{r} - \frac{1}{a}\right)}$$

$$\gamma = \arcsin\left[e\sin(E)\frac{\sqrt{\mu_M a}}{rV}\right]$$

$$\delta = \arcsin\left[\sin(\omega + \theta)\sin(i)\right]$$

$$\lambda = \arcsin\left[\frac{\tan\delta}{\tan(i)}\right] - \Omega$$

$$\chi = \arccos\left[\cos(\omega + \theta) - \frac{\sin(i)}{\cos\delta}\right]$$

(A.26)

A.3.4. Non-singular Kepler elements

During the calculation of the change in orbital elements, sometimes a number of Kepler elements cannot assume every possible value. Singularities occur when $e = 0$, and/or $i = 0°$ or $180°$. One kind of non-singular Kepler elements are the Modified Equinoctial Elements (MEE)s. The transformation from the ordinary Kepler elements to the MEEs is shown in Equation (A.27). This equation also includes the expressions to revert back to normal Kepler elements (see left equations). Here I is the retrograde factor and has a value of +1 for posigrade orbits and -1 for retrograde orbits. This is done to avoid singularities when $i = 180°$ and thus making the set non-singular.

$$p = a\left(1 - e^2\right)$$
$$f = e\cos(\omega + I\Omega)$$
$$g = e\sin(\omega + I\Omega)$$
$$h = \tan^I\left(\frac{i}{2}\right)\cos(\Omega)$$
$$k = \tan^I\left(\frac{i}{2}\right)\sin(\Omega)$$
$$L = \omega + \theta + I\Omega$$

$$a = \frac{p}{1 - \left(f^2 + g^2\right)}$$
$$e = \sqrt{f^2 + g^2}$$
$$i = 2\tan^{-I}\left[\sqrt{h^2 + k^2}\right]$$
$$\omega = L - \theta - I\Omega$$
$$\Omega = \text{atan2}\,(k, h)$$
$$\theta = L - \arccos\left[\frac{f}{e}\right]$$

(A.27)

B

Mars-GRAM 2005 input file

```
1    $INPUT
2      LSTFL    = 'LIST.txt'
3      OUTFL    = 'OUTPUT.txt'
4      TRAJFL   = 'TRAJDATA.txt'
5      profile  = 'null'
6      WaveFile = 'null'
7      DATADIR  = '/home/stachap/MarsGram/binFiles_TUDelft/'
8      GCMDIR   = '/home/stachap/MarsGram/binFiles_TUDelft/'
9      IERT     = 0
10     IUTC     = 1
11     MONTH    = 2
12     MDAY     = 28
13     MYEAR    = 2025
14     NPOS     = 32061
15     IHR      = 12
16     IMIN     = 0
17     SEC      = 0.0
18     LonEW    = 1
19     Dusttau  = 0
20     Dustmin  = 0.3
21     Dustmax  = 1.0
22     Dustnu   = 0.003
23     Dustdiam = 5.0
24     Dustdens = 3000.
25     ALS0     = 0.0
26     ALSDUR   = 48.
27     INTENS   = 0.0
28     RADMAX   = 0.0
29     DUSTLAT  = 0.0
30     DUSTLON  = 0.0
31     MapYear  = 0
32     F107     = 68.0
33     STDL     = 0.0
34     NR1      = 1234
35     NVARX    = 1
36     NVARY    = 0
37     LOGSCALE = 0
38     FLAT     = 21
39     FLON     = 74.5
40     FHGT     = -0.6
41     MOLAhgts = 1
42     hgtasfcm = 0.
43     zoffset  = 0.
44     ibougher = 0
45     DELHGT   = 0.01
46     DELLAT   = 0.0
47     DELLON   = 0.0
48     DELTIME  = 0.0
49     ΔTEX = 0.0
```

```
50    profnear = 0.0
51    proffar  = 0.0
52    rpscale  = 1.0
53    rwscale  = 1.0
54    wlscale  = 1.0
55    wmscale  = 0.0
56    blwinfac = 0.0
57    NMONTE   = 1
58    iup      = 13
59    WaveA0   = 1.0
60    WaveDate = 0.0
61    WaveA1   = 0.0
62    Wavephi1 = 0.0
63    phi1dot  = 0.0
64    WaveA2   = 0.0
65    Wavephi2 = 0.0
66    phi2dot  = 0.0
67    WaveA3   = 0.0
68    Wavephi3 = 0.0
69    phi3dot  = 0.0
70    iuwave   = 0
71    Wscale   = 20.
72    corlmin  = 0.0
73    ipclat   = 1
74    requa    = 3396.19
75    rpole    = 3376.20
76    idaydata = 1
77    $END
78
79    Explanation of variables:
80    LSTFL    =  List file name (CON for console listing)
81    OUTFL    =  Output file name
82    TRAJFL   =  (Optional) Trajectory input file. File contains time (sec)
83                 relative to start time, height (km), latitude (deg),
84                 longitude (deg W if LonEW=0, deg E if LonEW=1, see below)
85    profile  =  (Optional) auxiliary profile input file name
86    WaveFile =  (Optional) file for time-dependent wave coefficient data.
87                 See file description under parameter iuwave, below.
88    DATADIR  =  Directory for COSPAR data and topographic height data
89    GCMDIR   =  Directory for GCM binary data files
90    IERT     =  1 for time input as Earth-Receive time (ERT) or 0 Mars-event
91                 time (MET)
92    IUTC     =  1 for time input as Coordinated Universal Time (UTC), or 0
93                  for Terrestrial (Dynamical) Time (TT)
94    MONTH    =  (Integer) month of year
95    MDAY     =  (Integer) day of month
96    MYEAR    =  (Integer) year (4-digit; 1970-2069 can be 2-digit)
97    NPOS     =  max # positions to evaluate (0 = read data from trajectory
98                 input file)
99    IHR      =  Hour of day (ERT or MET, controlled by IERT and UTC or TT,
100                controlled by IUTC)
101   IMIN     =  minute of hour (meaning controlled by IERT and IUTC)
102   SEC      =  seconds of minute (meaning controlled by IERT and IUTC).
103                IHR:IMIN:SEC is time for initial position to be evaluated
104   LonEW    =  0 for input and output West longitudes positive; 1 for East
105                longitudes positive
106   Dusttau  =  Optical depth of background dust level (no time-developing
107                dust storm, just uniformly mixed dust), 0.1 to 3.0, or use
108                0 for assumed seasonal variation of background dust
109   Dustmin  =  Minimum seasonal dust tau if input Dusttau=0 (≥0.1)
110   Dustmax  =  Maximum seasonal dust tau if input Dusttau=0 (≤1.0)
111   Dustnu   =  Parameter for vertical distribution of dust density (Haberle
112                et al., J. Geophys. Res., 104, 8957, 1999)
113   Dustdiam =  Dust particle diameter (micrometers, assumed monodisperse)
114   Dustdens =  Dust particle density (kg/m**3)
115   ALS0     =  starting Ls value (degrees) for dust storm (0 = none)
116   ALSDUR   =  duration (in Ls degrees) for dust storm (default = 48)
117   INTENS   =  dust storm intensity (0.0 - 3.0)
118   RADMAX   =  max. radius (km) of dust storm (0 or >10000 = global)
119   DUSTLAT  =  Latitude (degrees) for center of dust storm
120   DUSTLON  =  Longitude (degrees) (West positive if LonEW=0, or East
```

```
121              positive if LonEW = 1) for center of dust storm
122  MapYear  =  1 or 2 for TES mapping year 1 or 2 GCM input data, or 0 for
123              Mars-GRAM 2001 GCM input data sets
124  F107     =  10.7 cm solar flux (10**-22 W/cm**2 at 1 AU)
125  NR1      =  starting random number (0 < NR1 < 30000)
126  NVARX    =  x-code for plotable output (1=hgt above MOLA areoid).
127              See file xycodes.txt
128  NVARY    =  y-code for 3-D plotable output (0 for 2-D plots)
129  LOGSCALE =  0=regular SI units, 1=log-base-10 scale, 2=percentage
130              deviations from COSPAR model, 3=SI units, with density
131              in kg/km**3 (suitable for high altitudes)
132  FLAT     =  initial latitude (N positive), degrees
133  FLON     =  initial longitude (West positive if LowEW = 0 or East
134              positive if LonEW = 1), degrees
135  FHGT     =  initial height (km); ≤-10 means evaluate at surface height;
136              > 3000 km means planeto-centric radius
137  MOLAhgts =  1 for input heights relative to MOLA areoid, otherwise
138              input heights are relative to reference ellipsoid
139  hgtasfcm =  height above surface (0-4500 m); use if FHGT ≤ -10. km
140  zoffset  =  constant height offset (km) for MTGCM data or constant
141              part of Ls-dependent (Bougher) height offset (0.0 means
142              no constant offset).  Positive offset increases density,
143              negative offset decreases density.
144  ibougher =  0 for no Ls-dependent (Bougher) height offset term; 1
145              means add Ls-dependent (Bougher) term, -A*Sin(Ls) (km),
146              to constant term (zoffset) [offset amplitude A = 2.5 for
147              MapYear=0 or 0.5 for MapYear > 0]; 2 means use global mean
148              height offset from data file hgtoffst.dat; 3 means use
149              daily average height offset at local position; 4 means
150              use height offset at current time and local position.
151              Value of zoffset is ignored if ibougher = 2, 3, or 4.
152  DELHGT   =  height increment (km) between steps
153  DELLAT   =  Latitude increment (deg) between steps (Northward positive)
154  DELLON   =  Longitude increment (deg) between steps (Westward positive
155              if LonEW = 0, Eastward positive if LonEW = 1)
156  DELTIME  =  time increment (sec) between steps
157  ΔTEX  =  adjustment for exospheric temperature (K)
158  profnear =  Lat-lon radius (degrees) within which weight for auxiliary
159              profile is 1.0 (Use profnear = 0.0 for no profile input)
160  proffar  =  Lat-lon radius (degrees) beyond which weight for auxiliary
161              profile is 0.0
162  rpscale  =  random density perturbation scale factor (0-2)
163  rwscale  =  random wind perturbation scale factor (≥0)
164  wlscale  =  scale factor for perturbation wavelengths (0.1-10)
165  wmscale  =  scale factor for mean winds
166  blwinfac =  scale factor for boundary layer slope winds (0 = none)
167  NMONTE   =  number of Monte Carlo runs
168  iup      =  0 for no LIST and graphics output, or unit number for output
169  WaveA0   =  Mean term of longitude-dependent wave multiplier for density
170  WaveDate =  Julian date for (primary) peak(s) of wave (0 for no traveling
171              component)
172  WaveA1   =  Amplitude of wave-1 component of longitude-dependent wave
173              multiplier for density
174  Wavephi1 =  Phase of wave-1 component of longitude-dependent wave
175              multiplier (longitude, with West positive if LonEW = 0,
176              East positive if LonEW = 1)
177  phi1dot  =  Rate of longitude movement (degrees per day) for wave-1
178              component (Westward positive if LonEW = 0, Eastward
179              positive if LonEW = 1)
180  WaveA2   =  Amplitude of wave-2 component of longitude-dependent wave
181              multiplier for density
182  Wavephi2 =  Phase of wave-2 component of longitude-dependent wave
183              multiplier (longitude, with West positive if LonEW = 0,
184              East positive if LonEW = 1)
185  phi2dot  =  Rate of longitude movement (degrees per day) for wave-2
186              component (Westward positive if LonEW = 0, Eastward
187              positive if LonEW = 1)
188  WaveA3   =  Amplitude of wave-3 component of longitude-dependent wave
189              multiplier for density
190  Wavephi3 =  Phase of wave-3 component of longitude-dependent wave
191              multiplier (longitude, with West positive if LonEW = 0,
```

```
192              East positive if LonEW = 1)
193   phi3dot   =  Rate of longitude movement (degrees per day) for wave-3
194                 component (Westward positive if LonEW = 0, Eastward
195                 positive if LonEW = 1)
196   iuwave    =  Unit number for (Optional) time-dependent wave coefficient
197                 data file "WaveFile" (or 0 for none).
198                 WaveFile contains time (sec) relative to start time, and
199                 wave model coefficients (WaveA0 thru Wavephi3) from the
200                 given time to the next time in the data file.
201   Wscale    =  Vertical scale (km) of longitude-dependent wave damping
202                 at altitudes below 100 km (10≤Wscale≤10,000 km)
203   corlmin   =  minimum relative step size for perturbation updates
204                 (0.0-1.0); 0.0 means always update perturbations, x.x
205                 means only update perturbations when corlim > x.x
206   ipclat    =  1 for Planeto-centric latitude and height input,
207                 0 for Planeto-graphic latitude and height input
208   requa     =  Equatorial radius (km) for reference ellipsoid
209   rpole     =  Polar radius (km) for reference ellipsoid
210   idaydata  =  1 for daily max/min data output; 0 for none
```

C

ATMOSPHERIC DATA FITTING

In Section 3.4.1 the final results of the atmospheric data fits were presented. However, before those results could be obtained, a few iterations of trial-and-error fits were required. These intermediate trials are presented for both the temperature data, in Appendix C.1, as well as for the density data, in Appendix C.2. The fit requirements for the polynomial function were set such that the errors created by the fit were less than the uncertainty of the latitude and longitude dependent data. This way the desired accuracy could still be reached. This uncertainty is caused by the difference in atmospheric data curves for the different latitudes and longitudes. The atmospheric data curve for the latitude and longitude corresponding to the launch site (21.0 °N and 74.5 °E) was taken as the reference curve and called the launch site curve. The differences between this launch site curve and the 8 other curves were used to define the maximum data curves difference. The *polyfit.m* function within Matlab was used to fit a polynomial to the data. This function also directly provides a standard deviation of the fit for each data point (in combination with the *polyval.m* function). One of the requirements was for the maximum standard deviation of the polynomial fit to be one order less than the maximum difference of the data curves with respect to the launch site curve. The second requirements for a proper fit was for the absolute maximum difference between the polynomial fit and the launch site curve to be less than the absolute maximum difference between the data curves and that same launch site curve.

C.1. TEMPERATURE

Initially, the temperature data curve was split into 6 different sections as portrayed in Figure C.1. The sections were selected on the basis of their individual shapes and the maximum order that was required, where the maximum order for temperature was set at 8. Fewer sections were however always preferred.

Unfortunately, the fourth quarter of section 3 caused this section to not meet the maximum standard deviation requirement because in that quarter the linear behaviour changes directions slightly and the differences between the different data curves become a lot smaller. Therefore section 3 was split into two different sections resulting in a total of 7 sections as shown in Figure C.2.

These sections all met the requirements and thus provided a proper fit to the data. This fit is shown in Figure C.3.

However, because fewer sections were preferred, an attempt was made to reduce the number of sections. Because of the inaccuracy in the Mars-GRAM model close to the planet surface, it was decided to delete the outliers near the surface (section 1) and stretch the outcome of the second polynomial fit to the surface instead. Also, it turned out that section 4 and 5 could be combined in such a way that the requirements were still met. This reduced the number of section from 7 to 5. The final fit was presented in Section 3.4.1 as well as the corresponding errors and polynomial coefficients.

C.2. DENSITY

For the density curve, because the data represents a logarithmic curve, initially an exponential atmosphere was fit. However, this did not meet any of the requirements for a proper fit as can be seen in . This is why a polynomial fit was attempted for the density curve as well with the same requirement as the temperature fits. The first fit was attempted with two sections as presented in Figure C.4.
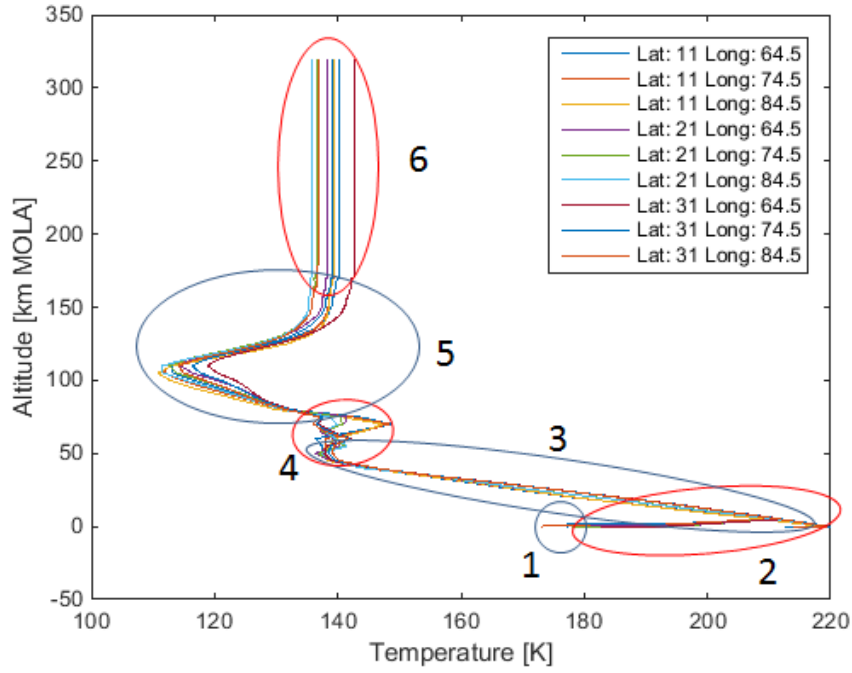
Figure C.1: Six different temperature curve sections
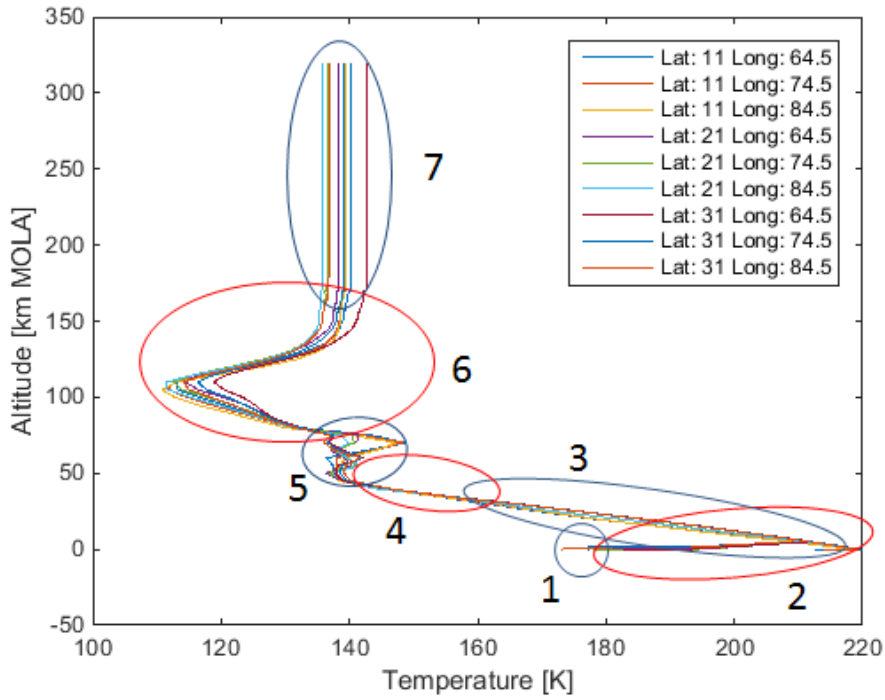
Figure C.2: Seven different temperature curve sections

However, the second section could not meet the requirements because of the initial part. This is why it was split into two sections as presented in Figure C.5.

This did meet the error requirements and resulted in the fit as shown in Figure C.6 with section 1 being
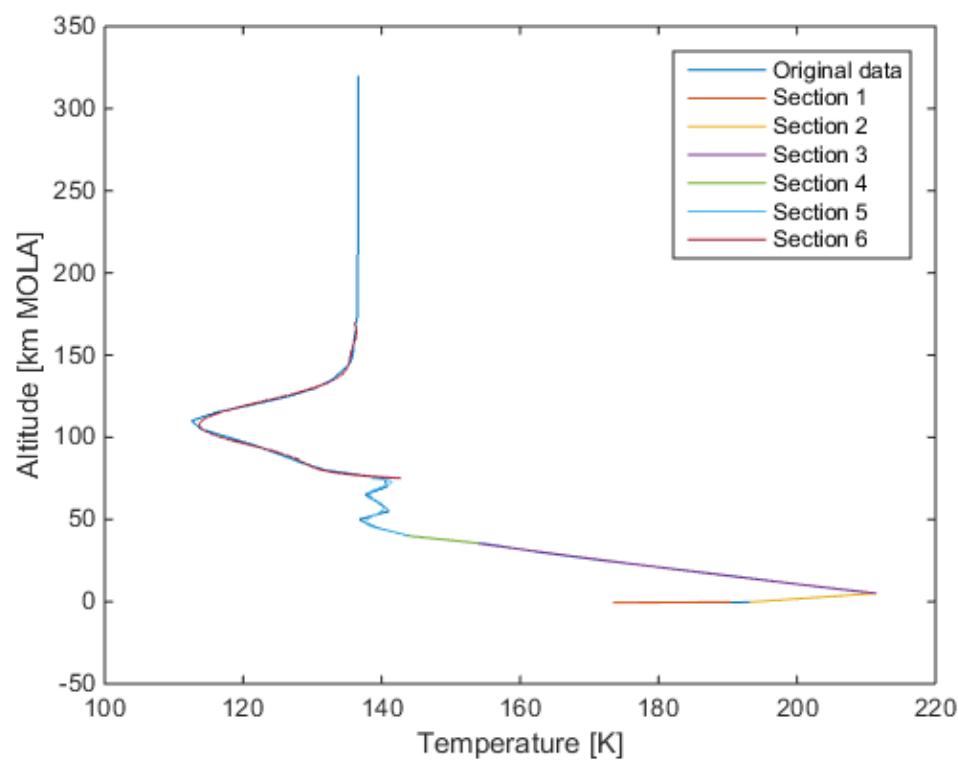
Figure C.3: All section fits for the launch site temperature data curve
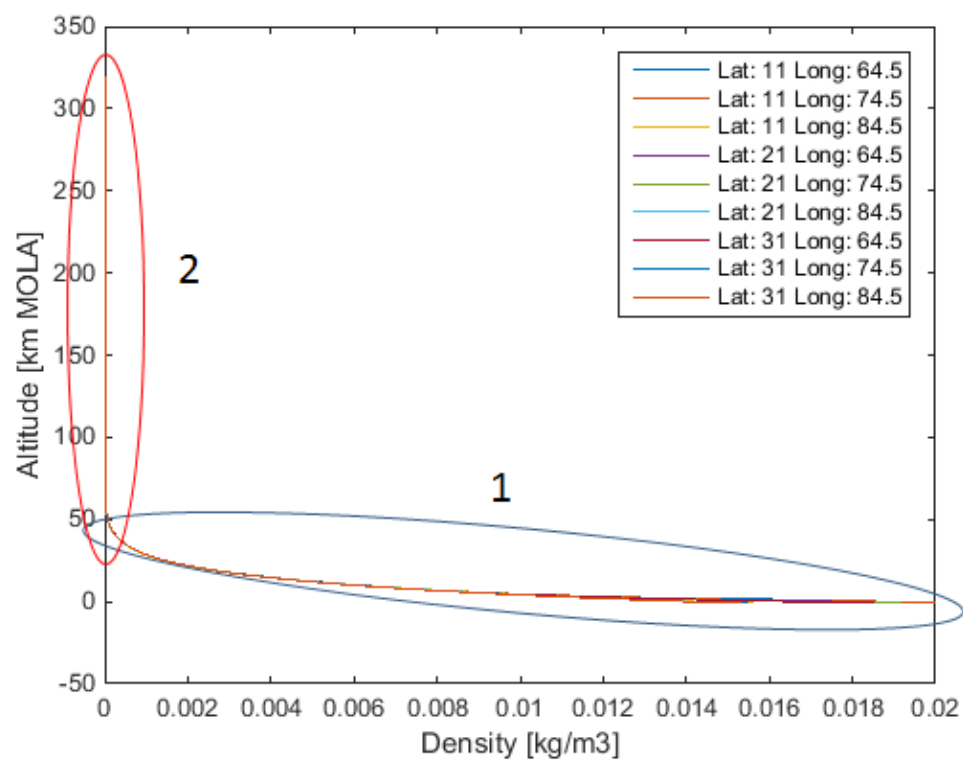
Figure C.4: Two different density curve sections
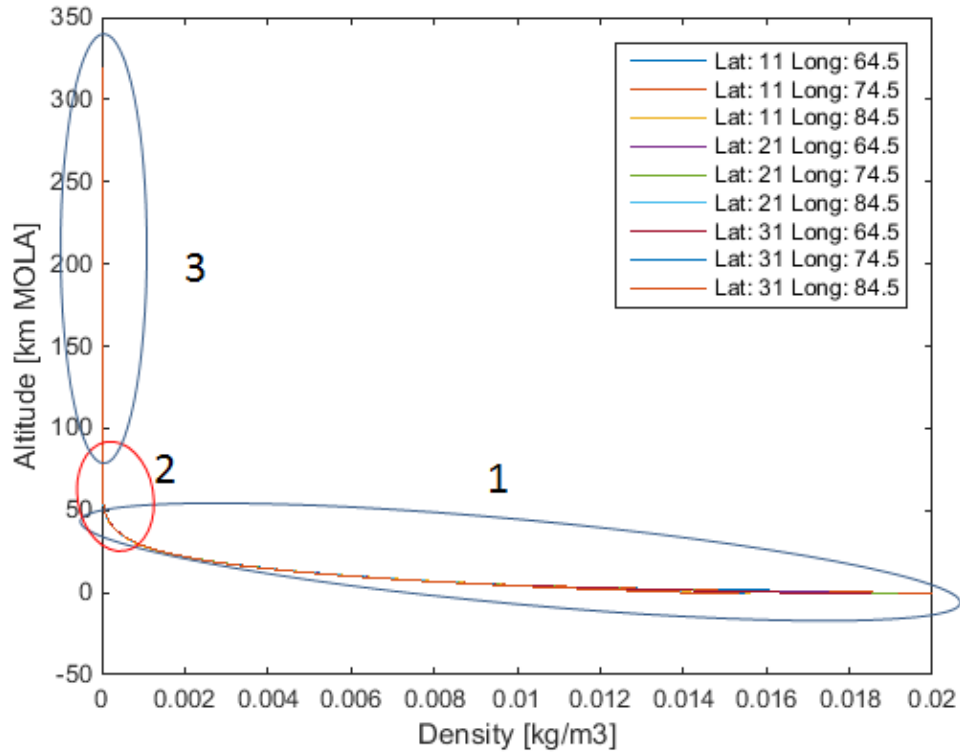
Figure C.5: Three different density curve sections

the lower part, section 2 the middle and section 3 the upper part.

However, in this case the fit for section three resulted in an oscillating behaviour around the actual data which caused the density values to drop below zero as shown in Figure C.7. Since this is unrealistic, an exponential atmospheric fit for only the third section was attempted (also shown in Figure C.7) however, this resulted in the same behaviour as the attempt for the entire curve. Therefore, it was decided to try a different exponential approach which eventually resulted in the fit described in Section 3.4.1.

Figure C.8 clearly shows that both the full exponential atmospheric fit and the polynomial fits were not a proper choice here. The figure shows the curved part of the curve.
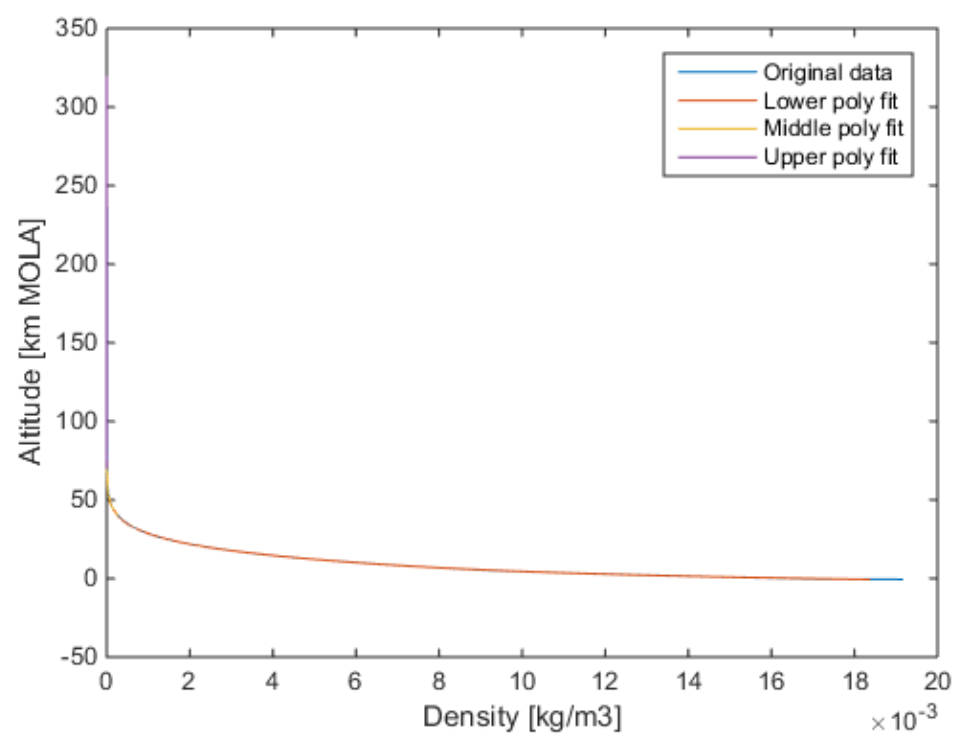
Figure C.6: All section fits for the launch site density data curve
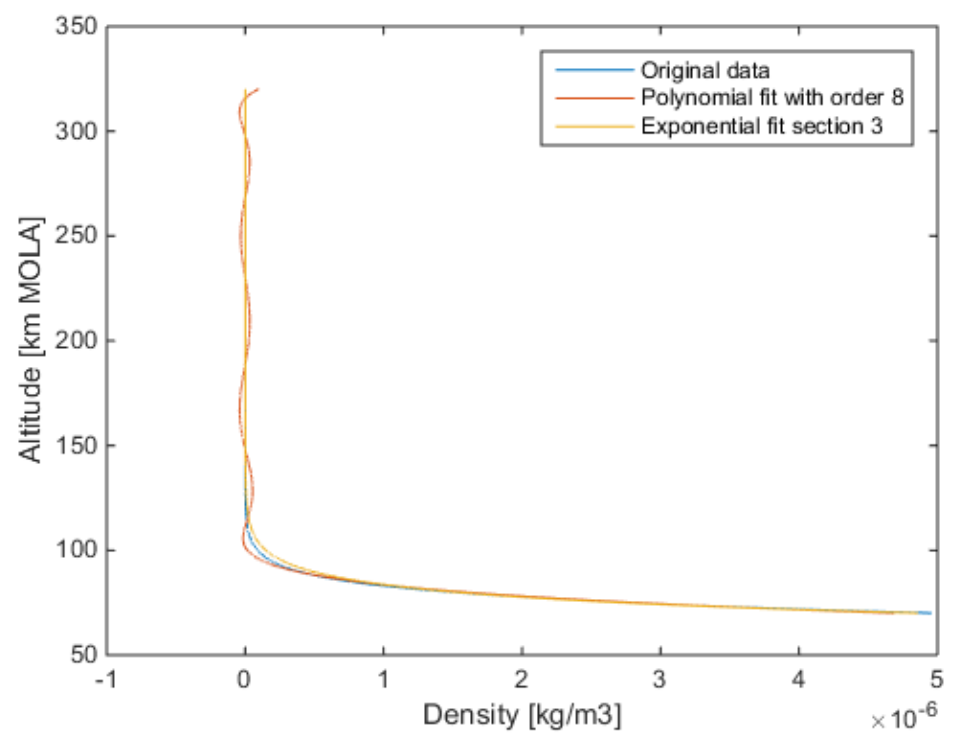
Figure C.7: Section 3 fit for the launch site density data curve
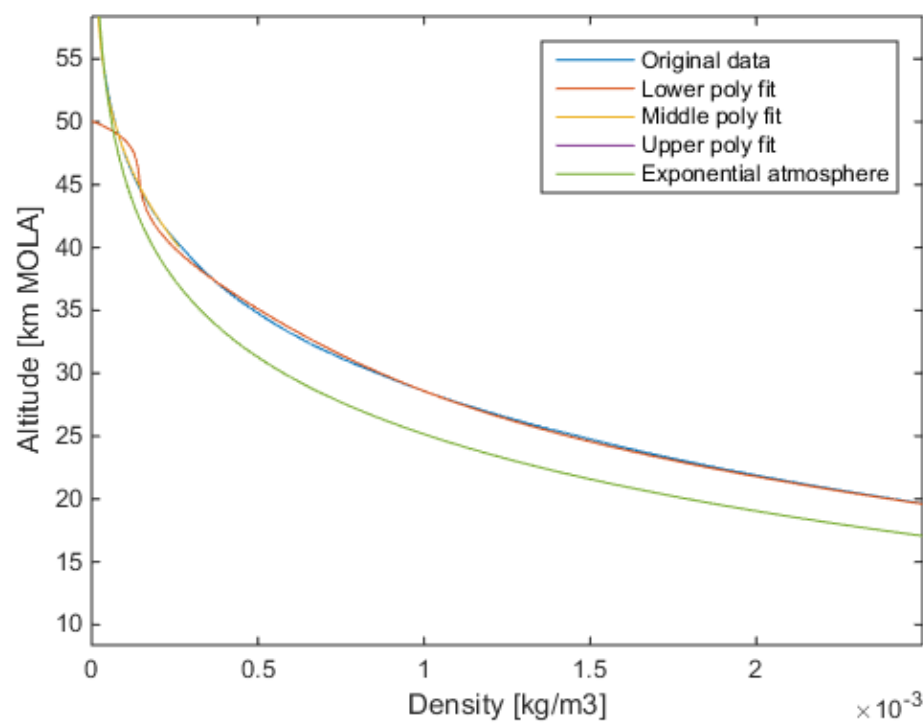
Figure C.8: Zoom in of the end of section 1 with the polynomial and exponential atmospheric fits

D

PROGRAM FILE DEFINITIONS

Both the RKF and TSI propagator architectures were presented in **??**(Figures 6.2 and 6.3 respectively). These included many different operation blocks. Each block is either a separate class, a combination of a header and source file (without it being a class), a function of either of these files or a function in the main file (MAVPropagator). The different files that include several blocks are MAVPropagator.h/.cpp, TaylorSeriesIntegration.h/.cpp, ascentDragForce.h/.cpp and ascentStateDerivativeFunction.h/.cpp, where this last file is also a class. The functions that will be implemented in these files are mentioned in Table D.1 all other blocks are described in Table D.2.

Table D.1: Large program files and included functions.

MAVPropagator	TaylorSeriesIntegration	ascentStateDerivativeFunction
Update current state	Compute auxiliaries	Compute current spherical state
Integration step	Thrust acceleration in B-frame	Compute gravitational acceleration
	Compute Taylor coefficients	Compute thrust and drag acceleration
ascentDragForce	Store state Taylor coefficients	Transfer to inertial frame
Compute speed of	Initial step-size	Compute total acceleration
sound and Mach	Provide Taylor series expansion	Compute mass flow rate
number	Estimate the max. trunc. error	
Compute drag force	Taylor series expansion incl. trunc. error	

Table D.2: Separate function files

Block	Kind of file
Planet characteristics	Class
Vehicle characteristics	Class
Auxiliary equations, derivatives and functions	Class
Current state and time	Class
Basic recurrence relations	Header and source
Full set of recurrence relations	Header and source
Determine next step-size	Header and source
Compute local air temperature	Header and source
Compute local air density	Header and source
Compute drag coefficient	Header and source

E

ALL RECURRENCE RELATIONS

In this appendix, all the reduced auxiliary functions that form the complete recurrence relations for each of the variables using the basic recurrence relations are provided for all three cases. Each case contains a table with the function definition, the corresponding equation and the basic recurrence relation category. All the reduced auxiliary derivatives are also described. All these expressions are a function of k, where $W(k)$ refers to the kth order reduced derivative. The same holds for $X(k)$ and $U(k)$. All the expressions hold for $k \geq 1$. In the tables, the (k) is neglected to make it more readable.

E.1. FIRST CARTESIAN CASE: EULER ANGLES

The first Cartesian case requires a large number of reduced auxiliary functions. These are all provided in Table E.1. For each function, the number, the equations and the category is provided.

Table E.1: Reduced auxiliary functions for the first Cartesian case.

Auxiliary function	Equation	Category
$W_{4,1} =$	$X_1^2 + X_2^2$	Multiplication
$W_{4,2} =$	$W_{4,1} + X_3^2$	Multiplication
$W_{4,3} =$	$\sqrt{W_{4,2}}$	Power
$W_{4,4} =$	$\sqrt{W_{4,1}}$	Power
$W_{4,5} =$	$\dfrac{X_2}{W_{4,4}}$	Division
$W_{4,6} =$	$\dfrac{X_1}{W_{4,4}}$	Division
$W_{4,7} =$	$\dfrac{X_3}{W_{4,3}}$	Division
$W_{4,8} =$	$\dfrac{W_{4,4}}{W_{4,3}}$	Division
$W_{4,9} =$	$X_4 + \Omega_M X_2$	Constant Multiplication
$W_{4,10} =$	$X_5 - \Omega_M X_1$	Constant Multiplication
$W_{4,11} =$	$W_{4,9}^2 + W_{4,10}^2 + X_6^2$	Multiplication
$W_{4,12} =$	$\sqrt{W_{4,11}}$	Power
$W_{4,13} =$	$-W_{4,6}W_{4,7}$	Multiplication
$W_{4,14} =$	$-W_{4,7}W_{4,5}$	Multiplication
$W_{4,15} =$	$-W_{4,8}W_{4,6}$	Multiplication
$W_{4,16} =$	$W_{4,8}W_{4,5}$	Multiplication
$W_{4,17} =$	$X_6 W_{4,8} + W_{4,9}W_{4,13} + W_{4,10}W_{4,14}$	Multiplication
$W_{4,18} =$	$W_{4,10}W_{4,6} - W_{4,9}W_{4,5}$	Multiplication

$W_{4,19} =$	$W_{4,9}W_{4,15} - X_6 W_{4,7} + W_{4,10}W_{4,16}$	Multiplication
$W_{4,20} =$	$W_{4,17}^2 + W_{4,18}^2$	Multiplication
$W_{4,21} =$	$\sqrt{W_{4,20}}$	Power
$W_{4,22} =$	$\dfrac{W_{4,18}}{W_{4,21}}$	Division
$W_{4,23} =$	$\dfrac{W_{4,17}}{W_{4,21}}$	Division
$W_{4,24} =$	$-\dfrac{W_{4,19}}{W_{4,12}}$	Division
$W_{4,25} =$	$\dfrac{W_{4,21}}{W_{4,12}}$	Division
$W_{4,26} =$	$c\psi_T$	Cosine
$W_{4,27} =$	$c\epsilon_T$	Cosine
$W_{4,28} =$	$s\psi_T$	Sine
$W_{4,29} =$	$s\epsilon_T$	Sine
$W_{4,30} =$	$W_{4,26}W_{4,27}$	Multiplication
$W_{4,31} =$	$W_{4,27}W_{4,28}$	Multiplication
$W_{4,32} =$	$\dfrac{1}{X_7}$	Division
$W_{4,33} =$	$T W_{4,32}$	Constant Multiplication
$W_{4,34} =$	$W_{4,33}W_{4,30}$	Multiplication
$W_{4,35} =$	$\dfrac{X_{27}}{X_7}$	Division
$W_{4,36} =$	$W_{4,34} - W_{4,35}$	Subtraction
$W_{4,37} =$	$W_{4,33}W_{4,31}$	Multiplication
$W_{4,38} =$	$W_{4,33}W_{4,29}$	Multiplication
$W_{4,39} =$	$-\mu_M \dfrac{X_1}{X_9}$	Division
$W_{4,40} =$	$-W_{4,7}W_{4,23}$	Multiplication
$W_{4,41} =$	$W_{4,8}W_{4,24}$	Multiplication
$W_{4,42} =$	$-W_{4,5}W_{4,22}$	Multiplication
$W_{4,43} =$	$-W_{4,5}W_{4,23}$	Multiplication
$W_{4,44} =$	$-W_{4,8}W_{4,25}$	Multiplication
$W_{4,45} =$	$W_{4,40}W_{4,25}$	Multiplication
$W_{4,46} =$	$W_{4,42}W_{4,25}$	Multiplication
$W_{4,47} =$	$-W_{4,13}W_{4,22}$	Multiplication
$W_{4,48} =$	$W_{4,40}W_{4,24}$	Multiplication
$W_{4,49} =$	$W_{4,42}W_{4,24}$	Multiplication
$W_{4,50} =$	$W_{4,6}\left(W_{4,45} + W_{4,41}\right) + W_{4,46}$	Multiplication
$W_{4,51} =$	$W_{4,6}\left(W_{4,48} + W_{4,44}\right) + W_{4,49}$	Multiplication
$W_{4,52} =$	$W_{4,39} + W_{4,36}W_{4,50} + W_{4,37}\left(W_{4,47} + W_{4,43}\right) - W_{4,38}W_{4,51}$	Multiplication
$W_{5,1} =$	$-\mu_M \dfrac{X_2}{X_9}$	Division
$W_{5,2} =$	$W_{4,6}W_{4,22}$	Multiplication
$W_{5,3} =$	$W_{4,5}\left(W_{4,45} + W_{4,41}\right) + W_{5,2}W_{4,25}$	Multiplication
$W_{5,4} =$	$-W_{4,14}W_{4,22} + W_{4,6}W_{4,23}$	Multiplication
$W_{5,5} =$	$W_{4,5}\left(W_{4,48} + W_{4,44}\right) + W_{5,2}W_{4,24}$	Multiplication
$W_{5,6} =$	$W_{5,1} + W_{4,36}W_{5,3} + W_{4,37}W_{5,4} - W_{4,38}W_{5,5}$	Multiplication
$W_{6,1} =$	$-\mu_M \dfrac{X_3}{X_9}$	Division
$W_{6,2} =$	$W_{4,7}W_{4,24}$	Multiplication
$W_{6,3} =$	$W_{4,8}W_{4,22}$	Multiplication
$W_{6,4} =$	$-W_{4,7}W_{4,25}$	Multiplication
$W_{6,5} =$	$-W_{4,44}W_{4,23} + W_{6,2}$	Multiplication

$W_{6,6} =$	$W_{4,41} W_{4,23} + W_{6,4}$	Multiplication
$W_{6,7} =$	$W_{6,1} + W_{4,36} W_{6,5} - W_{4,37} W_{6,3} - W_{4,38} W_{6,6}$	Multiplication
$W_{8,1} =$	$X_1 X_4$	Multiplication
$W_{8,2} =$	$X_2 X_5$	Multiplication
$W_{8,3} =$	$X_3 X_6$	Multiplication
$W_{9,0} =$	$X_9 U_8$	Multiplication
$W_{9,1} =$	$\dfrac{W_{9,0}}{X_8}$	Division
$W_{27,1} =$	$W_{4,3}$	Redefining
$W_{27,2} =$	$W_{27,1}^2$	Multiplication
$W_{27,3} =$	$W_{27,1}^3$	Power
$W_{27,4} =$	$W_{27,1}^4$	Power
$W_{27,5} =$	$W_{27,1}^5$	Power
$W_{27,6} =$	$W_{27,1}^6$	Power
$W_{27,7} =$	$W_{27,1}^7$	Power
$W_{27,8} =$	$W_{27,1}^8$	Power
$W_{27,9} =$	$W_{27,1}^9$	Power
$W_{27,10} =$	$W_{27,1}^{10}$	Power
$W_{27,11} =$	$P_{\rho 10} W_{27,10} + P_{\rho 9} W_{27,9} + \ldots + P_{\rho 1} W_{27,1} + P_{\rho 0}$	Constant Multiplication
$W_{27,12} =$	$e^{W_{27,11}}$	Exponential
$W_{27,13} =$	$T_a = \begin{cases} P_{T1,1} W_{27,1}, & \text{for } -0.6 \le h < 5.04 \\ P_{T3,2} W_{27,3} + P_{T2,2} W_{27,2} + P_{T1,2} W_{27,1}, & \text{for } 5.04 \le h < 35.53 \\ P_{T6,3} W_{27,6} + P_{T5,3} W_{27,5} + P_{T4,3} W_{27,4} + \ldots \\ \quad \ldots + P_{T3,3} W_{27,3} + P_{T2,3} W_{27,2} + P_{T1,3} W_{27,1}, & \text{for } 35.53 \le h < 75.07 \\ P_{T8,4} W_{27,8} + P_{T7,4} W_{27,7} + P_{T6,4} W_{27,6} + \ldots \\ \quad \ldots + P_{T5,4} W_{27,5} + P_{T4,4} W_{27,4} + P_{T3,4} W_{27,3} + \ldots \\ \quad \ldots + P_{T2,4} W_{27,2} + P_{T1,4} W_{27,1}, & \text{for } 75.07 \le h < 170.05 \\ 0, & \text{for } h \ge 170.05 \end{cases}$	Constant Multiplication
$W_{27,14} =$	$\sqrt{\gamma_a R_a^* W_{27,13}}$	Power
$W_{27,15} =$	$\dfrac{W_{4,12}}{W_{27,14}}$	Division
$W_{27,16} =$	$C_D = \begin{cases} 0, & \text{for } 0 \le M < 0.5 \\ P_{C_D 1,2} W_{27,15}, & \text{for } 0.5 \le M < 1 \\ P_{C_D 1,3} W_{27,15}, & \text{for } 1 \le M < 1.3 \\ P_{C_D 1,4} W_{27,15}, & \text{for } 1.3 \le M < 2.5 \\ P_{C_D 1,5} W_{27,15}, & \text{for } 2.5 \le M < 4 \\ 0, & \text{for } M \ge 4 \end{cases}$	Constant Multiplication
$W_{27,17} =$	$W_{4,12}^2$	Multiplication
$W_{27,18} =$	$W_{27,17} W_{27,16}$	Multiplication
$W_{27,19} =$	$\frac{1}{2} S W_{27,18} W_{27,12}$	Multiplication

The complete recurrence relation for each of the auxiliary variables can now be written as a function of the reduced auxiliary functions. These are shown by Equation (E.1) and hold for $k \ge 1$.

$$
\begin{aligned}
U_1(k) &= X_4(k) = \frac{U_4(k-1)}{k} & U_5(k) &= W_{5,6}(k) \\
U_2(k) &= X_5(k) = \frac{U_5(k-1)}{k} & U_6(k) &= W_{6,7}(k) \\
& & U_7(k) &= 0 \\
U_3(k) &= X_6(k) = \frac{U_6(k-1)}{k} & U_8(k) &= 2W_{8,1}(k) + 2W_{8,2}(k) + 2W_{8,3}(k) \\
U_4(k) &= W_{4,52}(k) & U_9(k) &= \frac{3}{2} W_{9,1}(k)
\end{aligned}
\tag{E.1}
$$

These equations are now all a function of the recurrence relations corresponding to the rest of the auxiliary functions, which are all basic recurrence relations as mentioned in Table E.1.

E.2. SECOND CARTESIAN CASE: UNIT VECTORS

The second Cartesian case is similar to the first one, however fewer reduced auxiliary functions are needed. These are all provided in Table E.2. For each function, the number, the equations and the category is provided. The numbers are not always the same as in the first case, so these should be read as completely new reduced auxiliary functions. In this case, $u4$, $u5$ and $u6$ are included in the table, because they were defined as recurrence multiplication relations.

Table E.2: Reduced auxiliary functions for the second Cartesian case.

Function	Equation	Category
$W_{4,1} =$	$X_1^2 + X_2^2$	Multiplication
$W_{4,2} =$	$W_{4,1} + X_3^2$	Multiplication
$W_{4,3} =$	$\sqrt{W_{4,2}}$	Power
$W_{4,4} =$	$\sqrt{W_{4,1}}$	Power
$W_{4,9} =$	$X_4 + \Omega_M X_2$	Constant Multiplication
$W_{4,10} =$	$X_5 - \Omega_M X_1$	Constant Multiplication
$W_{4,11} =$	$W_{4,9}^2 + W_{4,10}^2 + X_6^2$	Multiplication
$W_{4,12} =$	$\sqrt{W_{4,11}}$	Power
$W_{4,13} =$	$\dfrac{W_{4,9}}{W_{4,12}}$	Division
$W_{4,14} =$	$\dfrac{W_{4,10}}{W_{4,12}}$	Division
$W_{4,15} =$	$\dfrac{X_6}{W_{4,12}}$	Division
$W_{4,16} =$	$W_{4,10} X_3 - X_6 X_2$	Multiplication
$W_{4,17} =$	$X_6 X_1 - W_{4,9} X_3$	Multiplication
$W_{4,18} =$	$W_{4,9} X_2 - W_{4,10} X_1$	Multiplication
$W_{4,19} =$	$W_{4,16}^2 + W_{4,17}^2 + W_{4,18}^2$	Multiplication
$W_{4,20} =$	$\sqrt{W_{4,19}}$	Power
$W_{4,21} =$	$\dfrac{W_{4,16}}{W_{4,20}}$	Division
$W_{4,22} =$	$\dfrac{W_{4,17}}{W_{4,20}}$	Division
$W_{4,23} =$	$\dfrac{W_{4,18}}{W_{4,20}}$	Division
$W_{4,24} =$	$W_{4,16} W_{4,23} - W_{4,15} W_{4,22}$	Multiplication
$W_{4,25} =$	$W_{4,15} W_{4,21} - W_{4,13} W_{4,23}$	Multiplication
$W_{4,26} =$	$c\psi_T$	Cosine
$W_{4,27} =$	$c\epsilon_T$	Cosine
$W_{4,28} =$	$s\psi_T$	Sine
$W_{4,29} =$	$s\epsilon_T$	Sine
$W_{4,30} =$	$W_{4,26} W_{4,27}$	Multiplication
$W_{4,31} =$	$W_{4,27} W_{4,28}$	Multiplication
$W_{4,32} =$	$\dfrac{1}{X_7}$	Division
$W_{4,33} =$	$T W_{4,32}$	Constant Multiplication
$W_{4,34} =$	$W_{4,33} W_{4,30}$	Multiplication
$W_{4,35} =$	$\dfrac{X_{27}}{X_7}$	Division

$W_{4,36} =$	$W_{4,34} - W_{4,35}$	Subtraction
$W_{4,37} =$	$W_{4,33} W_{4,31}$	Multiplication
$W_{4,38} =$	$W_{4,33} W_{4,29}$	Multiplication
$W_{4,39} =$	$-\mu_M \dfrac{X_1}{X_9}$	Division
$W_{4,40} =$	$W_{4,13} W_{4,22} - W_{4,14} W_{4,21}$	Multiplication
$U_4 =$	$W_{4,39} + W_{4,36} W_{4,13} + W_{4,37} W_{4,21} - W_{4,38} W_{4,24}$	Multiplication
$W_{5,1} =$	$-\mu_M \dfrac{X_2}{X_9}$	Division
$U_5 =$	$W_{5,1} + W_{4,36} W_{4,14} + W_{4,37} W_{4,22} - W_{4,38} W_{4,25}$	Multiplication
$W_{6,1} =$	$-\mu_M \dfrac{X_3}{X_9}$	Division
$U_6 =$	$W_{6,1} + W_{4,36} W_{4,15} + W_{4,37} W_{4,23} - W_{4,38} W_{4,40}$	Multiplication
$W_{8,1} =$	$X_1 X_4$	Multiplication
$W_{8,2} =$	$X_2 X_5$	Multiplication
$W_{8,3} =$	$X_3 X_6$	Multiplication
$W_{9,0} =$	$X_9 U_8$	Multiplication
$W_{9,1} =$	$\dfrac{W_{9,0}}{X_8}$	Division
$W_{27,1} =$	$W_{4,3}$	Redefining
$W_{27,2} =$	$W_{27,1}^2$	Multiplication
$W_{27,3} =$	$W_{27,1}^3$	Power
$W_{27,4} =$	$W_{27,1}^4$	Power
$W_{27,5} =$	$W_{27,1}^5$	Power
$W_{27,6} =$	$W_{27,1}^6$	Power
$W_{27,7} =$	$W_{27,1}^7$	Power
$W_{27,8} =$	$W_{27,1}^8$	Power
$W_{27,9} =$	$W_{27,1}^9$	Power
$W_{27,10} =$	$W_{27,1}^{10}$	Power
$W_{27,11} =$	$P_{\rho 10} W_{27,10} + P_{\rho 9} W_{27,9} + \ldots + P_{\rho 1} W_{27,1} + P_{\rho 0}$	Constant Multiplication
$W_{27,12} =$	$e^{W_{27,11}}$	Exponential
$W_{27,13} =$	$T_a = \begin{cases} P_{T1,1} W_{27,1}, & \text{for } -0.6 \le h < 5.04 \\ P_{T3,2} W_{27,3} + P_{T2,2} W_{27,2} + P_{T1,2} W_{27,1}, & \text{for } 5.04 \le h < 35.53 \\ P_{T6,3} W_{27,6} + P_{T5,3} W_{27,5} + P_{T4,3} W_{27,4} + \ldots \\ \qquad \ldots + P_{T3,3} W_{27,3} + P_{T2,3} W_{27,2} + P_{T1,3} W_{27,1}, & \text{for } 35.53 \le h < 75.07 \\ P_{T8,4} W_{27,8} + P_{T7,4} W_{27,7} + P_{T6,4} W_{27,6} + \ldots \\ \qquad \ldots + P_{T5,4} W_{27,5} + P_{T4,4} W_{27,4} + P_{T3,4} W_{27,3} + \ldots \\ \qquad \ldots + P_{T2,4} W_{27,2} + P_{T1,4} W_{27,1}, & \text{for } 75.07 \le h < 170.05 \\ 0, & \text{for } h \ge 170.05 \end{cases}$	Constant Multiplication
$W_{27,14} =$	$\sqrt{\gamma_a R_a^* W_{27,13}}$	Power
$W_{27,15} =$	$\dfrac{W_{4,12}}{W_{27,14}}$	Division
$W_{27,16} =$	$C_D = \begin{cases} 0, & \text{for } 0 \le M < 0.5 \\ P_{C_D 1,2} W_{27,15}, & \text{for } 0.5 \le M < 1 \\ P_{C_D 1,3} W_{27,15}, & \text{for } 1 \le M < 1.3 \\ P_{C_D 1,4} W_{27,15}, & \text{for } 1.3 \le M < 2.5 \\ P_{C_D 1,5} W_{27,15}, & \text{for } 2.5 \le M < 4 \\ 0, & \text{for } M \ge 4 \end{cases}$	Constant Multiplication
$W_{27,17} =$	$W_{4,12}^2$	Multiplication
$W_{27,18} =$	$W_{27,17} W_{27,16}$	Multiplication

| $W_{27,19} =$ | $\frac{1}{2} S W_{27,18} W_{27,12}$ | Multiplication |

The complete recurrence relation for each of the auxiliary variables can again be written as a function of the reduced auxiliary functions. These are shown by Equation (E.2).

$$
\begin{aligned}
U_1(k) &= X_4(k) = \frac{U_4(k-1)}{k} \\
U_2(k) &= X_5(k) = \frac{U_5(k-1)}{k} \\
U_3(k) &= X_6(k) = \frac{U_6(k-1)}{k} \\
U_4(k) &= W_{4,39}(k) + W_{4,36}(k)W_{4,13}(k) + W_{4,37}(k)W_{4,21}(k) - W_{4,38}(k)W_{4,24}(k) \\
U_5(k) &= W_{5,1}(k) + W_{4,36}(k)W_{4,14}(k) + W_{4,37}(k)W_{4,22}(k) - W_{4,38}(k)W_{4,25}(k) \\
U_6(k) &= W_{6,1}(k) + W_{4,36}(k)W_{4,15}(k) + W_{4,37}(k)W_{4,23}(k) - W_{4,38}(k)W_{4,40}(k) \\
U_7(k) &= 0 \\
U_8(k) &= 2W_{8,1}(k) + 2W_{8,2}(k) + 2W_{8,3}(k) \\
U_9(k) &= \frac{3}{2} W_{9,1}(k)
\end{aligned}
\tag{E.2}
$$

E.3. SPHERICAL CASE

Since the Spherical case is very different from the Cartesian cases, it comes with its own auxiliary functions. The reduced versions are shown in Table E.3.

Table E.3: Reduced auxiliary functions for the Spherical case.

Auxiliary function	Equation	Category
$W_{4,4} =$	sX_{12}	Sine
$W_{4,5} =$	cX_{13}	Cosine
$W_{4,6} =$	cX_{12}	Cosine
$W_{4,7} =$	sX_{14}	Sine
$W_{4,8} =$	cX_{14}	Cosine
$W_{4,9} =$	sX_{13}	Sine
$W_{4,26} =$	$c\psi_T$	Cosine
$W_{4,27} =$	$c\epsilon_T$	Cosine
$W_{4,28} =$	$s\psi_T$	Sine
$W_{4,29} =$	$s\epsilon_T$	Sine
$W_{4,32} =$	$\frac{1}{X_7}$	Division
$W_{11,0} =$	$X_{15}W_{4,8}$	Multiplication
$W_{11,1} =$	$\frac{W_{11,0}}{X_{16}}$	Division
$W_{11,2} =$	$W_{11,1}W_{4,9}$	Multiplication
$W_{11,3} =$	$\frac{W_{11,2}}{W_{4,6}}$	Division
$W_{12,1} =$	$W_{11,1}W_{4,5}$	Multiplication
$W_{13,0} =$	$W_{4,28}W_{4,27}$	Multiplication
$W_{13,1} =$	$W_{4,7}W_{4,5}$	Multiplication
$W_{13,2} =$	$\Omega_M^2 X_{16}W_{4,6}$	Multiplication
$W_{13,3} =$	$W_{13,2}W_{4,4}$	Multiplication
$W_{13,4} =$	$TW_{13,0}W_{4,32}$	Multiplication
$W_{13,5} =$	$W_{13,3}W_{4,9} + W_{13,4}$	Multiplication
$W_{13,6} =$	$\frac{W_{13,5}}{X_{15}}$	Division

$W_{13,7} =$	$-2\Omega_M W_{4,6} W_{13,1} + W_{13,6}$	Multiplication
$W_{13,8} =$	$\dfrac{W_{13,7}}{W_{4,8}}$	Division
$W_{13,9} =$	$\left(2\Omega_M + W_{11,3}\right) W_{4,4} + W_{13,8}$	Multiplication
$W_{14,0} =$	$T W_{4,29} W_{4,32}$	Multiplication
$W_{14,1} =$	$W_{4,6} W_{4,8} + W_{13,1} W_{4,4}$	Multiplication
$W_{14,2} =$	$-\mu_M W_{4,8}$	Constant Multiplication
$W_{14,3} =$	X_{16}^2	Multiplication
$W_{14,4} =$	$\dfrac{W_{14,2}}{W_{14,3}}$	Division
$W_{14,5} =$	$W_{14,4} + W_{13,2} W_{14,1} + W_{14,0}$	Multiplication
$W_{14,6} =$	$\dfrac{W_{14,5}}{X_{15}}$	Division
$W_{14,7} =$	$2\Omega_M W_{4,6} W_{4,9} + W_{11,1} + W_{14,6}$	Multiplication
$W_{15,0} =$	$T W_{4,26} W_{4,27} - X_{27}$	Multiplication
$W_{15,1} =$	$\dfrac{W_{15,0}}{X_7}$	Division
$W_{15,2} =$	$-\mu_M W_{4,7}$	Constant Multiplication
$W_{15,3} =$	$\dfrac{W_{15,2}}{W_{14,3}}$	Division
$W_{15,4} =$	$W_{4,8} W_{4,5}$	Multiplication
$W_{15,5} =$	$W_{4,7} W_{4,6} - W_{15,4} W_{4,4}$	Multiplication
$W_{15,6} =$	$W_{13,2} W_{15,5} + W_{15,1} + W_{15,3}$	Multiplication
$W_{16,1} =$	$X_{15} W_{4,7}$	Multiplication
$W_{27,1} =$	$X_{29} U_{28}$	Multiplication
$W_{27,2} =$	$X_{28} U_{29}$	Multiplication
$W_{27,3} =$	$X_{28} X_{29}$	Multiplication
$W_{27,4} =$	$X_{15} \left(W_{27,1} + W_{27,2}\right)$	Multiplication
$W_{27,5} =$	$W_{27,3} U_{15}$	Multiplication
$W_{27,6} =$	$X_{15} \left(W_{27,4} + W_{27,5}\right)$	Multiplication
$W_{28,1} =$	$U_{30} X_{28}$	Multiplication
$W_{29,1} =$	$\begin{cases} 0, & \text{for } 0 \leq M < 0.5 \\ P_{C_D1,2} U_{32}, & \text{for } 0.5 \leq M < 1 \\ P_{C_D1,3} U_{32}, & \text{for } 1 \leq M < 1.3 \\ P_{C_D1,4} U_{32}, & \text{for } 1.3 \leq M < 2.5 \\ P_{C_D1,5} U_{32}, & \text{for } 2.5 \leq M < 4 \\ 0, & \text{for } M \geq 4 \end{cases}$	Constant Multiplication
$W_{30,1} =$	X_{31}^9	Power
$W_{30,2} =$	X_{31}^8	Power
$W_{30,3} =$	X_{31}^7	Power
$W_{30,4} =$	X_{31}^6	Power
$W_{30,5} =$	X_{31}^5	Power
$W_{30,6} =$	X_{31}^4	Power
$W_{30,7} =$	X_{31}^3	Power
$W_{30,8} =$	X_{31}^2	Multiplication
$W_{30,9} =$	$U_{31} \left(10 P_{\rho 10} W_{30,1} + \cdots + 3 P_{\rho 3} W_{30,8} + 2 P_{\rho 2} X_{31} + P_{\rho 1}\right)$	Multiplication
$W_{32,1} =$	$X_{33} U_{15}$	Multiplication
$W_{32,2} =$	$X_{15} U_{33}$	Multiplication
$W_{32,3} =$	X_{33}^2	Multiplication
$W_{32,4} =$	$\dfrac{W_{32,1} - W_{32,2}}{W_{32,3}}$	Division

$W_{33,1} =$	$\dfrac{U_{34}}{X_{33}}$		Division
$W_{34,1} =$	$\begin{cases} P_{T1,1}U_{31}, & \text{for } -0.6 \le h < 5.04 \\ \left(3P_{T3,2}W_{30,8} + 2P_{T2,2}X_{31}\right)U_{31} + P_{T1,2}U_{31}, & \text{for } 5.04 \le h < 35.53 \\ \left(6P_{T6,3}W_{30,5} + 5P_{T5,3}W_{30,6} + 4P_{T4,3}W_{30,7} + \ldots \right. \\ \qquad \left. \ldots + 3P_{T3,3}W_{30,8} + 2P_{T2,3}X_{31}\right)U_{31} + P_{T1,3}U_{31}, & \text{for } 35.53 \le h < 75.07 \\ \left(8P_{T8,4}W_{30,3} + 7P_{T7,4}W_{30,4} + 6P_{T6,4}W_{30,5} + 5P_{T5,4}W_{30,6} + \ldots \right. \\ \qquad \left. \ldots + 4P_{T4,4}W_{30,7} + 3P_{T3,4}W_{30,8} + 2P_{T2,4}X_{31}\right)U_{31} + P_{T1,4}U_{31}, & \text{for } 75.07 \le h < 170.05 \\ 0, & \text{for } h \ge 170.05 \end{cases}$		Multiplication

In this case, a number of extra auxiliary equations were used, which result in extra recurrence relations. These are all described in Equation (E.3) and hold for $k \ge 1$.

$$
\begin{aligned}
U_7(k) &= 0 \\
U_{11}(k) &= W_{11,3}(k) \\
U_{12}(k) &= W_{12,1}(k) \\
U_{13}(k) &= W_{13,9}(k) \\
U_{14}(k) &= W_{14,7}(k) \\
U_{15}(k) &= W_{15,6}(k) \\
U_{16}(k) &= W_{16,1}(k)
\end{aligned}
\qquad
\begin{aligned}
U_{27}(k) &= \frac{1}{2}SW_{27,6}(k) \\
U_{28}(k) &= W_{28,1}(k) \\
U_{29}(k) &= W_{29,1}(k) \\
U_{30}(k) &= W_{30,9}(k) \\
U_{31}(k) &= U_{16}(k) \\
U_{32}(k) &= W_{32,4}(k) \\
U_{33}(k) &= W_{33,1}(k) \\
U_{34}(k) &= W_{34,1}(k)
\end{aligned}
\qquad \text{(E.3)}
$$

F

PROPOSED SENSITIVITY ANALYSIS

The purpose of the sensitivity analysis is to determine the effects of the different parameters on the performance and the outcome of the program. The different test cases to determine these effects are described in Tables F.1 and F.2. The parameter cases that I give the most priority to are mentioned in Table F.1 and then in decreasing order of priority in Table F.2. The accuracy will always be compared to the nominal case. The differences are compared to the different cases per parameter. All cases are also computed for RKF and compared to the TSI results. For comparison purposes, a similar integration cut-off requirement is used for the different test cases (might vary per parameter though).

Table F.1: Test cases for the sensitivity analysis

Influencing parameter	Test case(s)	Focus for comparison
Maximum TSI order	Change the order from 2 till 30 (or higher depending on accuracy of computer).	Number of function evaluations required per order. Accuracy of the corresponding results. Speed of convergence.
Error tolerance	Vary from $1 \cdot 10^{-5}$ to $1 \cdot 10^{-14}$ with steps of 1 order	Number of function evaluations required per error tolerance. Accuracy of the corresponding results. Speed of convergence.
Initial TSI step-size	Vary from $1 \cdot 10^{-4}$ to 1 second. 10 steps per order.	Number of function evaluations required per step-size. Accuracy of the corresponding results. Speed of convergence.
Launch altitude	Between -0.6 and 0.5 km MOLA. Vary by 100 m each step.	Difference in propellant mass requirements. Difference in final state. Number of function evaluations required per altitude.
Launch latitude	From -90° to 90° with 20° steps. In combination with different longitudes creating different launch positions on Mars.	Difference in propellant mass requirements. Difference in final state. Number of function evaluations required per site. Accuracy of the corresponding results.
Launch longitude	From 0° to 330° with 30° steps. In combination with different longitudes creating different launch positions on Mars	Difference in propellant mass requirements. Difference in final state. Number of function evaluations required per site. Accuracy of the corresponding results.
RKF initiator time	Vary from 0.1 to 2 second with steps of 0.1 seconds.	Number of function evaluations required per case. Accuracy of the corresponding results. Speed of convergence.

Table F.2: Test cases for the sensitivity analysis continued

Influencing parameter	Test case(s)	Focus for comparison
Launch FPA	Vary from 0° to 90° with steps of 5°.	Difference in propellant mass requirements. Difference in final state. Number of function evaluations required per angle. Accuracy of the corresponding results.
Launch heading angle	Vary from 0° to 330° with steps of 30°.	Difference in propellant mass requirements. Difference in final state. Number of function evaluations required per angle. Accuracy of the corresponding results.
Launch ground velocity	Vary from $1 \cdot 10^{-6}$ to 0.1 km/s with steps of one order.	Difference in propellant mass requirements. Difference in final state. Number of function evaluations required per angle. Accuracy of the corresponding results.
MAV GLOM	Test range of masses as provided in the literature study based on the different reference MAV's.	Difference in propellant mass requirements. Difference in final state. Accuracy of the corresponding results.
Thrust	Test range of thrust values as provided in the literature study based on the different reference MAV's.	Difference in propellant mass requirements. Difference in final state. Accuracy of the corresponding results.
Specific impulse	Test a range of solid, hybrid and liquid specific impulses corresponding to the reference MAV's.	Difference in propellant mass requirements. Difference in final state. Accuracy of the corresponding results.
Burn time	Selected variation from the nominal test burn time. Both less and more time. Cut-off for integration set same altitude each time reachable by lowest burn time case.	Number of function evaluations per altitude.
Thrust elevation angle	Depending on the test case used, vary the angle by 50% in each direction. Can be combined with the thrust azimuth angle to show combined impact.	Difference in propellant mass requirements. Difference in final state.
Thrust azimuth angle	Depending on the test case used, vary the angle by 50% in each direction. Can be combined with the thrust elevation angle to show combined impact.	Difference in propellant mass requirements. Difference in final state.
Final orbit altitude	Vary from 250 km MOLA to 500 km MOLA with steps of 25 km MOLA. Possibly in combination with different burn times.	Difference in propellant mass requirements. Number of function evaluations per altitude.
Final orbit inclination	Vary from 0° to 160° with steps of 20°.	Difference in propellant mass requirements. Number of function evaluations per altitude.

G

PROPOSED SCHEDULE

In Table G.1, a proposed schedule per day is provided with the work that should be done on that day to meet the deadline. In bolt are the milestones that involve Delft.

Table G.1: Schedule

Date	Work
Monday 14/11	Get software running on new Linux computer. Finish draft chapter on verification and validation.
Tuesday 15/11	Finish draft chapter on models.
Wednesday 16/11	Finish draft chapter on standard integration methods.
Thursday 17/11	Write draft chapter on problem background.
Friday 18/11	Finish draft chapter on problem background.
Saturday 19/11	Produce results for sensitivity analysis.
Sunday 20/11	Write draft results chapter.
Monday 21/11	Finish draft results chapter. Write draft analysis chapter.
Tuesday 22/11	**Meeting with supervisors in Delft.** Finish draft analysis chapter.
Wednesday 23/11	Write draft chapter conclusions and recommendations. Write draft introduction.
Thursday 24/11	Read and adjust introduction, problem background and models chapter.
Friday 25/11	Read and adjust standard integration methods, TSI and Program simulation tool chapter.
Saturday 26/11	Read and adjust verification and validation chapter and appendices.
Sunday 27/11	Read and adjust results, analysis and conclusions and recommendations chapter.
Monday 28/11	Nomenclature and abbreviations.
Tuesday 29/11	Finalisation of report.
Wednesday 30/11	Finalisation of report.
Thursday 1/12	**Hand in holy draft.**